

Scalar induced gravity waves from ultra slow-roll Galileon inflation

Sayantana Choudhury^{1,*}, Ahaskar Karde^{1,†}, Sudhakar Panda^{1,‡} and M. Sami^{1,2,3,§}

¹*Centre For Cosmology and Science Popularization (CCSP),*

SGT University, Gurugram, Delhi- NCR, Haryana- 122505, India.

²*Center for Theoretical Physics, Eurasian National University, Astana 010008, Kazakhstan. and*

³*Chinese Academy of Sciences, 52 Sanlihe Rd, Xicheng District, Beijing.*

We consider the production of secondary gravity waves in Galileon inflation with an ultra-slow roll (USR) phase and show that the spectrum of scalar-induced gravitational waves (SIGWs) in this case is consistent with the recent NANOGrav 15-year data and with sensitivities of other ground and space-based missions, LISA, BBO, DECIGO, CE, ET, HLVK (consists of aLIGO, aVirgo, and KAGRA), and HLV(03). Thanks to the non-renormalization property of Galileon theory, the amplitude of the large fluctuation is controllable at the sharp transitions between SR and USR regions. We show that the behaviour of the GW spectrum, when one-loop effects are included in the scalar power spectrum, is preserved under a shift of the sharp transition scale with peak amplitude $\Omega_{\text{GW}} h^2 \sim \mathcal{O}(10^{-6})$, and hence it can cover a wide range of frequencies within $\mathcal{O}(10^{-9}\text{Hz} - 10^7\text{Hz})$. An analysis of the allowed mass range for primordial black holes (PBHs) is also performed, where we find that mass values ranging from $\mathcal{O}(1M_{\odot} - 10^{-18}M_{\odot})$ can be generated over the corresponding allowed range of low and high frequencies.

Contents

I. Introduction	2
II. Galileon Inflation	3
A. The Set up with ultra-slow roll realisation	3
1. The first slow-roll (SRI) phase	6
2. The ultra-slow roll (USR) phase	7
3. The second slow-roll (SRII) phase	10
B. Solutions from the perturbed second order action	13
C. Impact of the non-renormalization theorem	13
D. One-loop corrected power spectrum from third order action	14
E. PBH production and its comparison with recent studies	15
1. Calculation of the PBH mass fraction	17
III. Scalar Induced Gravitational Waves	17
IV. Results for the SIGW spectrum	20
V. Conclusion	23
VI. Appendix	24
A. General Mode Solutions	24
B. Couplings and Coefficients in three phases including one-loop effects	25
References	28

* sayantan_ccsp@sgtuniversity.org,

sayanphysics@gmail.com

† kardeahaskar@gmail.com

‡ panda@niser.ac.in

§ sami_ccsp@sgtuniversity.org, samijamia@gmail.com

I. Introduction

The first observational results on Gravitational Waves (GWs) generated from binary black hole mergers [1] provided us with an opportunity to study the physics of the early universe. Indeed, the GWs are a unique probe that directly brings information from the early universe before recombination. Their possible sources could include phase transitions in the early universe [2–9], domain walls [10–16], cosmic strings [9, 17–21], and most popularly, inflation [9, 22–45], where GWs (tensor perturbations) are generated naturally [46–53], enter the horizon and travel unimpeded to become visible to us today using the current and proposed observational experiments [54–56]. These GWs would appear to us in the form of random signals forming an often-called stochastic GW background (SGWB) when looking in all the possible directions in the universe for their sources located at large redshifts. The latest announcement from various PTA collaborations, NANOGrav [57–64], EPTA [65–70], PPTA [71–73], and CPTA [74], have confirmed the existence of an SGWB, which has attracted considerable work where the variety of cosmological models mentioned above are examined for being a possible source for the observed data. In this work, we will be concerned with the scalar-induced GWs scenario to explain the PTA signal.

The concept of GWs being induced by primordial density fluctuations was studied initially in the respective refs. [75–77]; however, it was confirmed that the magnitude of the produced GW spectrum was insufficient in terms of any meaningful observations. Later, the works of the authors in [78, 79] showed that the generation of induced GWs considered in the radiation and matter-dominated eras, including the radiation-matter equality phase, would be able to produce an enhanced spectrum amplitude by examining constraints on the spectral tilt, and details of the transfer function for production of the second-order GWs between the large scales observed today to the smallest scales, in the respective works. This led to the final induced GW spectrum having an observable amplitude but with the condition of having to consider only the very low-frequency regimes. Another interesting observation regarding this phenomenon was made by the authors in [80, 81], where they investigated the case of large enough primordial fluctuations which can lead to the collapse and formation of primordial black holes (PBHs) [30, 33, 79, 80, 82–174]. This work focuses on scalar-induced GWs production from Galileon inflation [175] in the presence of an ultra-slow-roll (USR) phase, which triggers the generation of large amplitude scalar perturbation. In particular, we want to discuss the observational status of the induced GWs spectrum and also examine the allowed mass range for the produced PBHs from Galileon inflation.

Recently, there has been an active pursuit to settle the arguments concerning the formation of PBHs and the effects on their masses from the one-loop corrections to the scalar power spectrum. Related discussions are present in refs. [118, 119, 121, 122, 124, 126–128, 130–134, 176, 177] which concern the single-field canonical models of inflation and the EFT treatment of inflation. Amidst this, the use of the Galileon theory in [127] has shown interesting results stemming from some important features forming the basis of our discussions in this work. See refs. [175, 178–230] to know about the underlying Galileon framework. It includes the unique Non-Renormalization theorem, which states that the theory is stable against radiative corrections to any of the calculated correlation functions. This further limits our work to only performing the regularization procedure while neglecting the important, but redundant in this case, procedures of renormalization and resummation which is a remarkable feature to consider. Using these properties of this theory, the one-loop corrected version of the scalar power spectrum is shown to have a controllable behaviour in terms of maintaining the perturbativity argument within the theory. When working with perturbation theory up to the second order, the observed spectrum of the scalar perturbations will act as a source for generating second-order tensor modes and hence SIGWs. The inclusion of quantum loop effects will then not greatly alter the behaviour of the spectrum and only result in an introduction of oscillatory features near the tail and peak regions. We are considering that the entire inflationary phase in this theory consists of three regions, namely the first slow-roll (SRI), ultra-slow roll (USR), and the second slow-roll (SR II), such that there exists a sharp transition when passing from SRI to USR and USR to SR II phases. The behavior of the scalar power spectrum at the transition scales, and similarly for the tensor power spectrum, is controllable due to the properties of this theory mentioned at the beginning. This fact has significant implications when controlling the non-Gaussianities [32, 128], and due to the phase corresponding to large primordial fluctuations having constraints on its duration, the perturbativity approximation does not break near the sharp transitions. This controlling feature results from properties intrinsic to the Galileon theory, which is not true for other single-field inflation models.

The nature of a transition, whether sharp or smooth, reflects significantly in the allowed PBH mass and its abundance. When quantum loop effects turn out to be necessary for the overall analysis of an inflationary paradigm to consider PBHs, then the need for performing renormalization and resummation is required to reach meaningful conclusions for the completion of inflation and on the mass of PBH [124–126]. An important consequence of the analysis done in the Galileon theory concerns the *no-go theorem* for the masses of PBHs [127, 128] such that the theory is able to evade the said theorem by being able to produce solar mass PBHs along with controlling the enhancement of perturbations with successful inflation. The behaviour of the induced GW spectrum investigated when having frequencies for the sharp transitions set in both the low and high-frequency regimes provides us with an opportunity

to see whether Galileon theory is able to produce a large enough GW signal that can lie within the existing observational results. Since shifting of the sharp transition scales does not affect the qualitative features of the scalar power spectrum as long as the perturbative arguments are maintained, we find that the induced GW spectrum can also show its presence where the high-frequency GW probes operate which includes LISA [231], BBO [232], DECIGO [233], Cosmic Explorer(CE) [234], Einstein Telescope(ET) [235], the HLVK network which consists of aLIGO in Hanford and Livingston [236], aVirgo [237], and KAGRA [238], and the HLV network during the third observation run (O3).

This paper is outlined as follows: In Sec. II, we provide a short overview of the Galileon theory which begins by analyzing the setup of interest in detail with proper realisation of each phase, including the evolution of the slow-roll parameters and the Galileon scalar field throughout, followed by analyzing its second-order perturbed action to get the mode solutions for the comoving curvature perturbation. Then we briefly discuss the significance of the non-renormalization theorem and introduce the third-order action responsible for the calculation of the one-loop effects. Lastly, we talk about the allowed mass range for producing PBH and compare the recent studies done in this regard. In Sec. III, we present a concise introduction to the theory of SIGWs and the radiation-dominated era contribution to the GW abundance formula which is going to be used by us. In Sec. IV, we use the results of the previous sections to present our key result for the induced GW spectrum from Galileon theory. There we analyze its qualitative features in detail and comment on their observational status and their relation with the masses of PBH. In Sec. V, we state our conclusions.

II. Galileon Inflation

In this section, we present a brief overview of our findings on the Galileon framework. We start with a discussion on the general action of the theory followed by the realisation of an ultra-slow roll (USR) phase in the present context. After this we provide an explanation for obtaining the mode solutions for the comoving curvature perturbation using the second-order perturbed action. Then we discuss the effects of mildly breaking the Galilean symmetry and the impact of the powerful non-renormalization theorem in the presence of a sharp transition scenario. We then discuss the third-order action in the theory responsible for one-loop effects to be used in the later sections. Finally, we discuss the case of allowed masses of PBH produced from the Galileon theory and comment on the recent studies related to this issue.

A. The Set up with ultra-slow roll realisation

The Galileon theory is a framework where the equations of motion are of second order despite the higher-derivative terms in the action ref.[239, 240],

$$S = \int d^4x \sqrt{-g} \left[\frac{M_{pl}^2}{2} R - V_0 + \sum_{i=1}^5 c_i \mathcal{L}_i \right] \quad (1)$$

which include the dimensionless coefficients c_i and the remaining Lagrangians are explicitly written as follows:

$$\begin{aligned} \mathcal{L}_1 &= \phi, \quad \mathcal{L}_2 = -\frac{1}{2}(\nabla\phi)^2, \quad \mathcal{L}_3 = \frac{1}{\Lambda^3}(\nabla\phi)^2\Box\phi, \\ \mathcal{L}_4 &= -\frac{1}{\Lambda^6}(\nabla\phi)^2 \left\{ (\Box\phi)^2 - (\nabla_\mu\nabla_\nu\phi)(\nabla^\mu\nabla^\nu\phi) - \frac{1}{4}R(\nabla\phi)^2 \right\}, \\ \mathcal{L}_5 &= \frac{1}{\Lambda^9}(\nabla\phi)^2 \left\{ (\Box\phi)^3 - 3(\Box\phi)(\nabla_\mu\nabla_\nu\phi)(\nabla^\mu\nabla^\nu\phi) + 2(\nabla_\mu\nabla_\nu\phi)(\nabla^\nu\nabla^\alpha\phi)(\nabla_\alpha\nabla^\mu\phi) - 6G_{\mu\nu}\nabla^\mu\nabla^\alpha\phi\nabla^\nu\phi\nabla_\alpha\phi \right\}. \end{aligned} \quad (2)$$

The action (1) has the Galilean shift symmetry as its defining property:

$$\phi \rightarrow \phi + a_\mu x^\mu + b, \quad (3)$$

where ϕ is the Galileon scalar field, a_μ is a constant vector and b a constant scalar defined in the $3+1$ dimensional space-time. The framework based upon the covariant action (1) is referred to as the Covariantized Galileon Theory (CGT).

Now we move towards studying the dynamics of this Galileon scalar field in a cosmological setting where the Galileon model lives on a quasi de Sitter background spacetime such that the background field, $\bar{\phi}(t)$, is homogeneous and time-dependent. Next, to study the inflationary scenario on such a spacetime we require that variation in the

effective potential of our theory must satisfy the condition $|\Delta V/V| \ll 1$. This gives us a value of the scale factor within our CGT framework as $a(t) = \exp(Ht)$, where the Hubble parameter H also defines the deviation from exact de sitter in form of the slow-roll parameter $\epsilon = -\dot{H}/H^2$. We now mention the action for the field $\phi(t)$ after collecting the first-order terms from integration by parts and discarding any boundary terms:

$$S^{(0)} = \int dt a^3 \mathcal{L} = \int d^4x a^3 \left\{ \dot{\phi}^2 \left(\frac{c_2}{2} + 2c_3 Z + \frac{9c_4}{2} Z^2 + 6c_5 Z^3 \right) + \lambda^3 \bar{\phi} \right\} \quad (4)$$

where the coupling parameter is defined as $Z \equiv H\dot{\phi}/\Lambda^3$ with Λ as a physical cut-off scale of the theory. In the regime where the coupling satisfies $Z \simeq 1$, we can incorporate the non-linearities within the galileon sector and also neglect any non-minimal couplings to gravity. This is the favourable regime in which we choose to work.

Let us briefly understand the behaviour of the scalar field in the de Sitter background through its evolution. To conduct inflation requires mildly breaking the shift symmetry, and this gets implemented starting with a linear term in the field $\bar{\phi}$ along the constant potential V_0 to give, $V = V_0 - c_1 \bar{\phi}$, where c_1 is a small and constant parameter. To get the equation of motion for $\bar{\phi}(t)$ is made simple by the fact that under the condition $M_p \rightarrow \infty$ while maintaining the relation $3H^2 M_p^2 = V_0$, gives us a scalar field on exact de Sitter space. There, we have an exact shift symmetry, which allows the conservation of the associated current to provide for the equation of motion for the field $\bar{\phi}$ as:

$$\ddot{\bar{\phi}} + 3H\dot{\bar{\phi}} - c_1 = 0. \quad (5)$$

and for this, there exists the solution with $3H\dot{\bar{\phi}} = c_1$. Now, with the eqn.(4) in mind, and using the definition of the Noether current for the above background action as $j^t = \partial \mathcal{L} / \partial \dot{\bar{\phi}}$ we can have the following relation:

$$\dot{\bar{\phi}}(c_2 + 6c_3 Z + 18c_4 Z^2 + 30c_5 Z^3) = \frac{c_1}{3H}, \quad (6)$$

where the existence of shift symmetry and the Galileon model having second-order equation of motions enables the identification of the j^t with $\dot{\bar{\phi}}$ and thus we can use the solution $\dot{\bar{\phi}} = c_1/3H$ as shown before. We restrict first to the case where the parameters c_4, c_5 , for the higher-derivative terms in eqn.(1), remain zero. This allows for a equation quadratic in $\dot{\bar{\phi}}$ from eqn.(6), solving which straightforwardly leads one to the solution:

$$\dot{\bar{\phi}} = \frac{f(c_1, c_2, c_3, \Lambda)}{H}, \quad \text{where} \quad f(c_1, c_2, c_3, \Lambda) \equiv \frac{\Lambda^3}{12} \frac{c_2}{c_3} \left[-1 + \sqrt{1 + \frac{8c_3}{c_2^2} \frac{c_1}{\Lambda^3}} \right], \quad (7)$$

and solving this gives us the evolution of the background field with time t or, as we will consider further, with the e-folding \mathcal{N} .

In order to determine the evolution of the function f , we take help from parameterization of the second-slow roll parameter, η , across the three phases in our setup of SRI-USR-SRII. In our construction, η undergoes a sharp transition at the boundary when going from SRI to USR and another sharp transition from USR to SRII. We use the Heaviside Theta function for the parameterization of η and from it derive the behaviour of the first slow-roll parameter ϵ as well the Hubble parameter H and the background scalar field $\bar{\phi}$.

Taking η as a constant value during each phase, we use its definition in terms of the scalar field to provide the following relations for the function f as:

$$\eta = -\frac{\ddot{\bar{\phi}}}{\dot{\bar{\phi}}H} = -\frac{1}{\dot{\bar{\phi}}} \frac{d}{d\mathcal{N}} \left(\frac{f}{H} \right) = -\frac{1}{f} \left(\frac{df}{d\mathcal{N}} - \frac{f}{H} \frac{dH}{d\mathcal{N}} \right), \quad (8)$$

where $d\mathcal{N} = Hdt$ is used. From this one can determine f as a function of \mathcal{N} by solving to get:

$$f(\mathcal{N}) = \frac{H(\mathcal{N})}{H(\mathcal{N}_i)} \exp(-\eta \Delta \mathcal{N}), \quad (9)$$

here \mathcal{N}_i is related to the initial condition at the beginning of each phase, it being \mathcal{N}_* for the SRI usually fixed at the pivot scale, \mathcal{N}_s for the USR, and \mathcal{N}_e for SRII. The notation $\Delta \mathcal{N}$ here refers to the subsequent change in e-foldings for each phase. We can also determine the first slow-roll parameter by using its relation with η as follows:

$$-\frac{\ddot{\bar{\phi}}}{\dot{\bar{\phi}}H} \equiv \eta = \epsilon - \frac{1}{2} \frac{d \ln \epsilon}{d\mathcal{N}} \implies \frac{d\epsilon}{d\mathcal{N}} = 2\epsilon(\epsilon - \eta), \quad (10)$$

integrating the above gives us:

$$\epsilon(\mathcal{N}) = \eta \left(1 - \left(1 - \frac{\eta}{\epsilon_i} \right) e^{2\eta\Delta\mathcal{N}} \right)^{-1}, \quad (11)$$

here also $\epsilon_i \equiv \epsilon(\mathcal{N}_i)$ is related to the initial condition at the beginning of each phase for the corresponding \mathcal{N}_i value. During the SRI phase, $\epsilon_{i,\text{SRI}} \sim 10^{-3}$ is chosen in our analysis at the pivot scale \mathcal{N}_* . It remains to understand the Hubble parameter with the e-folds, and this can be done directly from the definition of ϵ as follows:

$$\epsilon(\mathcal{N}) = -\frac{1}{H} \frac{dH}{d\mathcal{N}} = \eta \left(1 - \left(1 - \frac{\eta}{\epsilon_i} \right) e^{2\eta\Delta\mathcal{N}} \right)^{-1}, \quad (12)$$

where the second equality uses eqn.(11), and again from further integration one obtains for the respective phase:

$$H(\mathcal{N}) = H_i \left(\frac{\eta \exp(2\eta\mathcal{N})}{\epsilon_i - \exp(2\eta\mathcal{N})(\epsilon_i - \eta)} \right)^{-\frac{1}{2}}, \quad (13)$$

where $H_i \equiv H(\mathcal{N}_i)$ relates to the initial condition at the beginning of each phase for the corresponding \mathcal{N}_i value. We can now use the set of eqns.(11,13,7) to observe the behaviour of these parameters based on the η parameterization described before. From eqn.(7) we can now directly write for the field $\bar{\phi}$, with the help of the results of f and $H(\mathcal{N})$, the following relation:

$$\dot{\bar{\phi}} = H \frac{d\bar{\phi}}{d\mathcal{N}} = \frac{f}{H} \implies \frac{d\bar{\phi}}{d\mathcal{N}} = \frac{f(c_1, c_2, c_3, \Lambda)}{H(\mathcal{N})^2}, \quad (14)$$

In fig.(1) we present the evolution of the respective parameters as stated before. From fig.(1), we visualize how each of the parameters as well the background scalar field behaves across the three phases in our setup. Another crucial parameter involved in our study is the effective sound speed, c_s and it is defined in terms of few time-dependent coefficients which are also functions of the $c_i \forall i = 2, 3, 4, 5$. The definition of the respective c_i -dependent functions are as follows:

$$\mathcal{A} \equiv \frac{\dot{\bar{\phi}}^2}{2} \left(c_2 + 12c_3Z + 54c_4Z^2 + 120c_5Z^3 \right), \quad (15)$$

$$\mathcal{B} \equiv \frac{\dot{\bar{\phi}}^2}{2} \left\{ c_2 + 4c_3Z(2 - \eta) + 2c_4Z^2(13 - 6(\epsilon + 2\eta)) - 24c_5Z^3(2\epsilon + 1) \right\}. \quad (16)$$

and using this the parameter c_s is defined as, $c_s^2 = \mathcal{B}/\mathcal{A}$. The effective sound speed is a crucial parameter in that it contains almost all of the coefficients present within the original CGT action, see eqn.(1). The value of c_s ultimately facilitates a USR phase in our setup by considering what we now describe as a specific parameterization. It goes as follows: during the SRI phase, the value of the sound speed satisfies $c_s = c_{s,*}$ which is also its value set at the pivot scale, at $\mathcal{N} = \mathcal{N}_*$. Soon as we encounter our first sharp transition into the USR when $\mathcal{N} = \mathcal{N}_s$, here c_s suffers a sharp rise to its new value, $c_s = \tilde{c}_s = 1 \pm \delta$, where $\delta \ll 1$. When inside the USR, c_s drops quickly to its previous value of $c_{s,*}$. The same value of $c_s = \tilde{c}_s$ is achieved once again at the moment of another sharp transition at $\mathcal{N} = \mathcal{N}_e$ when we move into the SRII phase. Finally, throughout the SRII, we have $c_s = c_{s,*}$ till the phase comes to end at $\mathcal{N} = \mathcal{N}_{\text{end}}$. This parameterization is depicted using a schematic in fig.(2).

We can now analyze the distinct ranges and behaviour that the coefficients $c_i \forall i = 1, \dots, 5$, can achieve based on the causality and unitarity constraints we have on the values of the effective sound speed and the form of the functions of these coefficients as described in equations (7,15,16). Lastly, we also use the amplitude of the scalar power spectrum in the three phases to more accurately narrow the ranges of such coefficients. The analytical expressions can be found in the appendix VIA,VIB, but for our current purposes, we would require their amplitudes corresponding to the respective phase of interest, see [241] for a similar analysis on implementing the USR in CGT. We denote from hereon the tree-level power spectrum amplitude in SRI as $[\Delta_{\zeta, \text{Tree}}^2(k)]_{\text{SRI}} \sim \mathcal{O}(10^{-9})$, similarly in the USR we have, $[\Delta_{\zeta, \text{Tree}}^2(k)]_{\text{USR}} \sim \mathcal{O}(10^{-2})$, and in the SRII we have $[\Delta_{\zeta, \text{Tree}}^2(k)]_{\text{SRII}} \sim \mathcal{O}(10^{-5})$. We begin with the SRI phase and subsequently analyze the coefficients as we progress from one phase, through a sharp transition, and into the other phases. For a detailed construction of the SRI-USR-SRII phases in Galileon theory performed recently see [241].

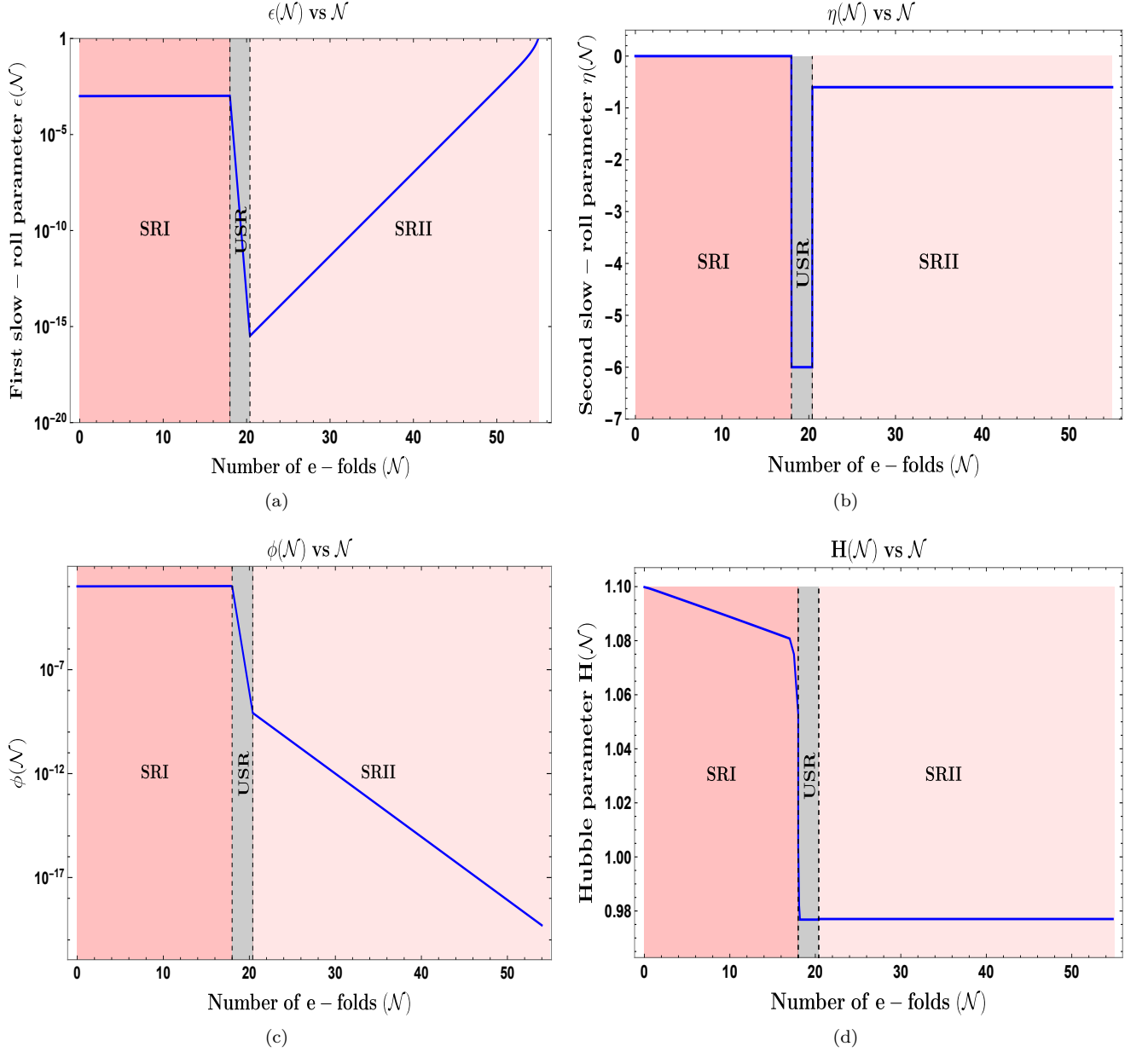


FIG. 1. Figure represents evolution of the various parameters, $\epsilon(\mathcal{N})$ in the top-left panel, $\eta(\mathcal{N})$ in the top-right panel, $\phi(\mathcal{N})$ in the bottom-left panel, $H(\mathcal{N})$ in the bottom-right panel, with respect to the e-folds \mathcal{N} and throughout the three phases of SRI-USR-SRII.

1. The first slow-roll (SRI) phase

We observe the behaviour of the coefficients $c_i \forall i : 1, \dots, 5$, during SRI using the eqn.(7) and constrain the remaining higher-derivative operators coefficients using existing constraint of $0.024 \leq c_s < 1$ on the effective sound speed. When using this sound speed parameter, we conduct the analysis for a set of values along the trend for the slow-roll parameters to understand the possible ranges of the involved coefficients.

The fig.(3) describes variation in the set of coefficients $c_i \forall i = 1, \dots, 5$ with respect to each other. In SRI, we choose for the initial conditions $\epsilon_i = \epsilon(\mathcal{N}_*) \sim \mathcal{O}(10^{-3})$, $\eta_i = \eta(\mathcal{N}_*) \sim -0.001$, and for the cut-off we choose $\Lambda \lesssim \mathcal{O}(10^{-1})M_p$. These slow-roll parameters remain almost constant in the SRI, as the fig.(1) confirms their behaviour. From the top-left panel, we observe that as the function f remains almost constant during SRI, large changes in c_3 for similar and fixed larger c_2 values change c_1 only within a tiny interval of $\mathcal{O}(1)$. We use the range for c_s to study the remaining

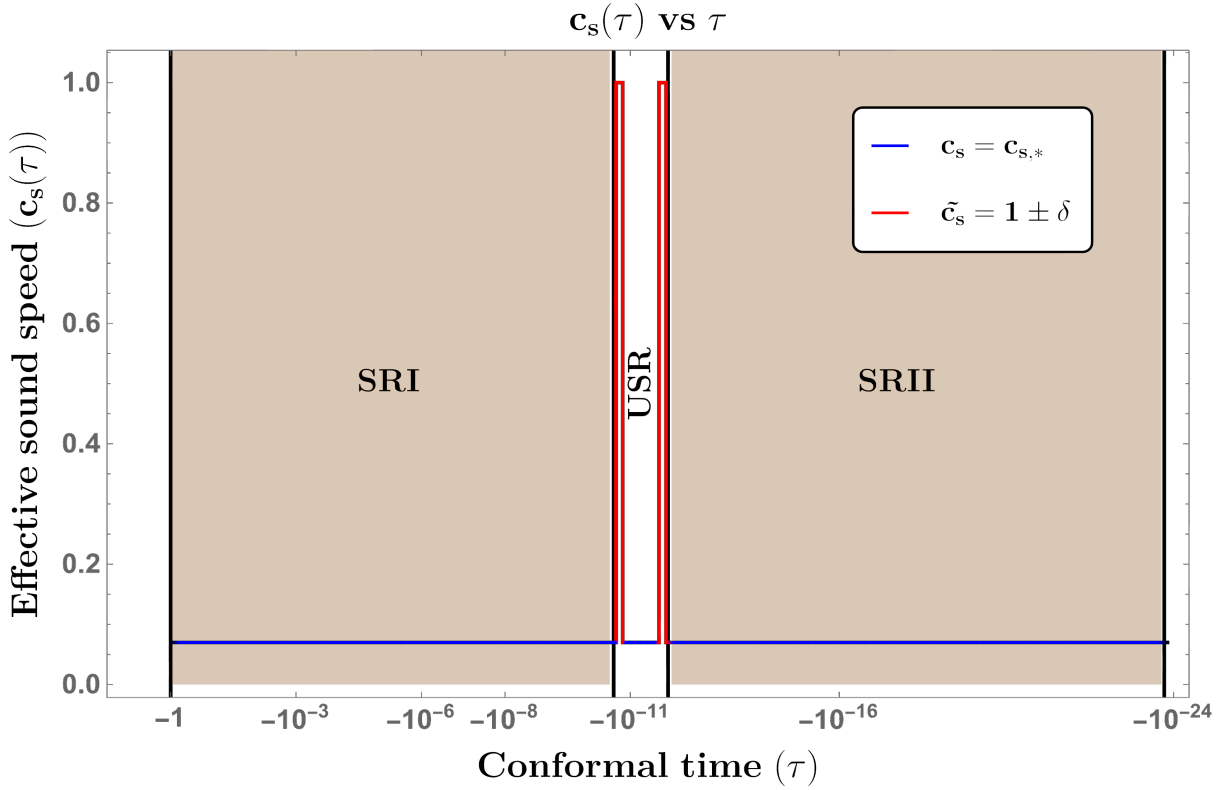


FIG. 2. Representative diagram of the parameterization used for the effective sound speed c_s as function of the conformal time τ . The red color highlights sudden change in c_s values corresponding to the moment of sharp transitions and the blue color represents c_s in the remaining duration of the phases.

coefficients for the next top-right and bottom panels. Here we observe that to achieve $0.024 \leq c_s < 0.2$, we can have $c_2 \sim \mathcal{O}(10^2)$ but then if $c_3 \sim \mathcal{O}(10^2)$ is also chosen, it further requires to have $(c_4, c_5) \sim \mathcal{O}(10^2)$ with $c_5 > c_4$. On the other hand, for $c_s \geq 0.2$, going higher in both $(c_3, c_4) \sim \mathcal{O}(10^2)$ with $c_4 > c_3$ and still having magnitude, which includes both signatures, of $c_5 \lesssim \mathcal{O}(10^2)$, also seen from the bottom panel, can help us achieve the desired values. Finally, the amplitude $[\Delta_{\zeta, \text{Tree}}^2(k)]_{\text{SRI}} \sim \mathcal{O}(10^{-9})$ also successfully constraints the coefficients (c_4, c_5) in the ranges as mentioned here before.

2. The ultra-slow roll (USR) phase

We examine the values for the coefficients $c_i \forall i : 1, \dots, 5$, during the USR using the eqn.(7) and constrain the remaining coefficients for the higher-derivative operators using existing bounds, $0.024 \leq c_s < 1$, on the effective sound speed parameter. The slow-roll parameters in this phase evolve as shown in the USR section of the fig.(1). The nature of the scalar field ϕ shows that it decreases at much faster rate in the USR and this implies the condition $\ddot{\phi} + 3H\dot{\phi} \rightarrow 0$. The first slow-roll parameter in the USR also goes as $\epsilon \propto a^{-6}$ while $\eta \sim \mathcal{O}(-6)$ holds throughout. For the rest of the analysis from the CGT Lagrangian perspective we proceed as follows.

We study the two scenarios, near the sharp transition and in the remainder of the USR. For the first scenario as stated above, we plot the behaviour in fig.(4). As before, when considering c_s , we fix an arbitrary set of slow-roll values along their respective trend in the USR to get the possible interval of values for the coefficients. When we are very close to the transition scale at $\mathcal{N} = \mathcal{N}_s$ (or $\tau = \tau_s$), the sound speed from fig.(2) is then seen to have values $c_s = 1 \pm \delta$ and we further use this to study the behaviour of the coefficients $c_i \forall i = 2, \dots, 5$ in fig.(4).

The top-left panel concerns with the function $f \equiv f(c_1, c_2, c_3, \Lambda)$. We notice now that a change with c_2 in between $\mathcal{O}(10 - 10^2)$ does not affect the allowed behaviour of (c_1, c_3) , and as we move inside after the sharp transition, the function f drops for which only lower values of $c_1 \lesssim \mathcal{O}(1)$ are allowed while c_3 can take values till $\mathcal{O}(10^3)$. With these estimates of the ranges for (c_2, c_3) we move towards the two top-right and bottom panels. There keeping $c_3 \sim \mathcal{O}(10^3)$ and for $c_5 \sim \mathcal{O}(10^4)$, $c_s \sim 1$ is possible to achieve and while changing c_2 does not make much difference, on the

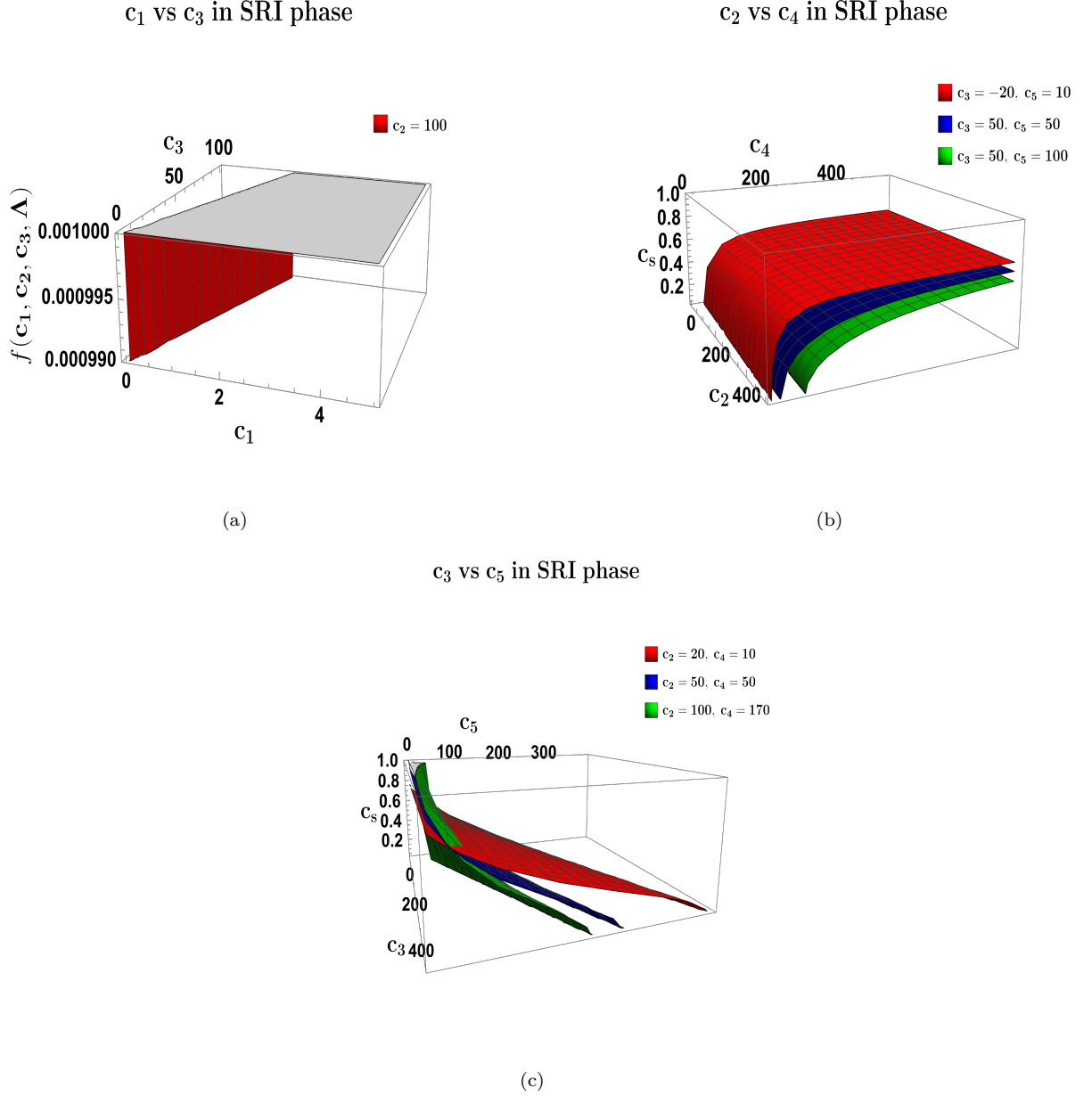


FIG. 3. Behaviour of the coefficients $c_i \forall i = 1, \dots, 5$, during the SRI phase. Top-left panel with red surface corresponds to allowed values (c_1, c_3) for fixed $c_2 = 100$. Top-right panel shows c_s values on the vertical for fixed set of (c_3, c_5) values and the allowed values of (c_2, c_4) from the red, blue, and green surfaces. Bottom panel shows c_s values on the vertical for fixed set of (c_2, c_4) values and the allowed values of (c_3, c_5) from the red, blue, and green surfaces.

contrary, slightly increasing c_5 can result into an increased interval of c_4 values. From the bottom panel, we see that increase in c_4 goes together with c_5 changing from $\mathcal{O}(10^3 - 10^4)$ if we are looking for large values of c_s , and c_3 can still stay within $c_3 \sim \mathcal{O}(10^2 - 10^4)$. However, going much large in c_5 does not help either as the surface drops also quickly for both $(c_4, c_5) \sim \mathcal{O}(10^4)$. Hence, these two coefficients must increase together and going beyond $\mathcal{O}(10^5)$ would result in $c_s > 1$. These ranges increase as the slow-roll and function f values follow their usual trend going more into the USR phase.

We now focus on the remainder of the USR interval, that is the moment after $\mathcal{N} = \mathcal{N}_s$ (or $\tau = \tau_s$). Here the values of c_s return back to its previous value in the SRI and we conduct the analysis accordingly. The same analysis is shown through the plots in fig.(5). The top-left panel focuses on the function f , which keeps decreasing during the length of the USR phase, and for that, we require large values of both $(c_2, c_3) \gtrsim \mathcal{O}(10^4)$. We can, however, do away with $(c_2, c_3) \sim \mathcal{O}(10^3)$ if we in turn keep $c_1 \ll \mathcal{O}(1)$. Hence, c_1 must decrease to even lower values than previous

cases. For the rest of the coefficients and effects of (c_2, c_3) on (c_4, c_5) we make use of the top-right and bottom panels. Observe that higher values of c_2 , that is $c_2 \gtrsim \mathcal{O}(10^4)$ are only necessary when $c_4 \sim \mathcal{O}(10^6)$, and this occurs when c_3 is of similar magnitude as c_2 while c_5 must now increase to at least $\mathcal{O}(10^{10})$ and this allows for achieving lower sound speed c_s values. For $(c_2, c_3) \sim \mathcal{O}(10^3 - 10^4)$, the higher one goes for $c_4 \gtrsim \mathcal{O}(10^7)$ while keeping $c_5 \sim \mathcal{O}(10^{10})$, one can achieve higher c_s values, and on the contrary, keeping $c_4 \sim \mathcal{O}(10^6)$ and increasing $c_5 \gtrsim \mathcal{O}(10^{10})$ one can get the values at the lower end of $0.024 \leq c_s < 0.2$. For the whole USR phase, the condition $[\Delta_{\zeta, \text{Tree}}^2(k)]_{\text{USR}} \sim \mathcal{O}(10^{-2})$ is also able to get satisfied for some set of values within the mentioned ranges of the coefficients.

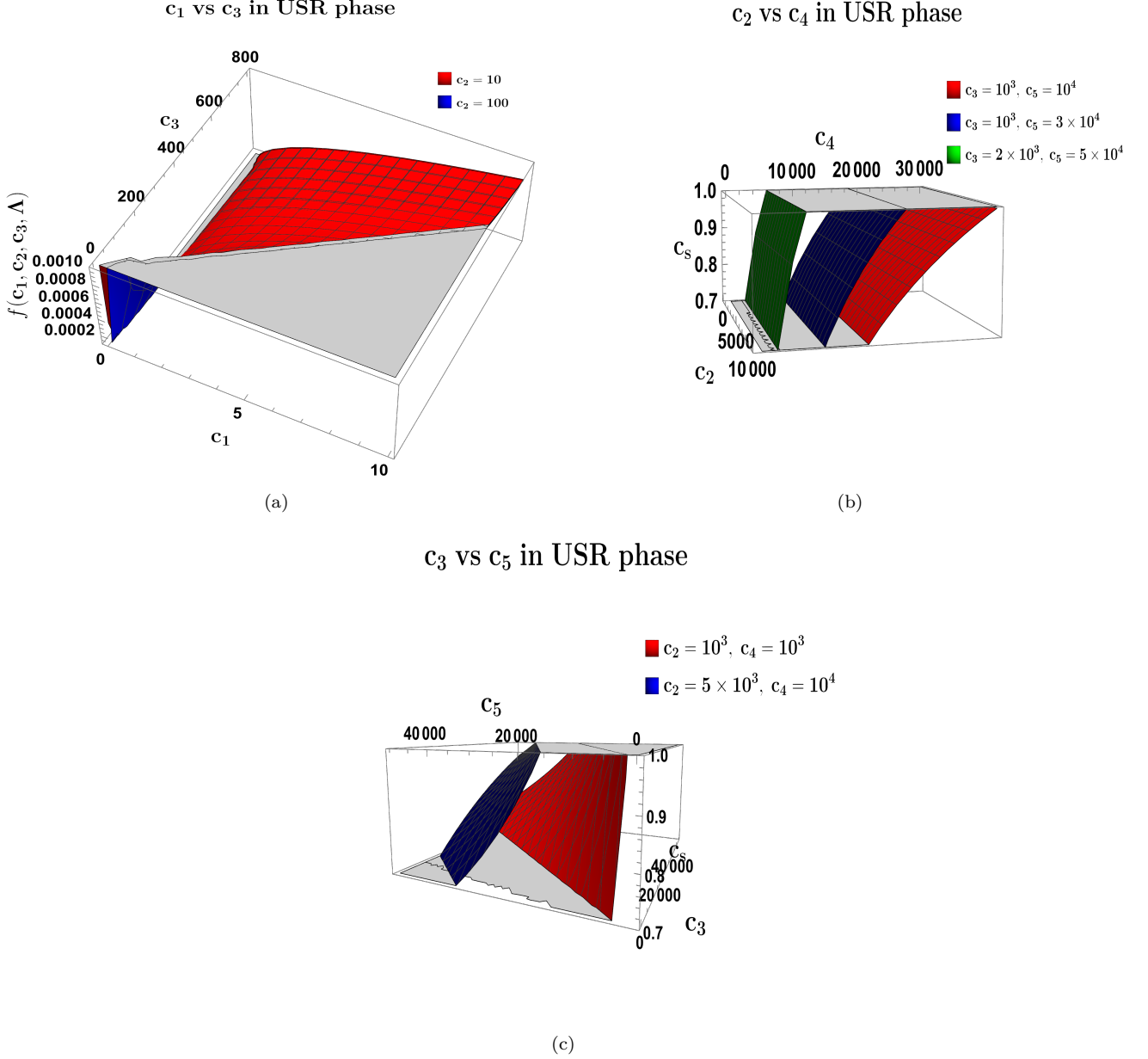


FIG. 4. Behaviour of the coefficients $c_i \forall i = 1, \dots, 5$, near the sharp transition of USR phase. Top-left panel with red surface corresponds to allowed values (c_1, c_3) for a fixed set of $c_2 = (10, 100)$ in red and blue surfaces. Top-right panel shows c_s values on the vertical for fixed set of (c_3, c_5) values and the allowed values of (c_2, c_4) from the red, blue, and green surfaces. Bottom panel shows c_s values on the vertical for fixed set of (c_2, c_4) values and the allowed values of (c_3, c_5) from the red, blue, and green surfaces.

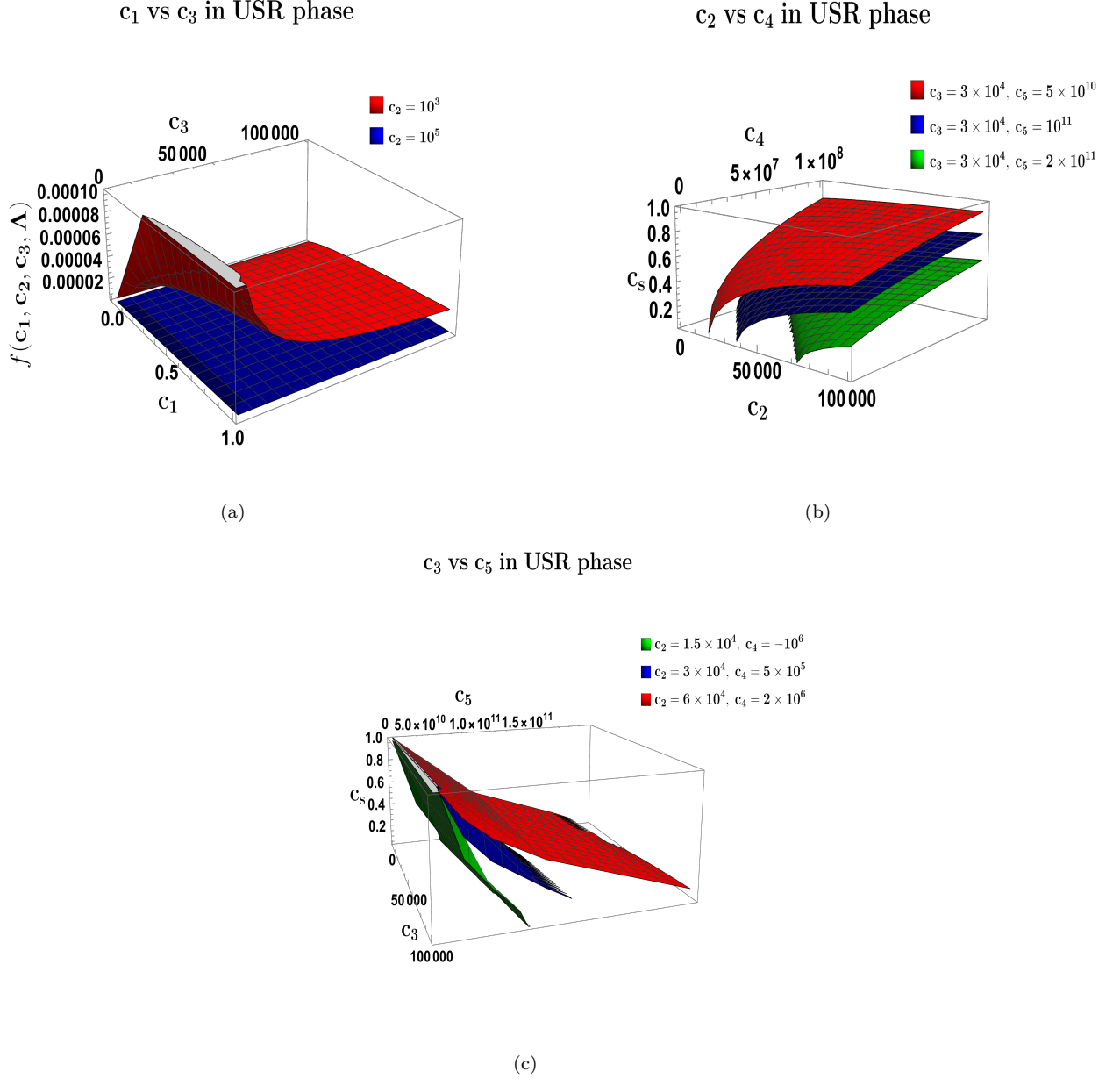


FIG. 5. Behaviour of the coefficients $c_i \forall i = 1, \dots, 5$, during the USR phase. Top-left panel with red surface corresponds to allowed values (c_1, c_3) for a fixed set of $c_2 = (10^3, 10^5)$ in red and blue surfaces. Top-right panel shows c_s values on the vertical for fixed set of (c_3, c_5) values and the allowed values of (c_2, c_4) from the red, blue, and green surfaces. Bottom panel shows c_s values on the vertical for fixed set of (c_2, c_4) values and the allowed values of (c_3, c_5) from the red, blue, and green surfaces.

3. The second slow-roll (SRII) phase

In this section, we examine the values of the coefficients $c_i \forall i : 1, \dots, 5$, during the SRII phase using the eqn.(7) and use the previously mentioned constraints on the effective sound speed. For the SRII also, we work in a similar fashion as in the USR, where we examine the coefficients near the sharp transition and then away from it for the remainder of the SRII phase. From the fig.(1), the scalar field decreases at a slower rate compared to the USR and ϵ climbs back until it becomes $\mathcal{O}(1)$ while $\eta \sim \mathcal{O}(-1)$ remains satisfied till end of inflation.

The fig.(6) shows the behaviour of the coefficients for the first scenario. The top-right panel shows the behaviour of (c_1, c_3) for fixed $c_2 \sim \mathcal{O}(10^4)$. Here we again notice for c_1 the same trend as for the previous cases as a consequence of which it keeps decreasing to $c_1 \sim \mathcal{O}(10^{-6})$ as the function f again decreases near the transition. The values for

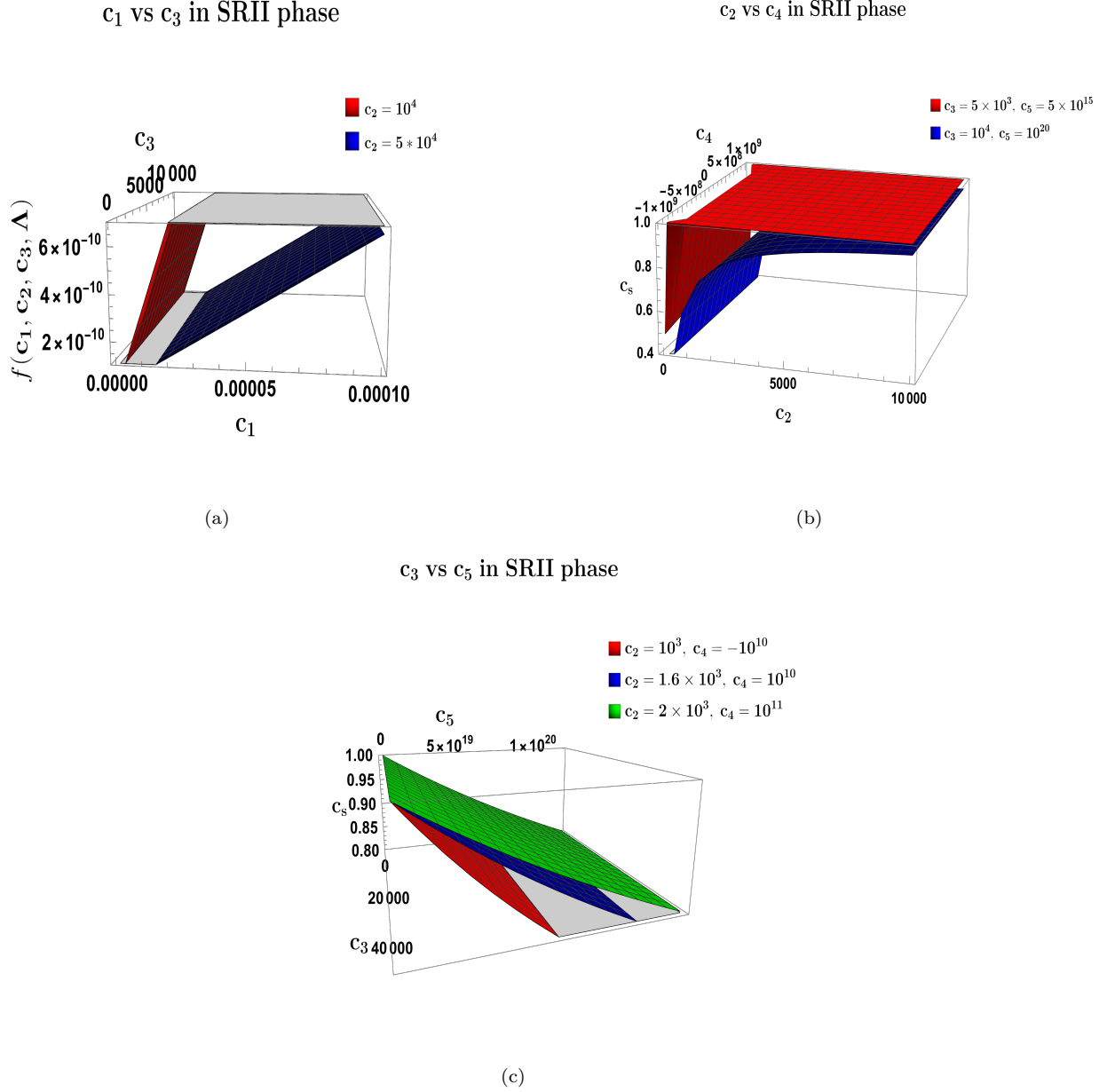


FIG. 6. Behaviour of the coefficients $c_i \forall i = 1, \dots, 5$, near the sharp transition into the SRII phase. Top-left panel with red surface corresponds to allowed values (c_1, c_3) for a fixed set of $c_2 \sim \mathcal{O}(10^4)$ in red and blue surfaces. Top-right panel shows c_s values on the vertical for fixed set of (c_3, c_5) values and the allowed values of (c_2, c_4) from the red, blue, and green surfaces. Bottom panel shows c_s values on the vertical for fixed set of (c_2, c_4) values and the allowed values of (c_3, c_5) from the red, blue, and green surfaces.

$c_2 \sim \mathcal{O}(10^4)$ is still sufficient to let us observe the desired f and changes in c_3 does not make much difference in the shape of the surfaces of allowed values. With this in mind, we move to the impact of (c_2, c_3) on the next set of coefficients (c_4, c_5) . From the top-right panel we can observe the fact that keeping $c_2 < \mathcal{O}(10^3)$ can push the magnitude of c_4 values to almost $\mathcal{O}(10^9)$ or higher while $c_5 \gtrsim \mathcal{O}(10^{15})$ is maintained, thus no significant on c_4 is observed long as c_5 is large. This nature is also clear from the plot in the bottom panel where c_3 does not affect much the allowed values of c_5 . Since this is near the transition, we must satisfy the values $c_s = 1 \pm \delta$. As we increase $c_3 \gtrsim \mathcal{O}(10^4)$ we must also have similar nature for c_2 and there the sensitivity to c_2 of c_s is seen to increase for such larger values, both from the top-right and the bottom panels. Upon further going for the larger magnitudes of $c_5 > \mathcal{O}(10^{16})$, while $c_2 < \mathcal{O}(10^3)$ and $c_3 > c_2$, can decrease c_s away from the desired condition.

Next we examine the remainder of the SRII phase in fig.(7). Further into the SRII the value of c_1 again decreases

to have $c_1 \sim \mathcal{O}(10^{-7})$ for both $(c_2, c_3) \sim \mathcal{O}(10^3)$. Thus, c_1 keeps on taking lower values as we cross different phases. From the constraint on the c_s values we have the analysis for the top-right and bottom panels. With $c_2 \sim \mathcal{O}(10^3)$, we notice that values in the range of $(c_2, c_3) \sim \mathcal{O}(10^2 - 10^3)$ are more preferred to achieve values with $c_s \leq 0.2$ and magnitude of $c_4 \sim \mathcal{O}(10^{23} - 10^{26})$. The range for c_5 is also seen to increase the more we get inside the SRII. From the bottom panel we notice that while c_3 does not much impact on the shape of the allowed surface, the values for c_5 do change with varying c_2 . As c_5 increases in the interval $c_5 \sim \mathcal{O}(10^{36} - 10^{40})$ we can cover the values within $1 \geq c_s \geq 0.024$ with having $c_4 \sim \mathcal{O}(10^{23} - 10^{27})$. The amplitude in this scenario, $[\Delta_{\zeta, \text{Tree}}^2(k)]_{\text{SRII}} \sim \mathcal{O}(10^{-5})$, allows for possible combination of values in the mentioned ranges for the coefficients.

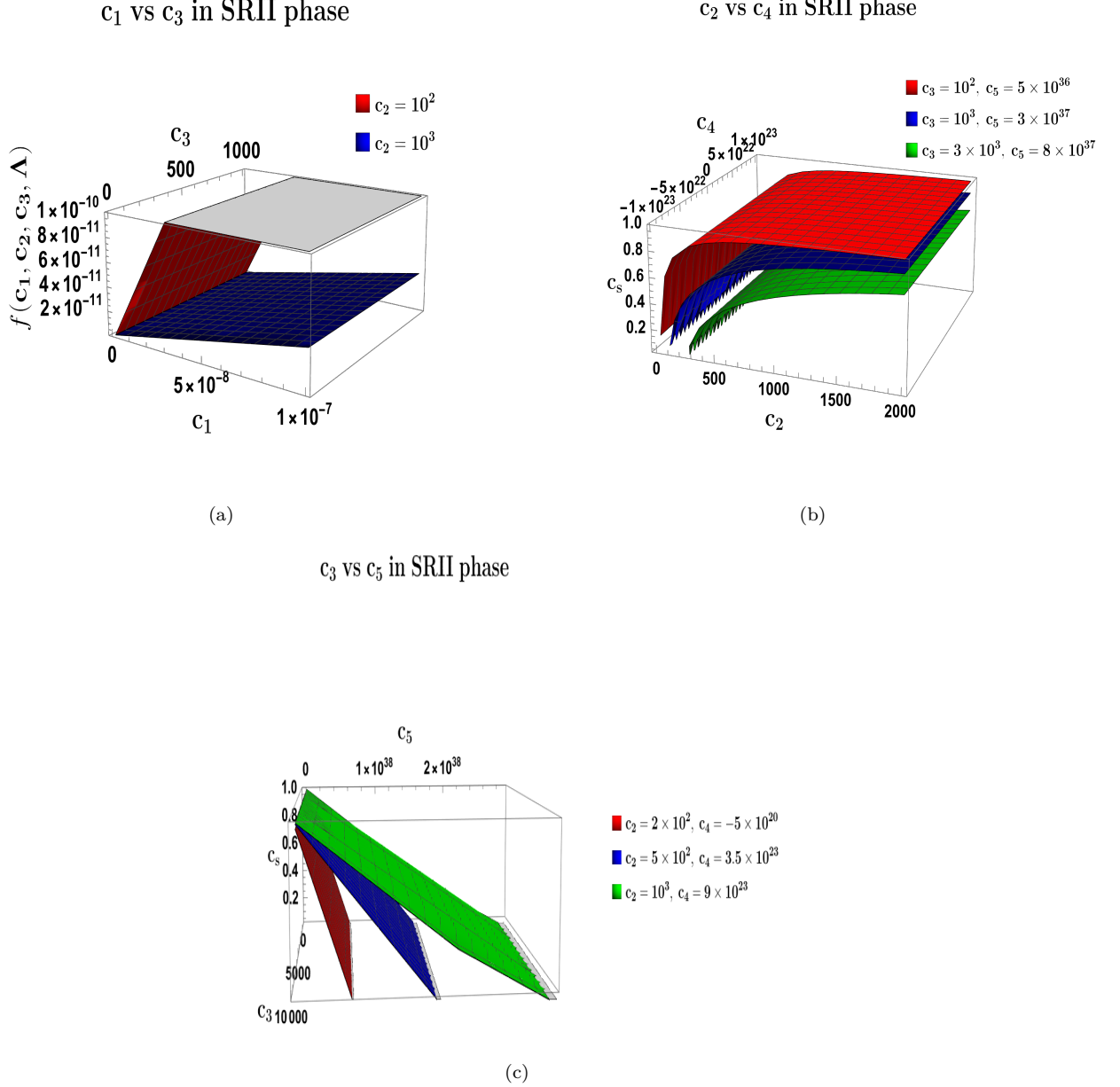


FIG. 7. Behaviour of the coefficients $c_i \forall i = 1, \dots, 5$, during the SRII phase. Top-left panel with red surface corresponds to allowed values (c_1, c_3) for a fixed set of $c_2 \sim \mathcal{O}(10^2 - 10^3)$ in red and blue surfaces. Top-right panel shows c_s values on the vertical for fixed set of (c_3, c_5) values and the allowed values of (c_2, c_4) from the red, blue, and green surfaces. Bottom panel shows c_s values on the vertical for fixed set of (c_2, c_4) values and the allowed values of (c_3, c_5) from the red, blue, and green surfaces.

B. Solutions from the perturbed second order action

Following the general discussion about the CGT action and for the background time-dependent Galileon field, we now present the mode solutions which comes from analysing the second-order action for the comoving curvature perturbations. To this effect, we quote the expression of the second-order action for the curvature perturbation:

$$S_\zeta^{(2)} = \int d\tau d^3x a(\tau)^2 \frac{\mathcal{A}}{H^2} \left(\zeta'^2 - c_s^2 (\partial_i \zeta)^2 \right) = \int d\tau \frac{d^3\mathbf{k}}{(2\pi)^3} a(\tau)^2 \frac{\mathcal{A}}{H^2} \left(|\zeta'_{\mathbf{k}}(\tau)|^2 - c_s^2 k^2 |\zeta_{\mathbf{k}}(\tau)|^2 \right) \quad (17)$$

where the second equation is written after performing the Fourier transform.

Variation of this action gives us the following second-order differential equation, commonly known as the Mukhanov-Sasaki equation for the scalar modes in Fourier space which is written as:

$$\zeta_{\mathbf{k}}''(\tau) + 2 \frac{z'(\tau)}{z(\tau)} \zeta_{\mathbf{k}}'(\tau) + c_s^2 k^2 \zeta_{\mathbf{k}}(\tau) = 0. \quad (18)$$

where we introduce a new variable $z(\tau) = a\sqrt{2\mathcal{A}}/H^2$ for the simplification purpose. We then solve the above differential equation in the three regions of interest during inflation, which includes the first slow-roll (SRI), the ultra-slow roll (USR), and the second slow-roll (SR II) phases. This method gives us the respective mode solutions in the three phases of interest written as follows:

$$\zeta_{\mathbf{k}}(\tau) = \left(\frac{iH^2}{2\mathcal{A}} \right) \frac{1}{(c_s k)^{3/2}} \times \begin{cases} \left[\alpha_{\mathbf{k}}^{(1)} (1 + ikc_s \tau) \exp(-ikc_s \tau) - \beta_{\mathbf{k}}^{(1)} (1 - ikc_s \tau) \exp(ikc_s \tau) \right] & \text{when } k < k_s \\ \left[\alpha_{\mathbf{k}}^{(2)} (1 + ikc_s \tau) \exp(-ikc_s \tau) - \beta_{\mathbf{k}}^{(2)} (1 - ikc_s \tau) \exp(ikc_s \tau) \right] & \text{when } k_s \leq k < k_e \\ \left[\alpha_{\mathbf{k}}^{(3)} (1 + ikc_s \tau) \exp(-ikc_s \tau) - \beta_{\mathbf{k}}^{(3)} (1 - ikc_s \tau) \exp(ikc_s \tau) \right] & \text{when } k_e \leq k \leq k_{\text{end}} \end{cases} \quad (19)$$

The general approach is to start with a quantum initial boundary condition which is taken to be the standard Bunch-Davies initial condition, which is actually a Euclidean vacuum state in this context. This gives us $\alpha_{\mathbf{k}}^{(1)} = 1$ and $\beta_{\mathbf{k}}^{(1)} = 0$. Then, due to having a sharp transition from one phase to another, new sets of Bogoliubov coefficients for the mode functions in the new phase can be obtained by making use of the Israel matching conditions at the sharp transition scales k_s (SRI to USR) and k_e (USR to SR II). This change in the behaviour of the Bogoliubov coefficients towards a Non-bunch Davies type vacuum is an important reason for the significant enhancement observed in the scalar power spectrum amplitude. Explicit expressions for the Bogoliubov coefficients are given in Appendix VI A.

C. Impact of the non-renormalization theorem

In this subsection, we briefly describe the implication of the non-renormalization theorem for Galileon inflation. The theorem states that the couplings of the theory remain protected against any radiative corrections even when the Galilean symmetry gets mildly broken. As a result, we can bypass the need to perform the renormalization and resummation procedures to obtain the one-loop corrected scalar power spectrum in Galileon theory. Other significant consequences of this theorem include the validity of successful inflation with having a prolonged SR II phase and the ability to control large fluctuations and their associated non-Gaussianities produced during the sharp transitions in the USR region.

For a successful inflation in this case, we require a mild breaking of the Galilean shift symmetry, which happens by going from a de-Sitter background to a quasi-de-Sitter one. The symmetry transformation of the terms built from curvature perturbation ζ is written by following the definition in eqn.(3):

$$\zeta \rightarrow \zeta - \frac{H}{\dot{\phi}} a \delta x, \quad \partial_i \zeta \rightarrow \partial_i \zeta - \frac{H}{\dot{\phi}} a_i, \quad \zeta' \rightarrow \zeta' - \frac{H}{\dot{\phi}} a_0, \quad \partial^2 \zeta \rightarrow \partial^2 \zeta. \quad (20)$$

where $\bar{\phi} \equiv \bar{\phi}(t)$ is the time-dependent background Galileon field. From the above equation, we see that only the term $\partial^2 \zeta$ remains invariant under Galilean symmetry, and the terms ζ , ζ' , and $\partial_i \zeta$ show mild breaking of the said symmetry. Based on this, let us briefly look into how radiative corrections become unimportant in the scalar power spectrum in Galileon theory. In single-field inflation, the dominant one-loop corrections to the scalar power spectrum come from the operator $\zeta' \zeta^2$, due to its coefficient containing the factor $\partial_\tau(\eta/c_s^2)$ which is large during a sharp transition.

However, this term is absent from the third-order action of Galileon theory even when it breaks the Galilean shift symmetry. This absence becomes evident by the use of eqn.(20), which converts the operator into a quantity evaluated at the boundary. There exist other terms in the Galileon theory which show mild symmetry breaking but are absent from the final third-order action because of the possibility of performing field redefinition or formation of boundary terms, reducing the allowed number of terms. Detailed discussion on this topic can be found by the authors in [127].

Keeping the above discussion in mind, only a few terms are allowed in the third-order action, which are called the bulk self-interaction terms and includes: $\zeta'^3, \zeta'^2 \partial^2 \zeta, \zeta' (\partial_i \zeta)^2, \partial^2 \zeta (\partial_i \zeta)^2$. These will be used in the next section to describe the third-order action necessary for calculating the one-loop effects.

D. One-loop corrected power spectrum from third order action

In this section, we consider the third-order action in the curvature perturbations which is constructed using the analysis done in the previous section. This action is formed using the Galilean symmetry-breaking terms introduced previously which collectively form the bulk self-interaction terms. The resulting action has the form [127, 128, 175]:

$$S_\zeta^3 = \int d\tau d^3x \frac{a(\tau)^2}{H^3} \left[\frac{\mathcal{G}_1}{a} \zeta'^3 + \frac{\mathcal{G}_2}{a^2} \zeta'^2 (\partial^2 \zeta) + \frac{\mathcal{G}_3}{a} \zeta' (\partial_i \zeta)^2 + \frac{\mathcal{G}_4}{a^2} (\partial_i \zeta)^2 (\partial^2 \zeta) \right] \quad (21)$$

where the couplings for each operator in the action have the following expressions:

$$\mathcal{G}_1 : \equiv \frac{2H\dot{\phi}^3}{\Lambda^3} \left(c_3 + 9c_4 Z + 30c_5 Z^2 \right), \quad (22)$$

$$\mathcal{G}_2 : \equiv -\frac{2\dot{\phi}^3}{\Lambda^3} \left(c_3 + 6c_4 Z + 18c_5 Z^2 \right), \quad (23)$$

$$\mathcal{G}_3 : \equiv -\frac{2H\dot{\phi}^3}{\Lambda^3} \left(c_3 + 7c_4 Z + 18c_5 Z^2 \right) - \frac{2\dot{\phi}^3 H \eta}{\Lambda^3} \left(c_3 + 6c_4 Z + 18c_5 Z^2 \right), \quad (24)$$

$$\mathcal{G}_4 : \equiv \frac{\dot{\phi}^3}{\Lambda^3} \left\{ c_3 + 3c_4 Z + 6c_5 \left[Z^2 + \frac{\dot{H}\dot{\phi}^2}{\Lambda^6} \right] \right\} - \frac{3\dot{\phi}^4 H \eta}{\Lambda^6} \left\{ c_4 + 4c_5 Z \right\}, \quad (25)$$

and the parameter Z is defined as $Z = H\dot{\phi}/\Lambda^2$.

The one-loop effects are calculated using the aforementioned third-order action by working with the Schwinger-Keldysh (in-in) formalism. After taking care of all the possible Wick contractions when calculating the one-loop contributions from each interaction operator, we perform the necessary temporal and momentum integrals to arrive at the result for the three phases. We now quote the total scalar power spectrum, which includes the one-loop corrections by combining the individual contributions in the following manner [127]:

$$\begin{aligned} \left[\Delta_\zeta^2(k) \right]_{\text{Total}} &= \left[\Delta_{\zeta, \text{Tree}}^2(k) \right]_{\text{SRI}} + \left[\Delta_{\zeta, \text{One-Loop}}^2(k) \right]_{\text{SRI}} + \left[\Delta_{\zeta, \text{Tree}}^2(k) \right]_{\text{USR}} \Theta(k - k_s) \\ &+ \left[\Delta_{\zeta, \text{One-Loop}}^2(k) \right]_{\text{USR}} \Theta(k - k_s) + \left[\Delta_{\zeta, \text{Tree}}^2(k) \right]_{\text{SRII}} \Theta(k - k_e) + \left[\Delta_{\zeta, \text{One-Loop}}^2(k) \right]_{\text{SRII}} \Theta(k - k_e), \\ &\approx \left[\Delta_{\zeta, \text{Tree}}^2(k) \right]_{\text{SRI}} \left\{ 1 + \left(\frac{k_e}{k_s} \right)^6 \left[|\alpha_{\mathbf{k}}^{(2)} - \beta_{\mathbf{k}}^{(2)}|^2 \Theta(k - k_e) + |\alpha_{\mathbf{k}}^{(3)} - \beta_{\mathbf{k}}^{(3)}|^2 \Theta(k - k_s) \right] \right\} \\ &+ \left[\Delta_{\zeta, \text{Tree}}^2(k) \right]_{\text{SRI}} \times \frac{1}{8\mathcal{A}_*^2 \pi^4} \left\{ - \sum_{i=1}^4 \mathcal{G}_{i, \text{SRI}} \mathbf{F}_{i, \text{SRI}}(k_s, k_*) + \sum_{i=1}^4 \mathcal{G}_{i, \text{USR}} \mathbf{F}_{i, \text{USR}}(k_e, k_s) \Theta(k - k_s) \right. \\ &\left. + \sum_{i=1}^4 \mathcal{G}_{i, \text{SRII}} \mathbf{F}_{i, \text{SRII}}(k_{\text{end}}, k_e) \Theta(k - k_e) \right\}. \end{aligned} \quad (26)$$

which involves the tree-level SRI power spectrum:

$$\left[\Delta_{\zeta, \text{Tree}}^2(k) \right]_{\text{SRI}} = \left(\frac{H^4}{8\pi^2 \mathcal{A} c_s^3} \right)_* \times \left(1 + \left(\frac{k}{k_s} \right)^2 \right). \quad (27)$$

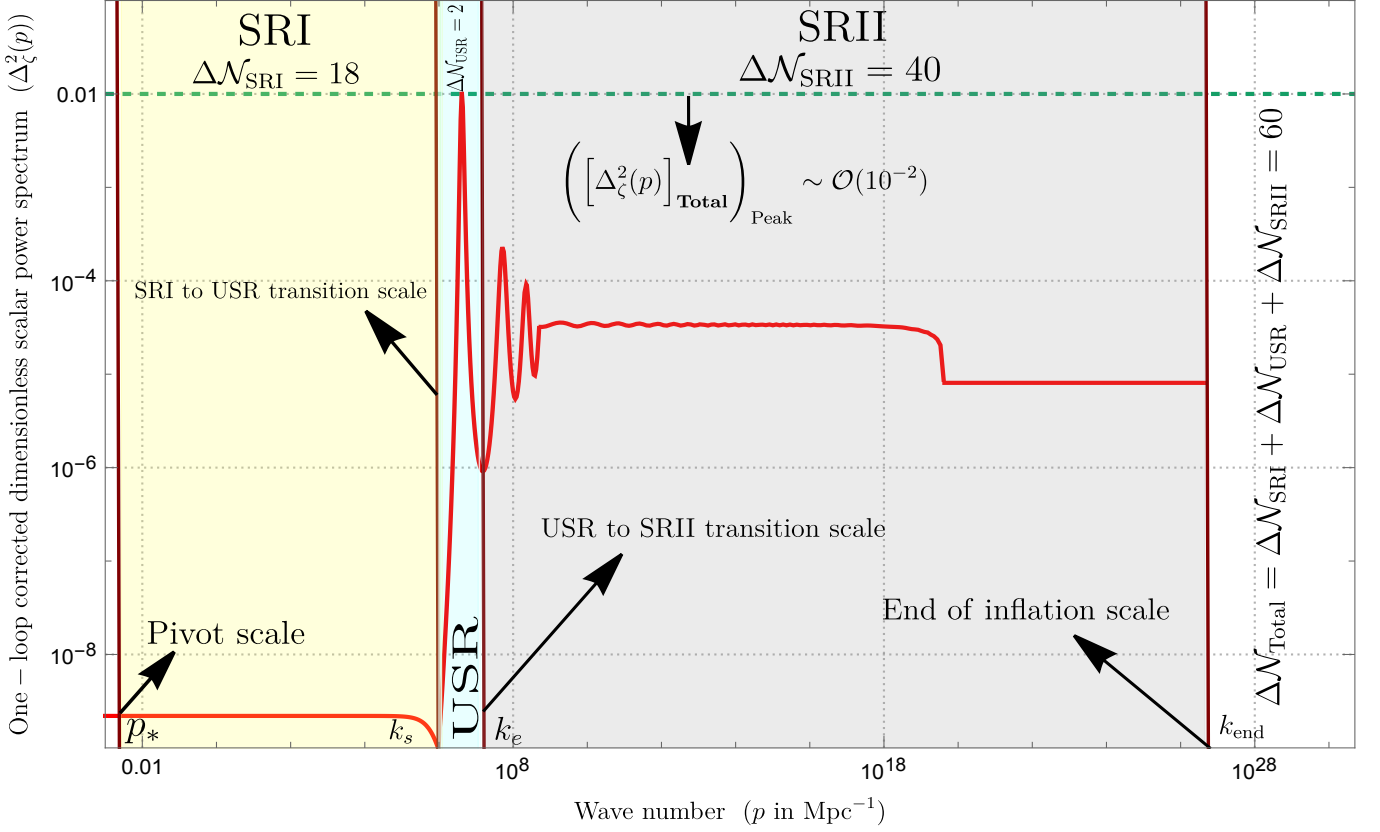
One – loop corrected dimensionless power spectrum from CGEFT vs wave number ($c_s = 0.05$)

FIG. 8. Figure represents behaviour of the total scalar power spectrum, which includes the one-loop corrections, plotted against the wavenumber. This is obtained for the value of the sound speed parameter $c_s = 0.05$. Other important parameters are taken to be as follows: pivot scale at $p_* = 0.02 \text{ Mpc}^{-1}$, the transition scale k_s (SRI to USR) at $= 10^6 \text{ Mpc}^{-1}$ and the transition scale k_e (USR to SRII) at $= 10^7 \text{ Mpc}^{-1}$ such that the condition $k_e/k_s \sim \mathcal{O}(10)$ is followed, and the end of SRII at $k_{\text{end}} = 10^{27} \text{ Mpc}^{-1}$ such that $\Delta\mathcal{N} = 60$ is achieved.

The explicit equations for the terms describing the one-loop effects above, which include $\mathcal{G}_{i,\text{SRI}}, \mathcal{G}_{i,\text{USR}}, \mathcal{G}_{i,\text{SRII}}$ and the leading order terms in $\mathbf{F}_{i,\text{SRI}}, \mathbf{F}_{i,\text{USR}}, \mathbf{F}_{i,\text{SRII}}$, are mentioned in the appendix [VIB](#). Detailed discussion on such terms can be found in a previous work by the authors in [\[127\]](#). The total scalar power spectrum hence formed after combining the tree and one-loop contributions, which are also mentioned in eqs.([71](#), [90](#)) along with discussions, will be used in a later section to evaluate the scalar-induced gravitational wave spectrum, which is the main focus of the next section.

E. PBH production and its comparison with recent studies

Here we address the question of allowed PBH masses, another crucial component of our analysis resting on the properties of Galileon theory before we study the theory behind the scalar-induced GWs.

The mass of PBH is calculated using the formula given as follows:

$$\begin{aligned}
\frac{M_{\text{PBH}}}{M_\odot} &= 1.13 \times 10^{15} \times \left(\frac{\gamma}{0.2}\right) \times \left(\frac{g_*}{106.75}\right)^{-1/6} \left(\frac{\tilde{c}_s k_s}{c_s k_*}\right)^{-2} \\
&= 1.13 \times 10^{15} \times \left(\frac{\gamma}{0.2}\right) \times \left(\frac{g_*}{106.75}\right)^{-1/6} \left(\frac{k_s}{k_*}\right)^{-2} \times c_s^2 (1 \mp 2\delta) \\
&= 1.13 \times 10^{15} \times \left(\frac{\gamma}{0.2}\right) \times \left(\frac{g_*}{106.75}\right)^{-1/6} \left(\frac{k_s}{k_*}\right)^{-2} \times c_s^2,
\end{aligned} \tag{28}$$

where the leading order term is considered in the last line. To get an estimate of the mass of PBHs produced, we use the fact that $\gamma \sim 0.2$ which is the critical collapse factor, $g_* \sim 106.75$ is the number of relativistic d.o.f, the pivot scale is at $k_* \sim 0.02 \text{Mpc}^{-1}$, the transition scale is set at $k_s \sim 10^6 \text{Mpc}^{-1}$, and using the effective sound speed values within the window of $0.024 < c_s < 1$ and the of solar mass value $M_\odot \sim 2 \times 10^{30} \text{Kg}$, we get the resulting range of $M_{\text{PBH}} \approx (10^{29} - 10^{30}) \text{Kg}$. Based on the above formula, one can further compute the evaporation time for the PBHs from galileon inflation as:

$$t_{\text{PBH}}^{\text{evap.}} = 10^{64} \left(\frac{M_{\text{PBH}}}{M_\odot}\right)^3 \text{ years} = 1.4429 \times 10^{109} \times \left(\frac{\gamma}{0.2}\right)^3 \times \left(\frac{g_*}{106.75}\right)^{-1/2} \left(\frac{k_s}{k_*}\right)^{-6} \times c_s^6 \text{ years}. \tag{29}$$

This equation can compute the evaporation time for PBHs within the mass range of solar mass and sub-solar mass. This particular time scale depends on the transition wavenumber and the effective sound speed values. For the case of PBH with $M_{\text{PBH}} \sim \mathcal{O}(M_\odot)$ and $M_{\text{PBH}} \sim \mathcal{O}(10^{-31} M_\odot)$, the time scale of evaporation is computed as:

$$t_{M_\odot}^{\text{evap.}} \approx 10^{64} \text{ years} \sim 10^{71} \text{ seconds} \tag{30}$$

$$t_{10^{-31} M_\odot}^{\text{evap.}} \approx 10^{-29} \text{ years} \sim 10^{-22} \text{ seconds} \tag{31}$$

The above calculated time scales represent the extremes of the interval where we can obtain the evaporation time for all PBHs ranging from large mass $M_{\text{PBH}} \sim \mathcal{O}(M_\odot)$ to the extremely small mass $M_{\text{PBH}} \sim \mathcal{O}(10^{-31} M_\odot \sim 10^2 \text{gm})$. This fact tells us that solar mass PBH can outlive the universe's current age, making them more helpful to study in cosmology. While, for the sub-solar mass PBH, the shortest time scale is negligibly small; as a result, it evaporated not long after it got produced in the early time. The above analysis is carried out by keeping the effective sound speed constraint $0.024 < c_s < 1$ satisfied, mainly we have taken $c_s = 0.05$. Hence, in Galileon theory, the causality and unitarity constraints are always respected to give meaningful results for a spectrum of PBHs in the above-mentioned mass range. This is in contrast when working with the EFT framework for single-field slow-roll inflation, where a violation of the said constraints is required to achieve better and more meaningful results relative to those from the causal case scenario [125]. Now we analyze the PBH mass formula in general to get more insights into the factors controlling their production. In eqn. (28), we used the fact that the speed of sound parameter is a time-dependent quantity such that its value at the pivot scale is fixed to be c_s . It moves abruptly to the value $\tilde{c}_s \approx 1 \pm \delta$, where $\delta \ll 1$, at the transition scale k_s , again reaches the value c_s during USR phase and then rapidly falls to the same value of \tilde{c}_s at the transition scale k_e , and finally comes to the value c_s when in the SRII phase till the end of inflation. See ref.[125] for a detailed study.

The important highlights concerning the mass of PBHs are listed as follows:

- Since the mass of PBH depends on the transition scale value $k_s \equiv k_{\text{PBH}}$, we notice that upon shifting the transition values to higher wavenumbers it is possible to generate PBHs with masses ranging from the almost solar to sub-solar masses $M_{\text{PBH}} \approx (1M_\odot - 10^{-18} M_\odot)$.
- The amplitude of the perturbations are controllable during the sharp transitions in the USR due to the non-renormalization theorem benefits. Until the perturbativity approximation of $k_e/k_s \sim \mathcal{O}(10)$ is satisfied, shifting of the transition scale k_s does not affect the existing features which include the amplitudes of the one-loop corrected scalar power spectrum in the SRI ($\mathcal{O}(10^{-9})$), USR ($\mathcal{O}(10^{-2})$), and SRII ($\mathcal{O}(10^{-5})$) phases.
- Due to the fact that the shifting of transition scale preserves the total scalar power spectrum features, we are able to cover a wide range of wavenumbers from $k \sim (10^{-2} - 10^{27} \text{Mpc}^{-1})$ which is reflected in the allowed mass of PBH and will be used in later sections to draw important conclusions for the GW spectrum induced by the one-loop corrected scalar power spectrum.

Finally, we would like to briefly compare our results on the allowed range of PBH masses with the recent findings in the literature. The authors in refs.[122, 130, 131] have discussed the properties of having a smooth transition such

that it can control the enhanced behavior of the perturbations when going from SRI to USR and USR to SRII phases and also allow for the generation of large mass PBHs when $k_{\text{PBH}} \sim 10^5 \text{Mpc}^{-1}$. Further studies have explored the same issue in [127, 128, 132–134]. In other studies [122, 130, 131], the authors have also shown explicitly that smooth transition can able to suppress the one-loop corrections in the final, loop-corrected, scalar power spectrum. Notably, the nature of the transition, smooth or sharp, is crucial to determine the status of the formed PBHs. In the case of a sharp transition, large mass PBHs are not allowed when renormalization and resummation procedures are included for the one-loop effects [124, 126], while in the studies [122, 127, 128, 130–134].

It may be noted that, while dealing with a smooth transition [122, 130, 131] and a sharp transition [118, 119, 121, 132, 134] have not mentioned the need for a renormalization and resummation procedure to arrive at the conclusion of controlled one-loop effects and the production of large mass PBHs. In the case of Galileon inflation, we have demonstrated that taking into account the one-loop corrections in the scalar power spectrum along with the non-renormalization theorem, it is possible to both control the large perturbations during sharp transitions and allow for solar mass as well as sub-solar mass PBH production from the underlying theory.

1. Calculation of the PBH mass fraction

Here we briefly outline the necessary computations required to evaluate the PBH mass fraction at formation time and the corresponding fraction of the current dark matter density present in the form of PBH, also known as its abundance.

Our computations are based on the Press-Schechter formalism to understand the estimates of PBH mass fraction. We begin by assuming that the perturbations in the primordial overdensity, as soon as it re-enters into the Horizon, collapse into forming the PBHs once it meets a critical condition criterion on its value, and this formation occurs primarily in a radiation-dominated Universe. The mass of the resulting PBH, depending on the volume of the Hubble horizon at the time of formation, is already given by the expression in eqn.(28). Based on this, one can compute the present day PBH abundance f_{PBH} as follows:

$$f_{\text{PBH}} = 1.68 \times 10^8 \left[\frac{\gamma}{0.2} \right]^{\frac{1}{2}} \left[\frac{g_*}{106.75} \right]^{-\frac{1}{4}} \left[\frac{M_{\text{PBH}}}{M_{\odot}} \right]^{-\frac{1}{2}} \times \beta(M_{\text{PBH}}), \quad (32)$$

which incorporates the PBH mass fraction β . This quantity gets evaluated within the Press-Schechter formalism after integrating over a Gaussian distribution for the overdensities $\delta(t, \mathbf{x})$ which informs about the likelihood that a certain value of overdensity is possible:

$$\beta(M_{\text{PBH}}) \simeq \gamma \left[\frac{\sigma_{M_{\text{PBH}}}}{\sqrt{2\pi}\delta_{\text{th}}} \right] \exp\left(-\frac{\delta_{\text{th}}^2}{2\sigma_{M_{\text{PBH}}}^2} \right), \quad (33)$$

where the integration gets performed above some limiting or threshold value of the overdensity denoted above by δ_{th} . Here, we adopt the criterion of the critical collapse theory, which allows one to determine the threshold value as equivalent to the equation of state of the RD fluid, $\delta \geq \delta_{\text{th}} = 1/3$. Another quantity essential to complete the estimate for $\beta(M_{\text{PBH}})$ is the variance of the distribution σ_{PBH} , and this is calculated with the aid of the scalar power spectrum amplitude, here it will be the one-loop corrected scalar power spectrum from eqn.(26), and this gets implemented as follows:

$$\sigma_{M_{\text{PBH}}}^2 = \frac{16}{81} \int_0^\infty \frac{dk}{k} (kR)^4 e^{-k^2 R^2/2} \left[\Delta_\zeta^2(k) \right]_{\text{Total}}, \quad (34)$$

where $R = 1/(\tilde{c}_s k_s)$ corresponds to the horizon scale over which the primordial perturbations are coarse-grained with the window function chosen to be a Gaussian in the above formula. The above discussion will prove sufficient to later analyze the PBH abundance resulting from the scalar power spectrum as shown in fig.(8).

III. Scalar Induced Gravitational Waves

In this section, we present a concise review of the theory behind the scalar-induced gravitational waves necessary to understand the calculation of the observationally relevant GW density parameter, which we will finally evaluate in the next section with the case of a one-loop corrected scalar power spectrum. We follow the refs.[78, 79, 242] for the derivation presented in this section.

To this end, let us start with a perturbed version of the spatially flat FLRW metric while working with the conformal Newtonian gauge:

$$ds^2 = a^2(\tau) \left\{ -(1 + 2\Phi)d\tau^2 + \left((1 - 2\Psi)\delta_{ij} + \frac{1}{2}h_{ij} \right) dx^i dx^j \right\}, \quad (35)$$

where Φ, Ψ are the first-order scalar perturbation modes, commonly referred to as the Bardeen potentials, and h_{ij} is the purely second-order tensor perturbation satisfying the additional property of $\delta^{ij}h_{ij} = \delta^{jk}\partial_k h_{ij} = 0$. The basic assumption to be followed in the further analysis of this metric is that the tensor perturbation modes only exist at second-order and no second-order scalar or vector modes are going to be considered. Also, in the absence of anisotropic stress, we can ultimately take $\Phi = \Psi$.

Using this metric, we proceed to solve the Einstein field equations for the second-order perturbations. Here we require an operator which extracts the transverse, traceless part of this equation since we are ultimately concerned with the evolution of the tensor modes. This is achieved through a projection operator $\hat{\mathcal{T}}_{ij}^{ab}$ having the properties:

$$\hat{\mathcal{T}}_{ij}^{ab}\hat{\mathcal{T}}_{mn}^{ij} = \hat{\mathcal{T}}_{mn}^{ab}, \quad \partial_j \hat{\mathcal{T}}_{ij}^{ab}\mathcal{P}_{ab} = \hat{\mathcal{T}}_{jj}^{ab}\mathcal{P}_{ab} = 0. \quad (36)$$

for an arbitrary second-rank tensor \mathcal{P}_{ab} . This operator is implemented onto the Einstein equations as follows:

$$\hat{\mathcal{T}}_{ij}^{ab}G_{ab}^{(2)} = \hat{\mathcal{T}}_{ij}^{ab}T_{ab}^{(2)} \quad (37)$$

where we have used the convention $M_p = 1/\sqrt{8\pi G} = 1$. This gives us the following equation for the tensor modes:

$$h_{ab}'' + 2\mathcal{H}h_{ab}' - \nabla^2 h_{ab} = -4\hat{\mathcal{T}}_{ab}^{ij}\mathcal{S}_{ij}, \quad (38)$$

where the notation $'$ denotes conformal time derivative throughout this section and \mathcal{S}_{ij} is a source term that contains quadratic contributions of the first-order scalar perturbations and whose explicit form will be given below shortly.

The analysis of the aforementioned equation is more illuminating in the Fourier space which includes the polarization information of the tensor modes and would ultimately help in obtaining the tensor power spectrum. For this, we start with the Fourier transform of h_{ab} :

$$h_{ab}(\tau, \mathbf{x}) = \int \frac{d^3\mathbf{k}}{(2\pi)^3} e^{i\mathbf{k}\cdot\mathbf{x}} (e_{ab}h_{\mathbf{k}}(\tau) + \bar{e}_{ab}\bar{h}_{\mathbf{k}}(\tau)), \quad (39)$$

which includes the two polarization tensors defined as:

$$e_{ab}(\mathbf{k}) = \frac{1}{\sqrt{2}} (e_a(\mathbf{k})e_b(\mathbf{k}) - \bar{e}_a(\mathbf{k})\bar{e}_b(\mathbf{k})), \quad \bar{e}_{ab}(\mathbf{k}) = \frac{1}{\sqrt{2}} (e_a(\mathbf{k})\bar{e}_b(\mathbf{k}) + \bar{e}_a(\mathbf{k})e_b(\mathbf{k})), \quad (40)$$

where $e_a(\mathbf{k}), \bar{e}_b(\mathbf{k})$ behaves as basis vectors, which are orthonormal and orthogonal to the momentum vector \mathbf{k} and hence satisfy $e_a(\mathbf{k})\cdot\bar{e}_b(\mathbf{k}) = 0$. As for the RHS in eqn.(38), we can write it using the polarization tensors and Fourier transform of the source as:

$$\hat{\mathcal{T}}_{ab}^{ij}\mathcal{S}_{ij} = \int \frac{d^3\mathbf{k}}{(2\pi)^3} e^{i\mathbf{k}\cdot\mathbf{x}} [e_{ab}(\mathbf{k})e^{ij}(\mathbf{k}) + \bar{e}_{ab}(\mathbf{k})\bar{e}^{ij}(\mathbf{k})]\mathcal{S}_{ij}(\mathbf{k}) \quad (41)$$

The above equations are combined together to give us the following Fourier space version of Eqn.(38):

$$h_{\mathbf{k}}'' + 2\mathcal{H}h_{\mathbf{k}}' + k^2 h_{\mathbf{k}} = \mathcal{S}(\mathbf{k}, \tau), \quad (42)$$

with the RHS defined to be:

$$\mathcal{S}(\mathbf{k}, \tau) = \int \frac{d^3\mathbf{q}}{(2\pi)^3} e^{ij}(\mathbf{k})q_i q_j F(\mathbf{k}, \mathbf{q}, \tau). \quad (43)$$

Solving eqn.(42) requires knowledge of the time-dependent behaviour of the scalar perturbations present inside the function $F(\mathbf{k}, \mathbf{q}, \tau)$ written explicitly as:

$$F(\mathbf{k}, \mathbf{q}, \tau) = \frac{4}{3(1+w)} \left(2(5+3w)\Phi_q(\tau)\Phi_{k-q}(\tau) + \frac{4}{\mathcal{H}}(\Phi_q(\tau)\Phi'_{k-q}(\tau) + \Phi_{k-q}(\tau)\Phi'_q(\tau)) + \frac{4}{\mathcal{H}^2}\Phi'_q(\tau)\Phi'_{k-q}(\tau) \right) \quad (44)$$

which is obtained using the relations from first-order Einstein equations and the parameter $w = P/\rho$ denotes the equation of state. The Hubble parameter in this section is defined as $\mathcal{H} = \partial_\tau \ln(a(\tau)) = 2/(1 + 3w)\tau$. In our subsequent analysis, we will work with only one polarization mode.

In general, we solve the inhomogeneous differential equation, eqn.(42), using Green's function method. To see this, consider a change in variable $h_{\mathbf{k}}(\tau) \rightarrow a(\tau)h_{\mathbf{k}}(\tau)$ which gives us the following solution for the same differential equation:

$$h_{\mathbf{k}}(\tau) = \frac{1}{a(\tau)} \int_{\tau_0}^{\tau} d\tilde{\tau} G_{\mathbf{k}}(\tau, \tilde{\tau}) a(\tilde{\tau}) \mathcal{S}(\mathbf{k}, \tilde{\tau}). \quad (45)$$

where the Green's function $G_{\mathbf{k}}(\tau, \tilde{\tau})$ satisfies:

$$G_{\mathbf{k}}''(\tau, \tilde{\tau}) + \left(k^2 - \frac{a''(\tau)}{a(\tau)} \right) G_{\mathbf{k}}(\tau, \tilde{\tau}) = \delta(\tau - \tilde{\tau}). \quad (46)$$

Now, from the definition of the tensor power spectrum, we write the following expressions based on our current analysis:

$$\langle h_{\mathbf{k}}(\tau) h_{\tilde{\mathbf{k}}}(\tau) \rangle = \frac{2\pi^2}{k^3} \delta(\mathbf{k} + \tilde{\mathbf{k}}) \Delta_h^2(k, \tau) \quad (47)$$

$$= \frac{1}{a(\tau)^2} \int_{\tau_0}^{\tau} d\tilde{\tau}_1 \int_{\tau_0}^{\tau} d\tilde{\tau}_2 a(\tau_1) G_{\mathbf{k}}(\tau, \tau_1) a(\tau_2) G_{\tilde{\mathbf{k}}}(\tau, \tau_2) \langle \mathcal{S}(\mathbf{k}, \tilde{\tau}_1) \mathcal{S}(\tilde{\mathbf{k}}, \tilde{\tau}_2) \rangle. \quad (48)$$

To simplify this further we use the fact that if the perturbations originated during the inflationary epoch then the behaviour of the gravitational potential, $\Phi_{\mathbf{k}}(\tau)$, can be understood using a decomposition into (a) : the transfer function $\Phi(k\tau)$ which helps to describe the evolution of the potential, and (b) : a component describing the primordial scalar perturbations amplitude, $\phi_{\mathbf{k}}$, which follows Gaussian statistics. Hence, we can write the function $F(\mathbf{k}, \mathbf{q}, \tau)$ using the transfer function and its derivatives and pull the primordial perturbation part outside the function.

We are left to evaluate the correlation function of the source functions in terms of the correlations between the scalar perturbations. After using Wick's theorem to perform the contractions, we get only 2 connected components which are proportional to $\delta(\mathbf{k} + \tilde{\mathbf{k}}) \delta(\mathbf{q} + \tilde{\mathbf{q}}) \Delta_\phi^2(q) \Delta_\phi^2(|\mathbf{k} - \mathbf{q}|)$ and $\delta(\mathbf{k} + \tilde{\mathbf{k}}) \delta(\mathbf{k} - \mathbf{q} + \tilde{\mathbf{q}}) \Delta_\phi^2(q) \Delta_\phi^2(|\mathbf{k} - \mathbf{q}|)$. An important point to further note is the invariance under the change of variables and $\mathbf{k} \rightarrow -\mathbf{k}$ in the function $F(\mathbf{k}, \mathbf{q}, \tau)$ and the invariance of the projection $e^{ij}(\mathbf{k}) q_i q_j = q^2 \sin^2 \theta \cos 2\beta / \sqrt{2}$ under $\mathbf{k} \rightarrow -\mathbf{k}$, where θ represents angle between \mathbf{k}, \mathbf{q} with $\cos \theta = \alpha = \mathbf{k} \cdot \mathbf{q} / kq$ and β is the azimuth angle.

Using these facts we write down the complete expression for the tensor power spectrum:

$$\Delta_h^2(k, \tau) = \int_0^\infty dq \int_{-1}^1 d\alpha \frac{k^3 q^3}{|\mathbf{k} - \mathbf{q}|^3} (1 - \alpha^2)^2 \Delta_\phi^2(q) \Delta_\phi^2(|\mathbf{k} - \mathbf{q}|) \mathcal{G}(k, q, \tau), \quad (49)$$

where the function \mathcal{G} is of the form:

$$\mathcal{G}(k, q, \tau) = \frac{2}{a(\tau)^2} \int_{\tau_0}^{\tau} d\tau_1 \int_{\tau_0}^{\tau} d\tau_2 a(\tau_1) G_{\mathbf{k}}(\tau, \tau_1) a(\tau_2) G_{\mathbf{k}}(\tau, \tau_2) F(\mathbf{k}, \mathbf{q}, \tau_1) F(\mathbf{k}, \mathbf{q}, \tau_2). \quad (50)$$

Let us note that the function F contains the necessary information regarding the evolution of the gravitational potentials through the transfer function. Hence, we require the solutions of the following equation for the time-dependent potentials in the absence of any entropy perturbations:

$$\Phi_{\mathbf{k}}''(\tau) + 3\mathcal{H}(1 + w)\Phi_{\mathbf{k}}'(\tau) + (2\mathcal{H}' + (1 + 3w)\mathcal{H}^2 + wk^2)\Phi_{\mathbf{k}}(\tau) = 0. \quad (51)$$

In the super-Hubble limit, it is possible to relate the two-point correlation function of primordial perturbations with the correlation function of the comoving curvature perturbations. To achieve this, we need to consider a particular gauge condition more suitable for outside the horizon. In this gauge, the perturbations in the scalar field satisfy $\delta\phi(\mathbf{x}, \tau) = 0$, which then enables us to write the comoving curvature perturbation as follows:

$$\zeta(\mathbf{x}, \tau) = -\Phi(\mathbf{x}, \tau) \left(\frac{5 + 3w}{3 + 3w} \right) - \frac{2\Phi'}{3\mathcal{H}(1 + w)}. \quad (52)$$

From eqn.(51), in the super-Hubble limit, the potential Φ comes out as a constant and this gives us the required relation for the Fourier modes:

$$\zeta_{\mathbf{k}} = -\frac{5 + 3w}{3 + 3w} \phi_{\mathbf{k}} \quad \implies \quad \Delta_\zeta^2(k) = \left(\frac{5 + 3w}{3 + 3w} \right)^2 \Delta_\phi^2(k). \quad (53)$$

The integral in eqn.(49) can be simplified even further when considering a variable change from $q, \alpha \rightarrow u, v$ where u, v are the new dimensionless variables with the form $u = |\mathbf{k} - \mathbf{q}|/k$ and $v = q/k$. The advantage of this substitution is to make the symmetries of the integrand under variable exchange more explicit which is discussed in the paragraph before eqn.(49). The final version of the tensor power spectrum in terms of the newly defined dimensionless variables follows the relation [243]:

$$\Delta_h^2(\tau, k) = 4 \int_0^\infty dv \int_{|1-v|}^{1+v} du \left(\frac{4v^2 - (1 + v^2 - u^2)^2}{4vu} \right)^2 \left(\frac{5 + 3w}{3 + 3w} \right)^4 \mathcal{I}^2(u, v, x) \Delta_\zeta^2(kv) \Delta_\zeta^2(ku), \quad (54)$$

with the function $\mathcal{I}(u, v, x)$ is defined as follows:

$$\mathcal{I}(u, v, x) = \int_0^x d\tilde{x} \frac{a(\tilde{\tau})}{a(\tau)} k G_{\mathbf{k}}(\tau, \tilde{\tau}) F(u, v, \tilde{x}) \quad (55)$$

where $x \equiv k\tau$ substitution is used.

Now, the fraction of the total energy density in GWs is related to the tensor power spectrum through the relation [243]:

$$\Omega_{\text{GW}}(\tau, k) = \frac{\rho_{\text{GW}}(\tau, k)}{\rho_{\text{total}}(\tau)} = \frac{1}{24} \left(\frac{k}{a(\tau)H(\tau)} \right)^2 \overline{\Delta_h^2(\tau, k)}, \quad (56)$$

where the overline represents the time-averaging at a given point within the horizon. We are ultimately interested in the above quantity detected through observations. To determine this quantity at the current time, we first take the late-time limit, $k\tau \rightarrow \infty$, of the integral \mathcal{I}^2 in eqn.(54) and then take the time average of the remaining quantity as given in eqn.(56). The final formula for the GW spectrum assumed primarily to be produced during the radiation-dominated (RD) era requires the knowledge of the associated Green's function and the approximation $a(\tilde{\tau})/a(\tau) \approx \tilde{\tau}/\tau$ which, along with the necessary steps mentioned before to observe the spectrum today, later reduce the eqn.(56) into the following form [60]:

$$\Omega_{\text{GW}}(f) = 0.39 \left(\frac{g_*(T_c)}{106.75} \right)^{-1/3} \Omega_{r,0} \int_0^\infty dv \int_{|1-v|}^{1+v} du \mathcal{K}(u, v) \Delta_\zeta^2(ku) \Delta_\zeta^2(kv) \quad (57)$$

where the kernel function from the RD era is [243]:

$$\mathcal{K}(u, v) = \frac{3(4v^2 - (1 + v^2 - u^2)^2)^2(u^2 + v^2 - 3)^4}{1024u^8v^8} \left(\left(\ln \frac{|3 - (u + v)^2|}{|3 - (u - v)^2|} - \frac{4uv}{u^2 + v^2 - 3} \right)^2 + \pi^2 \Theta(u + v - \sqrt{3}) \right) \quad (58)$$

and pre-factors outside the integral include the energy density fraction of radiation at present time $\Omega_{r,0}$, the total number of relativistic d.o.f in SM 106.75, and $g_*(T_c)$ is the total relativistic d.o.f at the temperature T_c which is evaluated at the time when the perturbations re-enter the horizon in the RD era. The following conversion between frequency and wavenumber is adopted:

$$f = 1.6 \times 10^{-9} \text{Hz} \left(\frac{k}{10^6 \text{Mpc}^{-1}} \right) \quad (59)$$

IV. Results for the SIGW spectrum

In this section, we discuss our results for the induced GW spectrum using the one-loop corrected scalar power spectrum obtained in eqn.(26) during inflation in the Galileon theory. The behavior of the obtained GW spectrum is analyzed, and the possible range of masses for the PBHs is discussed while covering the whole frequency range allowed by the observations. In fig.(9), we present the scalar-induced GW spectrum results plotted against the allowed frequency range. This range consists of the low-frequency regime where the NANOGrav results are observed and the high-frequency regime where various other observational experiments, both existing and planned, can probe.

The values in range ($10^{-17}\text{Hz}, 10^{-8}\text{Hz}$) include part of the spectrum which contains information from the pivot scale $k_* \sim (10^{-2}\text{Mpc}^{-1} \approx 10^{-17}\text{Hz})$ up to the transition wavenumber $k_{\text{PBH}} \sim 10^7\text{Mpc}^{-1}$ ($f_{\text{PBH}} \sim 10^{-8}\text{Hz}$). As we move higher in the frequency range from the frequency at the pivot scale, the spectrum shows a rise in amplitude, including small oscillations, which result from the highly oscillating integrand involved in the spectrum calculation. Up to a

Scalar induced gravitational waves from ultra slow – roll Galileon inflation

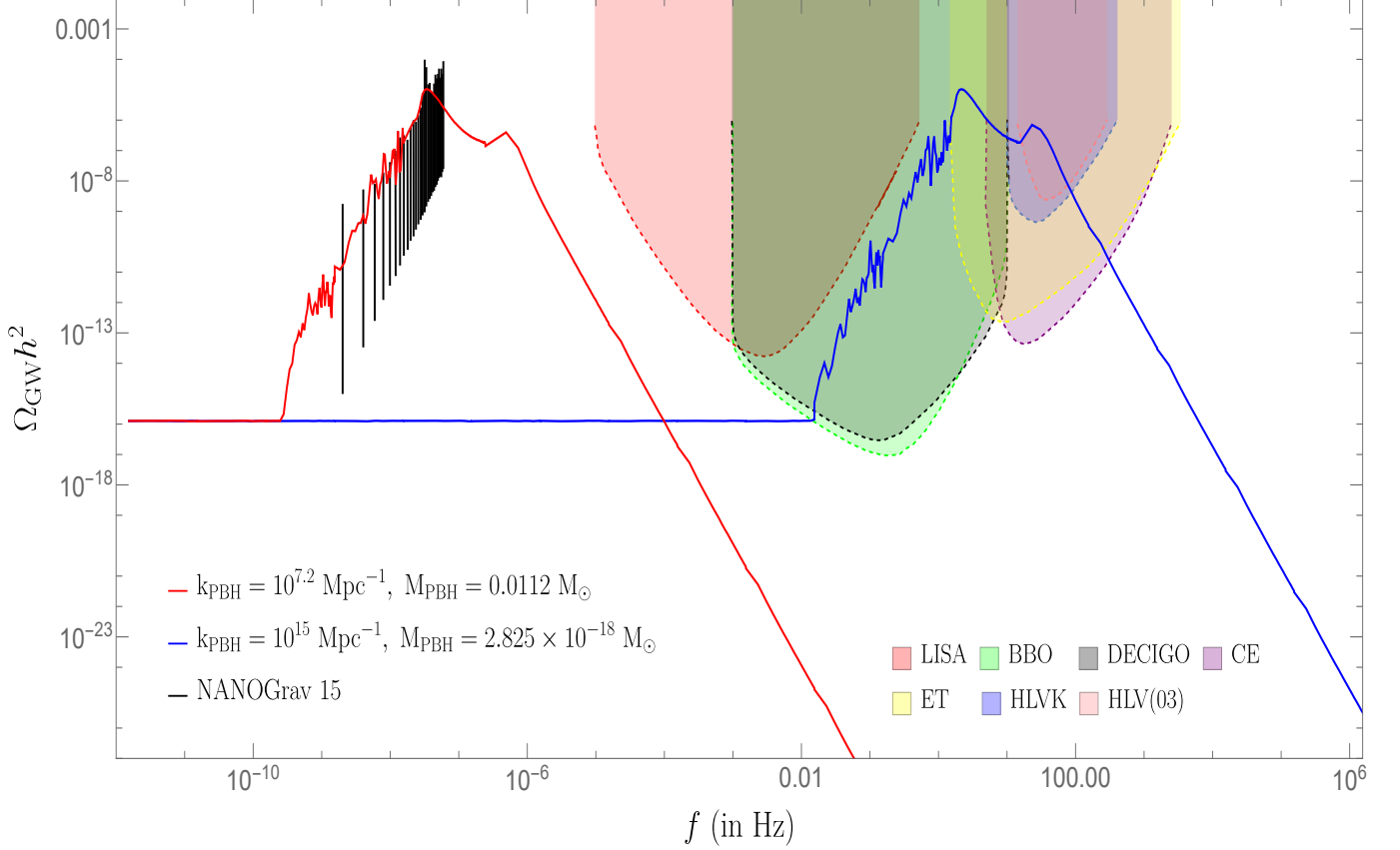


FIG. 9. The plot represents the scalar-induced GW spectrum generated using the one-loop corrected version of the scalar power spectrum obtained in Galileon inflation. This figure contains 2 separate features each distinguished by colors red and blue which indicate different scenarios. The red spectrum is where the amplitude of the generated signal coincides with the observational result from NANOGrav 15-year signal and it also indicates the production of $M_{\text{PBH}} \sim 0.01 M_{\odot}$ ($2 \times 10^{28} \text{ Kg}$) for a transition scale of $f_{\text{PBH}} \sim 10^{-8} \text{ Hz}$. The blue spectrum is where the amplitude of the signal lies within the proposed sensitivity curves of the existing and future experiments to detect high-frequency GWs, which include the following: LISA, BBO, DECIGO, Cosmic Explorer(CE), Einstein Telescope(ET), HLVK network (consisting of detectors: aLIGO in Hanford and Livingston, aVirgo, and KAGRA), and the HLV network during the third observation run (O3). This blue curve also shows a similar spectrum of GWs generated at a high-frequency value, near the transition scale $f_{\text{PBH}} \sim 1 \text{ Hz}$ where sub-solar PBH, $M_{\text{PBH}} \sim 10^{-18} M_{\odot}$ ($2 \times 10^2 \text{ Kg}$), are generated.

specific frequency, the behavior of the power spectrum changes, and we see that for a small region, the spectrum achieves a peak amplitude of $\Omega_{\text{GW}} h^2 \sim \mathcal{O}(10^{-5})$ which occurs as a result of the sharp transition encountered at the scale k_{PBH} . After the peak, the amplitude of the spectrum starts to fall before going through a bump-like feature visible in the plot right after the frequency $f \sim 10^{-7} \text{ Hz}$. This feature is reminiscent of the similar effect observed in the one-loop corrected scalar power spectrum, fig.(8), for the comoving curvature perturbation, which occurs right after the transition at the wavenumber k_e during the end of USR. Then, as we proceed towards completing the necessary e-foldings $\mathcal{N} = 60$, the amplitude of the spectrum falls linearly and at a rate faster compared to its rise in the region before the peak, which results from the behavior of the scalar power spectrum in the frequency region corresponding to the SRII phase.

As we can see, the peak value of the GW spectrum shown in the plot coincides with the results observed in the NANOGrav 15-year Data Set. These observations show that inflation in Galileon theory has the required feature to produce the primordial GWs and nearly solar mass PBHs, $M_{\text{PBH}} \sim 0.01 M_{\odot}$.

The interesting feature to note in fig.(9) comes further when we shift the transition scale to higher wavenumbers where $k_{\text{PBH}} \sim \mathcal{O}(10^{15} \text{ Mpc}^{-1} \approx 1 \text{ Hz})$. There we observe a similar kind of behavior for the GW spectrum as was with the case when considering almost solar mass PBH, but this time, masses of the produced PBH are tiny, in the

sub-solar regime $M_{\text{PBH}} \sim 10^{-18} M_{\odot}$. For this case, the peak value of the GW spectrum falls into the sensitivity curves of the proposed and operational space and earth-based probes of GWs, which are in the background of the above figure for comparison. Maintaining the perturbativity approximation and benefits of the non-renormalization theorem has the GW spectrum preserve its behavior near the sharp transitions and have successful inflation after the end of the USR.

Hence, Galileon theory has the power to accommodate the possibility of producing PBHs within the sub-solar and solar mass range depending on the transition wavenumber k_{PBH} position and can produce enough amount of GW signal which can fall into the experimentally observed low-frequency regime of NANOGrav 15, as well as in the allowed sensitivity of the high-frequency regime probes.

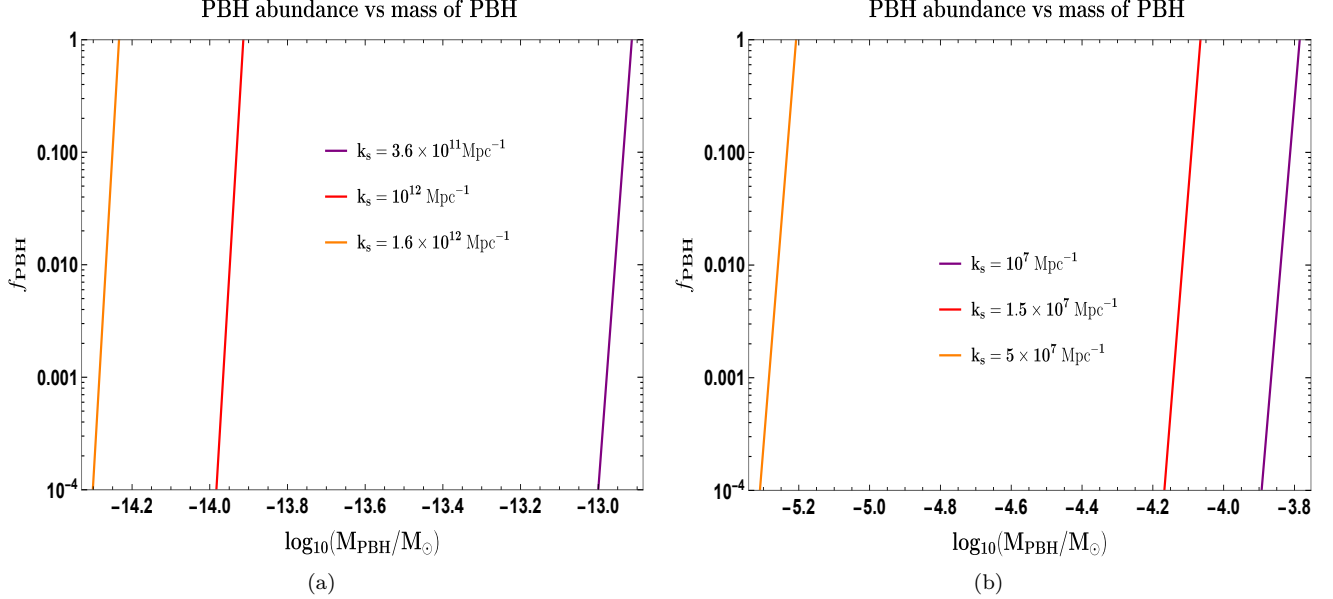


FIG. 10. PBH abundance as function of their masses. The *left panel* shows PBH abundance for masses in the range $\mathcal{O}(10^{-15} - 10^{-13})M_{\odot}$ corresponding to the small scales. The *right panel* shows PBH abundance for masses in the range $\mathcal{O}(10^{-6} - 10^{-3})M_{\odot}$ corresponding to frequency interval of the NANOGrav15 signal.

The fig.(10) shows behaviour for the PBH abundance as a function of the PBH masses. We analyze the abundance for two regions, one concerning the frequency range corresponding to the NANOGrav 15 signal window (*right panel*) and the other concerning the PBHs formed at large wavenumbers or small scales (*left panel*) where, from the one-loop corrected scalar power spectrum in fig.(8), one can notice an amplitude of $\mathcal{O}(10^{-5})$. Here, we use a crucial point highlighted through our plot in fig.(9), which shows the invariance of the obtained GW spectrum under translation in wavenumber. This property is also highlighted under discussions in the section II E for working with the Galileon theory. To reiterate, until we can maintain the necessary perturbativity approximation, especially having $k_e/k_s \sim \mathcal{O}(10)$, we control the scalar power spectrum amplitude from achieving values greater than $\mathcal{O}(1)$, and thus, we are free to shift the sharp transition wavenumber to the value of our choosing. By doing so, we will observe successful inflation in our setup, owing to the benefits of the non-renormalization theorem. Since the amplitude from the fig.(8) is quite small on the small scales, when PBH formation is of main concern as it requires at least $\mathcal{O}(10^{-2})$ for the power spectrum amplitude, we utilize here the translation property mentioned above to our advantage. By keeping the wavenumber around $k_s \sim \mathcal{O}(10^{11} - 10^{12})\text{Mpc}^{-1}$, it allows to produce PBHs with masses in the range $\mathcal{O}(10^{-15} - 10^{-13})M_{\odot}$ and there the corresponding abundance is not restricted due to strong constraints coming from PBH evaporation. Such restriction are large as we consider PBHs of even smaller masses such as $M_{\text{PBH}} < \mathcal{O}(10^{-16})$ where PBH evaporation constraints are the most stringent and there, with an amplitude of the scalar power spectrum of the order $\mathcal{O}(10^{-5})$, produces highly suppressed value of the variance which ultimately produces almost vanishing f_{PBH} . In the right panel, we show the PBH abundance for the wavenumbers associated with the frequency interval of the NANOGrav15 signal. The observed mass range corresponding to the sharp transitions at the frequencies significant to the NANOGrav15 is seen to lie within $M_{\text{PBH}} \sim \mathcal{O}(10^{-3} - 10^{-5})$ with sufficient abundance for such PBH masses.

V. Conclusion

In this paper, we have considered the scalar-induced gravitational waves using the one-loop corrected scalar power spectrum from Galileon inflation. We first briefly reviewed the Galileon theory by introducing the action for the Covariantized Galileon Theory, with detailing the implementation of various phases in our setup during inflation and then outlining the procedure to develop solutions for the comoving curvature perturbations modes in the three regions, SRI, USR, and SRII, by using the second-order action in this theory. The defining feature of this theory, other than the ability to evade the emergence of unwanted ghosts, is its non-renormalization theorem which allows us not to consider any renormalization and resummation procedure for the loop effects in its correlations. This feature helped us to manage a sufficient number of e-foldings of expansion and control the one-loop effects in theory, which later form part of the total scalar power spectrum necessary for further analysis regarding the GWs abundance calculation. We then presented a concise overview of the theory behind the scalar-induced gravitational waves (SIGWs) which tells us that the second-order tensor mode solutions involved quadratic contributions of the first-order scalar perturbations. After deriving the expression for the tensor power spectrum in terms of the scalar power spectrum, the next step was to numerically solve the integral for the GW abundance and plot the resulting behavior against the allowed frequency range. The features of this plot represent the key findings of our overall analysis done in this work.

We observed that the amount of GW abundance, $\Omega_{\text{GW}}h^2$, produced through the use of one-loop corrected scalar power spectrum in the low-frequency region, $10^{-8}\text{Hz} \leq f \leq 10^{-6}\text{Hz}$, is such that it gives a sufficient overlap and thus indicates an agreement with the observational result from the NANOGrav 15-year signal. In the high-frequency region, after the peak value is achieved, the obtained spectrum falls rapidly compared to its ascent near the low-frequency values. The peak enhancement in the signal is due to a sharp transition feature when going from the SRI to USR phase. This behavior is known to exist for the total dimensionless scalar power spectrum in plot fig.(8) near the scales labeled as $k_s \sim 10^6\text{Mpc}^{-1}$ and $k_e \sim 10^7\text{Mpc}^{-1}$. There the property of accommodating a long enough SRII region required for successful inflation, $\Delta\mathcal{N}_{\text{Total}} = 60$, is also reflected in the tensor power spectrum, and equivalently the GW spectrum, when it is extended to even higher frequencies and their corresponding lower amplitudes relative to the current values.

The scale of the transition wave number determines the mass of the PBH being produced. Using the eqn.(28), we were able to find the allowed range of mass values, $(1M_\odot - 10^{-18}M_\odot)$, of the produced PBH when the transition scale is set between $k_{\text{PBH}} \sim (10^7\text{Mpc}^{-1} - 10^{15}\text{Mpc}^{-1})$. Hence, by keeping the transition scale near to the required value in the frequency range of the NANOGrav signal, $k_{\text{PBH}} \sim (10^7\text{Mpc}^{-1} \approx 10^{-8}\text{Hz})$, we have shown that Galileon theory can produce almost solar mass PBH, $M_{\text{PBH}} \sim 0.01M_\odot$, and along with that generate enough amount of observable signal in the GW spectrum. Next, we examined the case where the transition scale is pushed to the domain of higher frequencies where the existing and proposed GW experiments are able to probe the effect. We found that Galileon theory is also able to produce a sufficient amount of signal in the spectrum such that it falls under the parameter space of these experiments. The observed spectrum exactly mimics the behavior for the case of a transition scale in the lower frequencies. This is important from the perspective of future investigations regarding the observation of SIGWs in higher frequencies as a signal for new physics models. Due to the setting of the transition at such high wave numbers, $k_{\text{PBH}} \sim (10^{15}\text{Mpc}^{-1} \approx 1\text{Hz})$, we are also able to predict the production of small mass PBHs in the sub-solar category, $M_{\text{PBH}} \sim 10^{-18}M_\odot$, and also producing an observable amount of signal in the GW spectrum. This is again the result of the intrinsic properties of the Galileon theory, which does not depend on the scale of transition until we are able to satisfy the perturbativity criteria, which is maintained throughout our analysis by keeping $k_e/k_s \sim \mathcal{O}(10)$, where k_s, k_e are the respective scales at the SRI to USR and USR to SRII transitions. Thus, have demonstrated the possibility of generating a measurable spectrum of the GW abundance either in the low-frequency (NANOGrav) region or the high-frequency region of the ground- and space-based GW detectors and the production of corresponding masses of PBHs ranging from $(1M_\odot - 10^{-18}M_\odot)$.

Acknowledgements

SC would like to thank the work-friendly environment of The Thanu Padmanabhan Centre For Cosmology and Science Popularization (CCSP), SGT University, Gurugram, for providing tremendous support in research. SC would also like to thank all the members of Quantum Aspects of the Space-Time & Matter (QASTM) for elaborative discussions. MS is supported by Science and Engineering Research Board (SERB), DST, Government of India under the Grant Agreement number CRG/2022/004120 (Core Research Grant). MS is also partially supported by the Ministry of Education and Science of the Republic of Kazakhstan, Grant No. 0118RK00935 and CAS President's International Fellowship Initiative (PIFI). Last but not least, we would like to acknowledge our debt to the people belonging to the various parts of the world for their generous and steady support for research in natural sciences.

VI. Appendix

A. General Mode Solutions

In this appendix, we focus on the calculation of the comoving curvature perturbations modes for our inflationary setup with the phases SRI, USR, and SRII involved within the CGT. The contents of this appendix is based on the detailed study provided in the refs.[127, 128].

To begin, we must work with the perturbation theory in second order in the curvature perturbations, and for this, we would need the second-order perturbed action. This action is written in the Fourier space as follows:

$$S_{\zeta}^{(2)} = \int d\tau \frac{d^3\mathbf{k}}{(2\pi)^3} a(\tau)^2 \frac{\mathcal{A}}{H^2} \left(|\zeta'_{\mathbf{k}}(\tau)|^2 - c_s^2 k^2 |\zeta_{\mathbf{k}}(\tau)|^2 \right) = \int d\tau \frac{d^3\mathbf{k}}{(2\pi)^3} a(\tau)^2 \frac{\mathcal{B}}{c_s^2 H^2} \left(|\zeta'_{\mathbf{k}}(\tau)|^2 - c_s^2 k^2 |\zeta_{\mathbf{k}}(\tau)|^2 \right) \quad (60)$$

where \mathcal{A} and \mathcal{B} are the same time-dependent coefficients as defined in eqns.(15,16), and which form the relation, $c_s^2 = \mathcal{B}/\mathcal{A}$, for the effective speed of sound parameter in the CGT as discussed before. Here we can observe the significance of these new coefficients as being directly involved in the action $S_{\zeta}^{(2)}$ and from here they will participate in the mode solutions for the curvature perturbations which further incorporates them into the scalar power spectrum.

Now, solving the above second order action would give us the following equation of motion:

$$\zeta_{\mathbf{k}}''(\tau) + 2 \frac{z'(\tau)}{z(\tau)} \zeta_{\mathbf{k}}'(\tau) + c_s^2 k^2 \zeta_{\mathbf{k}}(\tau) = 0. \quad (61)$$

with $z(\tau) = a\sqrt{2\mathcal{A}}/H^2$. It is this equation whose solutions in the three phases are to be analyzed. This is performed by setting of the initial conditions for the SRI phase as the Bunch-Davies quantum vacuum state and in the subsequent phases we are required to solve the boundary conditions during the transitions to eventually determine their complete solutions. We now describe the mode solutions for each phase.

- **For the SRI phase:**

The general mode solution in this phase for the second-order Fourier space equation of motion turns out to be:

$$\zeta_{\mathbf{k}}(\tau) = \left(\frac{iH^2}{2\sqrt{\mathcal{A}}} \right) \frac{1}{(c_s k)^{3/2}} \times \left[\alpha_{\mathbf{k}}^{(1)} (1 + ikc_s \tau) \exp(-ikc_s \tau) - \beta_{\mathbf{k}}^{(1)} (1 - ikc_s \tau) \exp(ikc_s \tau) \right] \quad (62)$$

where the conformal time window is the interval with $\tau < \tau_s$. The Bogoliubov coefficients for this phase are obtained as the result of fixing the Bunch-Davies initial condition:

$$\alpha_{\mathbf{k}}^{(1)} = 1, \quad (63)$$

$$\beta_{\mathbf{k}}^{(1)} = 0. \quad (64)$$

Throughout this phase, the slow-roll parameter $\epsilon(\tau)$ is almost a constant while for the other slow-roll parameter $\eta(\tau) \sim 0$.

- **For the USR phase:**

The general mode solution in this phase, for the conformal time window $\tau \in [\tau_s, \tau_e]$, is obtained to be as follows:

$$\zeta_{\mathbf{k}}(\tau) = \left(\frac{iH^2}{2\sqrt{\mathcal{A}}} \right) \left(\frac{\tau_s}{\tau} \right)^3 \frac{1}{(c_s k)^{3/2}} \times \left[\alpha_{\mathbf{k}}^{(2)} (1 + ikc_s \tau) \exp(-ikc_s \tau) - \beta_{\mathbf{k}}^{(2)} (1 - ikc_s \tau) \exp(ikc_s \tau) \right]. \quad (65)$$

The parameter ϵ behaves very differently for this phase with having a time-dependent form: $\epsilon(\tau) = \epsilon(\tau/\tau_s)^6$. This effect is reflected in the above equation. To have the complete solution requires the solving of the continuity and differentiability conditions at the transition scale τ_s . As a result, we obtain the following Bogoliubov coefficients:

$$\alpha_{\mathbf{k}}^{(2)} = 1 + \frac{3k_s^3}{2ik^3} \left(1 + \left(\frac{k}{k_s} \right)^2 \right), \quad (66)$$

$$\beta_{\mathbf{k}}^{(2)} = \frac{3k_s^3}{2ik^3} \left(1 - i \left(\frac{k}{k_s} \right)^2 \right)^2 \exp \left(2i \frac{k}{k_s} \right). \quad (67)$$

However, the parameter $\eta(\tau)$ here satisfies $\eta \sim -6$ which indicates an extreme jump from the previous value and is the cause for the enhancement in the fluctuations.

- **For the SRII phase:**

The general mode solution in this phase, for the conformal time window $\tau \in [\tau_e, \tau_{\text{end}}]$, is obtained to be as follows:

$$\zeta_{\mathbf{k}}(\tau) = \left(\frac{iH^2}{2\sqrt{\mathcal{A}}} \right) \left(\frac{\tau_s}{\tau_e} \right)^3 \frac{1}{(c_s k)^{3/2}} \times \left[\alpha_{\mathbf{k}}^{(3)} (1 + ikc_s \tau) \exp(-ikc_s \tau) - \beta_{\mathbf{k}}^{(3)} (1 - ikc_s \tau) \exp(ikc_s \tau) \right]. \quad (68)$$

The parameter ϵ in this phase has the behaviour where it varies slowly as a result of its form: $\epsilon(\tau) = \epsilon(\tau_e/\tau_s)$. This fact is crucial for the above solution. Again, through the use of the boundary conditions we get the following form of the Bogoliubov coefficients in this phase:

$$\begin{aligned} \alpha_{\mathbf{k}}^{(3)} &= -\frac{k_s^3 k_e^3}{4k^6} \left[9 \left(-\frac{k}{k_e} + i \right)^2 \left(\frac{k}{k_s} + i \right)^2 \exp \left(2ik \left(\frac{1}{k_s} - \frac{1}{k_e} \right) \right) \right. \\ &\quad \left. - \left\{ \left(\frac{k}{k_e} \right)^2 \left(-2\frac{k}{k_e} - 3i \right) - 3i \right\} \left\{ \left(\frac{k}{k_s} \right)^2 \left(-2\frac{k}{k_s} + 3i \right) + 3i \right\} \right] \\ \beta_{\mathbf{k}}^{(3)} &= \frac{3k_s^3 k_e^3}{4k^6} \left[\left(\frac{k}{k_s} + i \right)^2 \left\{ \left(\frac{k}{k_e} \right)^2 \left(2i\frac{k}{k_e} \right) + 3 \right\} \exp \left(2i\frac{k}{k_s} \right) \right. \\ &\quad \left. + i \left(\frac{k}{k_e} + i \right)^2 \left\{ 3i + \left(\frac{k}{k_s} \right)^2 \left(-2\frac{k}{k_s} + 3i \right) \right\} \exp \left(2i\frac{k}{k_e} \right) \right]. \quad (70) \end{aligned}$$

For this phase, the parameter $\eta(\tau)$ has an almost constant value throughout. This is quite similar to the behavior of the same parameter in the SRI phase. This nature is also reflected in the final behaviour of the power spectrum during this phase.

In all the equations above we have used the horizon crossing condition $-kc_s \tau = 1$ which is valid in all three phases during the sharp transitions at k_s from the SRI to USR phase and at k_e for the USR to SRII phase. These equations are sufficient to write the tree-level scalar power spectrum in the super-horizon limit, which we now mention as:

$$\Delta_{\zeta, \text{Tree}}^2(k) = \left(\frac{H^4}{8\pi^2 \mathcal{A} c_s^3} \right)_* \times \begin{cases} 1 + \left(\frac{k}{k_s} \right)^2 & \text{when } k < k_s \text{ (SRI)} \\ \left(\frac{k_e}{k_s} \right)^6 \left| \alpha_{\mathbf{k}}^{(2)} - \beta_{\mathbf{k}}^{(2)} \right|^2 & \text{when } k_s \leq k < k_e \text{ (USR)} \\ \left(\frac{k_e}{k_s} \right)^6 \left| \alpha_{\mathbf{k}}^{(3)} - \beta_{\mathbf{k}}^{(3)} \right|^2 & \text{when } k_e \leq k \leq k_{\text{end}} \text{ (SRII)} \end{cases} \quad (71)$$

B. Couplings and Coefficients in three phases including one-loop effects

In this appendix, we present the expressions for the couplings and the momentum-dependent functions which are necessary to describe the one-loop contributions to the total scalar power spectrum.

- **For the SRI phase:** The one-loop effect from the SRI phase which contributes into the total scalar power spectrum is written as follows:

$$\left[\Delta_{\zeta, \text{One-Loop}}^2(k) \right]_{\text{SRI}} = \left[\Delta_{\zeta, \text{Tree}}^2(k) \right]_{\text{SRI}} \times \left(- \sum_{i=1}^4 \mathcal{G}_{i, \text{SRI}} \mathbf{F}_{i, \text{SRI}}(k_s, k_*) \right) \quad (72)$$

the values for $\mathcal{G}_{i, \text{SRI}} \forall i = 1, 2, 3, 4$ are defined using the CGT couplings:

$$\begin{aligned} \mathcal{G}_{1, \text{SRI}} &= \mathcal{G}_1^2(\tau_*) \\ \mathcal{G}_{2, \text{SRI}} &= -\mathcal{G}_2^2(\tau_*) H^2(\tau_*) c_s^2 \\ \mathcal{G}_{3, \text{SRI}} &= -\frac{\mathcal{G}_3^2(\tau_*)}{c_s^2} \\ \mathcal{G}_{4, \text{SRI}} &= \frac{\mathcal{G}_4^2(\tau_*) H^2(\tau_*)}{c_s^6} \end{aligned} \quad (73)$$

and the momentum-dependent functions $\mathbf{F}_{i,\mathbf{SRI}}$ are defined using the notation $\mathcal{K}_{*,s} \equiv k_*/k_s$ as follows:

$$\mathbf{F}_{1,\mathbf{SRI}}(k_s, k_*) = \frac{1}{2} \left[3 + \mathcal{K}_{*,s}^2 \right], \quad (74)$$

$$\mathbf{F}_{2,\mathbf{SRI}}(k_s, k_*) = \left[\frac{17}{42} - \frac{2}{3} \mathcal{K}_{*,s}^6 + \frac{24}{7} \mathcal{K}_{*,s}^7 - \frac{9}{2} \mathcal{K}_{*,s}^8 \right], \quad (75)$$

$$\mathbf{F}_{3,\mathbf{SRI}}(k_s, k_*) = -\frac{2}{3} \left[1 - \mathcal{K}_{*,s}^6 \right], \quad (76)$$

$$\mathbf{F}_{4,\mathbf{SRI}}(k_s, k_*) = -\frac{1}{2} \left[1 - \mathcal{K}_{*,s}^2 \right]. \quad (77)$$

- **For the USR phase:** The one-loop effect from the USR phase which contributes into the total scalar power spectrum is written as follows:

$$\left[\Delta_{\zeta, \mathbf{One-Loop}}^2(k) \right]_{\mathbf{USR}} = \left[\Delta_{\zeta, \mathbf{Tree}}^2(k) \right]_{\mathbf{SRI}} \times \left(\sum_{i=1}^4 \mathcal{G}_{i,\mathbf{USR}} \mathbf{F}_{i,\mathbf{SRI}}(k_e, k_s) \right) \quad (78)$$

the values for $\mathcal{G}_{i,\mathbf{USR}} \forall i = 1, 2, 3, 4$ are defined using the CGT couplings:

$$\begin{aligned} \mathcal{G}_{1,\mathbf{USR}} &= \left(\frac{\mathcal{G}_1^2(\tau_e)}{c_s^3} \mathcal{K}_{e,s}^6 - \frac{\mathcal{G}_1^2(\tau_s)}{c_s^3} \right) \\ \mathcal{G}_{2,\mathbf{USR}} &= \left(\frac{\mathcal{G}_2^2(\tau_e) H^2(\tau_e)}{c_s^5} \mathcal{K}_{e,s}^4 - \frac{\mathcal{G}_2^2(\tau_s) H^2(\tau_s)}{c_s^5} \right) \\ \mathcal{G}_{3,\mathbf{USR}} &= \left(\frac{\mathcal{G}_3^2(\tau_e)}{c_s^6} \mathcal{K}_{e,s}^3 - \frac{\mathcal{G}_3^2(\tau_s)}{c_s^6} \right) \\ \mathcal{G}_{4,\mathbf{USR}} &= \left(\frac{\mathcal{G}_2^2(\tau_e) H^2(\tau_e)}{c_s^7} \mathcal{K}_{e,s}^2 - \frac{\mathcal{G}_2^2(\tau_s) H^2(\tau_s)}{c_s^7} \right). \end{aligned} \quad (79)$$

where we have used the notation $\mathcal{K}_{e,s} \equiv k_e/k_s$, and $\mathcal{K}_{s,e} \equiv k_s/k_e$. Using these same notations further we write the momentum-dependent functions $\mathbf{F}_{i,\mathbf{USR}}$ as follows:

$$\begin{aligned} \mathbf{F}_{1,\mathbf{USR}}(k_e, k_s) &= \left[\frac{1}{4} + \frac{9}{4} \mathcal{K}_{s,e}^2 - \frac{1}{4} \mathcal{K}_{s,e}^4 - 9 \mathcal{K}_{s,e}^4 \ln \mathcal{K}_{s,e} - 6 \sin(1 + \mathcal{K}_{e,s}) \sin(1 - \mathcal{K}_{e,s}) \right. \\ &\quad \left. - \frac{9}{8} \mathcal{K}_{s,e}^2 \left\{ 2 \left(\frac{k_e}{k_s} \right) \sin(2\mathcal{K}_{e,s}) - \cos(2\mathcal{K}_{e,s}) \right\} - 6 \mathcal{K}_{s,e} \sin(2\mathcal{K}_{e,s}) \right. \\ &\quad \left. - \frac{69}{16} \cos(2\mathcal{K}_{e,s}) - \frac{3}{4} \mathcal{K}_{s,e}^2 \left\{ 2 \mathcal{K}_{e,s} \cos(2\mathcal{K}_{e,s}) - \sin(2\mathcal{K}_{e,s}) \right\} \right], \end{aligned} \quad (80)$$

$$\mathbf{F}_{2,\mathbf{USR}}(k_e, k_s) = \left[\frac{1}{8} + \frac{9}{12} \mathcal{K}_{s,e}^2 + \frac{9}{4} \mathcal{K}_{s,e}^4 + \frac{9}{4} \mathcal{K}_{s,e}^6 - \frac{43}{8} \mathcal{K}_{s,e}^8 - \frac{9}{8} \cos(2\mathcal{K}_{e,s}) \right], \quad (81)$$

$$\begin{aligned} \mathbf{F}_{3,\mathbf{USR}}(k_e, k_s) &= \left[\frac{1}{8} + \frac{9}{12} \mathcal{K}_{s,e}^2 + \frac{9}{4} \mathcal{K}_{s,e}^4 + \frac{9}{4} \mathcal{K}_{s,e}^6 - \frac{43}{8} \mathcal{K}_{s,e}^8 - \frac{9}{8} \cos(2\mathcal{K}_{e,s}) \right] \\ &= \mathbf{F}_{2,\mathbf{USR}}(k_e, k_s), \end{aligned} \quad (82)$$

$$\mathbf{F}_{4,\mathbf{USR}}(k_e, k_s) = \left[\frac{1}{12} + \frac{9}{20} \mathcal{K}_{s,e}^2 + \frac{9}{8} \mathcal{K}_{s,e}^4 + \frac{9}{12} \mathcal{K}_{s,e}^6 - \frac{299}{230} \mathcal{K}_{s,e}^{12} \right]. \quad (83)$$

- **For the SRII phase:** The one-loop effect from the SRII phase which contributes into the total scalar power spectrum is written as follows:

$$\left[\Delta_{\zeta, \text{One-Loop}}^2(k) \right]_{\text{SRII}} = \left[\Delta_{\zeta, \text{Tree}}^2(k) \right]_{\text{SRI}} \times \left(\sum_{i=1}^4 \mathcal{G}_{i, \text{SRII}} \mathbf{F}_{i, \text{SRII}}(k_{\text{end}}, k_e) \right) \quad (84)$$

the values for $\mathcal{G}_{i, \text{SRII}} \forall i = 1, 2, 3, 4$ are defined using the CGT couplings:

$$\begin{aligned} \mathcal{G}_{1, \text{SRII}} &= \left(\frac{\mathcal{G}_1^2(\tau_{\text{end}})}{c_s^3} \mathcal{K}_{e,s}^6 - \frac{\mathcal{G}_1^2(\tau_e)}{c_s^3} \right) \\ \mathcal{G}_{2, \text{SRII}} &= \left(\frac{\mathcal{G}_2^2(\tau_{\text{end}}) H^2(\tau_{\text{end}})}{c_s^5} \mathcal{K}_{e,s}^4 - \frac{\mathcal{G}_2^2(\tau_e) H^2(\tau_e)}{c_s^5} \right) \\ \mathcal{G}_{3, \text{SRII}} &= \left(\frac{\mathcal{G}_3^2(\tau_{\text{end}})}{c_s^6} \mathcal{K}_{e,s}^3 - \frac{\mathcal{G}_3^2(\tau_e)}{c_s^6} \right) \\ \mathcal{G}_{4, \text{SRII}} &= \left(\frac{\mathcal{G}_4^2(\tau_{\text{end}}) H^2(\tau_{\text{end}})}{c_s^7} \mathcal{K}_{e,s}^2 - \frac{\mathcal{G}_4^2(\tau_e) H^2(\tau_e)}{c_s^7} \right) \end{aligned} \quad (85)$$

where $\mathcal{K}_{e,s}$ and $\mathcal{K}_{s,e}$ are previously defined in the USR phase. The momentum-dependent functions $\mathbf{F}_{i, \text{SRII}}$ are defined here after taking out only the leading order contributions and "... " are used to represent the suppressed quantities. To write the expressions more concisely, we choose the following notation:

$$\mathcal{K}_{\text{end},e} \equiv \frac{k_{\text{end}}}{k_e}, \quad \mathcal{K}_{\text{end},s} \equiv \frac{k_{\text{end}}}{k_s}, \quad \mathcal{K}_{e,\text{end}} \equiv \frac{k_e}{k_{\text{end}}}, \quad \mathcal{K}_{s,\text{end}} \equiv \frac{k_s}{k_{\text{end}}} \quad (86)$$

The final result is written as follows:

$$\begin{aligned} \mathbf{F}_{1, \text{SRII}}(k_{\text{end}}, k_e) &= \left[\frac{81}{64} + \frac{81}{40} (1 + \mathcal{K}_{s,e}) - \frac{9}{8} (1 + \mathcal{K}_{s,e}^2) + \frac{1}{6} \left((1 + \mathcal{K}_{s,e})^2 + 2\mathcal{K}_{s,e} \right) + \frac{1}{8} \mathcal{K}_{s,e}^2 + 6 + \frac{2}{7} \mathcal{K}_{s,e} (1 + \mathcal{K}_{s,e}) \right. \\ &\quad + \frac{27}{8} (1 + \mathcal{K}_{s,e}^6) - \frac{3}{4} \mathcal{K}_{e,\text{end}} \cos(2\mathcal{K}_{\text{end},e}) + 4\mathcal{K}_{e,\text{end}}^2 \ln(\mathcal{K}_{e,\text{end}}) - \frac{3}{4} \sin(1 + \mathcal{K}_{\text{end},s}) \sin(1 - \mathcal{K}_{\text{end},s}) \\ &\quad - \frac{9}{4} \frac{\mathcal{K}_{s,e}}{(1 - \mathcal{K}_{s,e})^2} \left\{ \cos(2(\mathcal{K}_{\text{end},e} - \mathcal{K}_{\text{end},s})) \right\} - \frac{9}{4} \frac{1}{(1 - \mathcal{K}_{s,e})} \left\{ \mathcal{K}_{s,\text{end}} \sin(2(\mathcal{K}_{\text{end},e} - \mathcal{K}_{\text{end},s})) \right\} \\ &\quad - 9 \frac{(1 + \mathcal{K}_{s,e})^2}{(1 - \mathcal{K}_{s,e})} \left\{ \sin(2(\mathcal{K}_{\text{end},e} - \mathcal{K}_{\text{end},s})) \right\} + \frac{9}{8} \left\{ 8 - 18\mathcal{K}_{s,e}^4 (1 + \mathcal{K}_{s,e}) \right\} \\ &\quad \left\{ \cos(2(\mathcal{K}_{\text{end},e} - \mathcal{K}_{\text{end},s})) - \mathcal{K}_{e,\text{end}} \cos(2(1 - \mathcal{K}_{e,s})) \right\} - \frac{9}{16} \mathcal{K}_{s,e}^2 (9 + 44\mathcal{K}_{s,e}^2) \ln \mathcal{K}_{e,\text{end}} \\ &\quad + 9\mathcal{K}_{s,e}^4 (1 + \mathcal{K}_{s,e}^2) + \frac{9}{7} \mathcal{K}_{s,e}^6 + 22\mathcal{K}_{s,e}^2 (1 - \mathcal{K}_{e,\text{end}}) \\ &\quad \left. - \frac{27}{16} \mathcal{K}_{s,e}^4 \mathcal{K}_{e,\text{end}} \left\{ \sin(2\mathcal{K}_{\text{end},e}) - \mathcal{K}_{e,\text{end}} \cos(2\mathcal{K}_{\text{end},e}) \right\} \dots \right], \\ \mathbf{F}_{2, \text{SRII}}(k_{\text{end}}, k_e) &= \left[\frac{81}{16} \ln \mathcal{K}_{e,\text{end}} + \frac{81}{8} (1 - \mathcal{K}_{e,\text{end}}) (1 + \mathcal{K}_{s,e}) + 5\mathcal{K}_{s,e}^6 \ln \mathcal{K}_{e,\text{end}} \right. \\ &\quad + \frac{1}{2} \left((1 + \mathcal{K}_{s,e})^2 + 2\mathcal{K}_{s,e} \right) + \frac{2}{3} (1 - \mathcal{K}_{e,\text{end}}^3) \mathcal{K}_{s,e} (1 + \mathcal{K}_{s,e}) + \frac{1}{4} \mathcal{K}_{s,e}^2 + \frac{1}{4} + \frac{27}{64} - \frac{27}{8} (1 + \mathcal{K}_{s,e}^6) \\ &\quad + \frac{3}{8} (1 + \mathcal{K}_{s,e}^2) - \frac{9}{16} \frac{\mathcal{K}_{s,e}^3}{(1 - \mathcal{K}_{s,e})^2} \left\{ \cos(2(\mathcal{K}_{\text{end},e} - \mathcal{K}_{\text{end},s})) \right\} \\ &\quad \left. - \frac{27}{4} \frac{1}{(1 - \mathcal{K}_{s,e})} \left\{ \mathcal{K}_{s,\text{end}} \sin(2(\mathcal{K}_{\text{end},e} - \mathcal{K}_{\text{end},s})) \right\} + \frac{81}{16} \frac{(1 + \mathcal{K}_{s,e}^2)}{(1 - \mathcal{K}_{s,e})} \left\{ \cos(2(\mathcal{K}_{\text{end},e} - \mathcal{K}_{\text{end},s})) \right\} \right] \end{aligned} \quad (87)$$

$$\begin{aligned}
& -\frac{9}{16} \frac{\mathcal{K}_{s,e}^3}{(1-\mathcal{K}_{s,e})} \left\{ \sin(2(\mathcal{K}_{\text{end},e} - \mathcal{K}_{\text{end},s})) \right\} - \frac{9}{16} \left(1 + \left(\frac{k_e}{k_s} \right) \right) \left\{ \mathcal{K}_{e,\text{end}} \cos(2(\mathcal{K}_{\text{end},e} - \mathcal{K}_{\text{end},s})) \right\} \\
& + \frac{27}{16} \mathcal{K}_{s,e}^6 + \frac{81}{64} \mathcal{K}_{s,e}^6 - \frac{9}{32} \mathcal{K}_{s,e}^2 (9 + 8\mathcal{K}_{s,e}^2 + 36\mathcal{K}_{s,e}^4) (1 - \mathcal{K}_{e,\text{end}}) - \frac{81}{16} \mathcal{K}_{s,e}^4 (1 + \mathcal{K}_{s,e}^2) \\
& + (1 + 4\mathcal{K}_{s,e}^2 + \mathcal{K}_{s,e}^4) \ln \mathcal{K}_{e,\text{end}} - \frac{3}{4} \mathcal{K}_{e,\text{end}} \cos(2\mathcal{K}_{\text{end},e}) \cdots \Big] = \mathbf{F}_{3,\text{SRII}}(k_{\text{end}}, k_e), \tag{88}
\end{aligned}$$

$$\begin{aligned}
\mathbf{F}_{4,\text{SRII}}(k_{\text{end}}, k_e) = & \left[\frac{81}{16} + \frac{27}{8} (1 + \mathcal{K}_{s,e}) + \frac{81}{16} \mathcal{K}_{s,e}^6 \ln \mathcal{K}_{e,\text{end}} + \frac{81}{32} ((1 + \mathcal{K}_{s,e})^2 + 2\mathcal{K}_{s,e}) \right. \\
& + 10\mathcal{K}_{s,e} (1 + \mathcal{K}_{s,e}) + \frac{1}{12} + \frac{9}{40} (1 + \mathcal{K}_{s,e}^2) + \frac{27}{64} (1 + \mathcal{K}_{s,e}^6) + \frac{81}{128} + 6\mathcal{K}_{s,e}^2 \ln \mathcal{K}_{e,\text{end}} \\
& - \frac{9}{16} \frac{(1 + \mathcal{K}_{s,e})^2}{(1 - \mathcal{K}_{s,e})^2} \left\{ \cos(2(\mathcal{K}_{\text{end},e} - \mathcal{K}_{\text{end},s})) \right\} - \frac{27}{8} \frac{(1 + \mathcal{K}_{s,e})^2}{(1 - \mathcal{K}_{s,e})^3} \left\{ \sin(2(\mathcal{K}_{\text{end},e} - \mathcal{K}_{\text{end},s})) \right\} \\
& - \frac{27}{4} \frac{(1 + \mathcal{K}_{s,e})^2}{(1 - \mathcal{K}_{s,e})} \left\{ \mathcal{K}_{e,\text{end}}^2 \sin(2(\mathcal{K}_{\text{end},e} - \mathcal{K}_{\text{end},s})) \right\} + \frac{9}{80} \mathcal{K}_{s,e}^2 (9 + 44\mathcal{K}_{s,e}^2) + \frac{27}{8} \mathcal{K}_{s,e}^4 (1 + \mathcal{K}_{s,e}^2) \\
& \left. + \frac{81}{16} \mathcal{K}_{s,e}^6 (1 - \mathcal{K}_{e,\text{end}}) + \frac{99}{56} + \frac{1}{4} \mathcal{K}_{e,\text{end}}^2 + \frac{81}{32} \mathcal{K}_{s,e}^6 \mathcal{K}_{e,\text{end}} \left\{ \sin(2\mathcal{K}_{\text{end},e}) - \mathcal{K}_{e,\text{end}} \cos(2\mathcal{K}_{\text{end},e}) \right\} \cdots \right]. \tag{89}
\end{aligned}$$

In terms of the above equations defined for all the three phases, the one-loop corrections to the scalar power spectrum from each of these phases can be written using the following expression:

$$\Delta_{\zeta, \text{One-Loop}}^2(k) = \left[\Delta_{\zeta, \text{Tree}}^2(k) \right]_{\text{SRI}} \times \begin{cases} -\sum_{i=1}^4 \mathcal{G}_{i,\text{SRI}} \mathbf{F}_{i,\text{SRI}}(k_s, k_*) & \text{when } k < k_s \text{ (SRI)} \\ \sum_{i=1}^4 \mathcal{G}_{i,\text{USR}} \mathbf{F}_{i,\text{USR}}(k_e, k_s) \Theta(k - k_s) & \text{when } k_s \leq k < k_e \text{ (USR)} \\ \sum_{i=1}^4 \mathcal{G}_{i,\text{SRII}} \mathbf{F}_{i,\text{SRII}}(k_{\text{end}}, k_e) \Theta(k - k_e) & \text{when } k_e \leq k \leq k_{\text{end}} \text{ (SRII)} \end{cases} \tag{90}$$

Combining Eqs.(71, 90) gives us the total dimensionless one-loop corrected version of the primordial scalar power spectrum which we ultimately utilize to generate the scalar-induced GW spectrum in Galileon inflation.

-
- [1] **LIGO Scientific, Virgo** Collaboration, B. P. Abbott *et al.*, “Observation of Gravitational Waves from a Binary Black Hole Merger,” *Phys. Rev. Lett.* **116** no. 6, (2016) 061102, [arXiv:1602.03837 \[gr-qc\]](#).
 - [2] L. Zu, C. Zhang, Y.-Y. Li, Y.-C. Gu, Y.-L. S. Tsai, and Y.-Z. Fan, “Mirror QCD phase transition as the origin of the nanohertz Stochastic Gravitational-Wave Background,” [arXiv:2306.16769 \[astro-ph.HE\]](#).
 - [3] K. T. Abe and Y. Tada, “Translating nano-Hertz gravitational wave background into primordial perturbations taking account of the cosmological QCD phase transition,” [arXiv:2307.01653 \[astro-ph.CO\]](#).
 - [4] Y. Gouttenoire, “First-order Phase Transition interpretation of PTA signal produces solar-mass Black Holes,” [arXiv:2307.04239 \[hep-ph\]](#).
 - [5] **NANOGrav** Collaboration, Z. Arzoumanian *et al.*, “Searching for Gravitational Waves from Cosmological Phase Transitions with the NANOGrav 12.5-Year Dataset,” *Phys. Rev. Lett.* **127** no. 25, (2021) 251302, [arXiv:2104.13930 \[astro-ph.CO\]](#).
 - [6] X. Xue *et al.*, “Constraining Cosmological Phase Transitions with the Parkes Pulsar Timing Array,” *Phys. Rev. Lett.* **127** no. 25, (2021) 251303, [arXiv:2110.03096 \[astro-ph.CO\]](#).
 - [7] Y. Nakai, M. Suzuki, F. Takahashi, and M. Yamada, “Gravitational Waves and Dark Radiation from Dark Phase Transition: Connecting NANOGrav Pulsar Timing Data and Hubble Tension,” *Phys. Lett. B* **816** (2021) 136238, [arXiv:2009.09754 \[astro-ph.CO\]](#).
 - [8] P. Athron, A. Fowlie, C.-T. Lu, L. Morris, L. Wu, Y. Wu, and Z. Xu, “Can supercooled phase transitions explain the gravitational wave background observed by pulsar timing arrays?,” [arXiv:2306.17239 \[hep-ph\]](#).
 - [9] E. Mudge, E. Morgante, C. Puchades-Ibáñez, N. Ramberg, W. Ratzinger, S. Schenk, and P. Schwaller, “Primordial gravitational waves in the nano-Hertz regime and PTA data – towards solving the GW inverse problem,” [arXiv:2306.14856 \[hep-ph\]](#).

- [10] N. Kitajima, J. Lee, K. Murai, F. Takahashi, and W. Yin, “Nanohertz Gravitational Waves from Axion Domain Walls Coupled to QCD,” [arXiv:2306.17146 \[hep-ph\]](#).
- [11] E. Babichev, D. Gorbunov, S. Ramazanov, R. Samanta, and A. Vikman, “NANOGrav spectral index $\gamma = 3$ from melting domain walls,” [arXiv:2307.04582 \[hep-ph\]](#).
- [12] Z. Zhang, C. Cai, Y.-H. Su, S. Wang, Z.-H. Yu, and H.-H. Zhang, “Nano-Hertz gravitational waves from collapsing domain walls associated with freeze-in dark matter in light of pulsar timing array observations,” [arXiv:2307.11495 \[hep-ph\]](#).
- [13] Z.-M. Zeng, J. Liu, and Z.-K. Guo, “Enhanced curvature perturbations from spherical domain walls nucleated during inflation,” [arXiv:2301.07230 \[astro-ph.CO\]](#).
- [14] R. Z. Ferreira, A. Notari, O. Pujolas, and F. Rompineve, “Gravitational waves from domain walls in Pulsar Timing Array datasets,” *JCAP* **02** (2023) 001, [arXiv:2204.04228 \[astro-ph.CO\]](#).
- [15] H. An and C. Yang, “Gravitational Waves Produced by Domain Walls During Inflation,” [arXiv:2304.02361 \[hep-ph\]](#).
- [16] X.-F. Li, “Probing the high temperature symmetry breaking with gravitational waves from domain walls,” [arXiv:2307.03163 \[hep-ph\]](#).
- [17] J. Ellis and M. Lewicki, “Cosmic String Interpretation of NANOGrav Pulsar Timing Data,” *Phys. Rev. Lett.* **126** no. 4, (2021) 041304, [arXiv:2009.06555 \[astro-ph.CO\]](#).
- [18] S. Blasi, V. Brdar, and K. Schmitz, “Has NANOGrav found first evidence for cosmic strings?,” *Phys. Rev. Lett.* **126** no. 4, (2021) 041305, [arXiv:2009.06607 \[astro-ph.CO\]](#).
- [19] W. Buchmuller, V. Domcke, and K. Schmitz, “From NANOGrav to LIGO with metastable cosmic strings,” *Phys. Lett. B* **811** (2020) 135914, [arXiv:2009.10649 \[astro-ph.CO\]](#).
- [20] J. J. Blanco-Pillado, K. D. Olum, and J. M. Wachter, “Comparison of cosmic string and superstring models to NANOGrav 12.5-year results,” *Phys. Rev. D* **103** no. 10, (2021) 103512, [arXiv:2102.08194 \[astro-ph.CO\]](#).
- [21] W. Buchmuller, V. Domcke, and K. Schmitz, “Stochastic gravitational-wave background from metastable cosmic strings,” *JCAP* **12** no. 12, (2021) 006, [arXiv:2107.04578 \[hep-ph\]](#).
- [22] K. Inomata, K. Kohri, and T. Terada, “The Detected Stochastic Gravitational Waves and Subsolar-Mass Primordial Black Holes,” [arXiv:2306.17834 \[astro-ph.CO\]](#).
- [23] Q.-H. Zhu, Z.-C. Zhao, and S. Wang, “Joint implications of BBN, CMB, and PTA Datasets for Scalar-Induced Gravitational Waves of Second and Third orders,” [arXiv:2307.03095 \[astro-ph.CO\]](#).
- [24] S. A. Hosseini Mansoori, F. Felegray, A. Talebian, and M. Sami, “PBHs and GWs from \mathbb{T}^2 -inflation and NANOGrav 15-year data,” [arXiv:2307.06757 \[astro-ph.CO\]](#).
- [25] B. Das, N. Jaman, and M. Sami, “Gravitational Waves Background (NANOGrav) from Quintessential Inflation,” [arXiv:2307.12913 \[gr-qc\]](#).
- [26] S. Balaji, G. Domènech, and G. Franciolini, “Scalar-induced gravitational wave interpretation of PTA data: the role of scalar fluctuation propagation speed,” [arXiv:2307.08552 \[gr-qc\]](#).
- [27] Y.-F. Cai, X.-C. He, X. Ma, S.-F. Yan, and G.-W. Yuan, “Limits on scalar-induced gravitational waves from the stochastic background by pulsar timing array observations,” [arXiv:2306.17822 \[gr-qc\]](#).
- [28] S. Wang, Z.-C. Zhao, J.-P. Li, and Q.-H. Zhu, “Exploring the Implications of 2023 Pulsar Timing Array Datasets for Scalar-Induced Gravitational Waves and Primordial Black Holes,” [arXiv:2307.00572 \[astro-ph.CO\]](#).
- [29] Z. Yi, Q. Gao, Y. Gong, Y. Wang, and F. Zhang, “The waveform of the scalar induced gravitational waves in light of Pulsar Timing Array data,” [arXiv:2307.02467 \[gr-qc\]](#).
- [30] S. Choudhury and A. Mazumdar, “Primordial blackholes and gravitational waves for an inflection-point model of inflation,” *Phys. Lett. B* **733** (2014) 270–275, [arXiv:1307.5119 \[astro-ph.CO\]](#).
- [31] S. Choudhury, “Single field inflation in the light of NANOGrav 15-year Data: Quintessential interpretation of blue tilted tensor spectrum through Non-Bunch Davies initial condition,” [arXiv:2307.03249 \[astro-ph.CO\]](#).
- [32] S. Choudhury, A. Karde, K. Dey, S. Panda, and M. Sami, “Primordial non-Gaussianity as a saviour for PBH overproduction in SIGWs generated by Pulsar Timing Arrays for Galileon inflation,” [arXiv:2310.11034 \[astro-ph.CO\]](#).
- [33] G. Bhattacharya, S. Choudhury, K. Dey, S. Ghosh, A. Karde, and N. S. Mishra, “Evading no-go for PBH formation and production of SIGWs using Multiple Sharp Transitions in EFT of single field inflation,” [arXiv:2309.00973 \[astro-ph.CO\]](#).
- [34] S. Vagnozzi, “Inflationary interpretation of the stochastic gravitational wave background signal detected by pulsar timing array experiments,” *JHEAp* **39** (2023) 81–98, [arXiv:2306.16912 \[astro-ph.CO\]](#).
- [35] G. Franciolini, A. Iovino, Junior., V. Vaskonen, and H. Veermäe, “The recent gravitational wave observation by pulsar timing arrays and primordial black holes: the importance of non-gaussianities,” [arXiv:2306.17149 \[astro-ph.CO\]](#).
- [36] M. A. Gorji, M. Sasaki, and T. Suyama, “Extra-tensor-induced origin for the PTA signal: No primordial black hole production,” [arXiv:2307.13109 \[astro-ph.CO\]](#).
- [37] V. De Luca, A. Kehagias, and A. Riotto, “How Well Do We Know the Primordial Black Hole Abundance? The Crucial Role of Non-Linearities when Approaching the Horizon,” [arXiv:2307.13633 \[astro-ph.CO\]](#).
- [38] L. Frosina and A. Urbano, “On the inflationary interpretation of the nHz gravitational-wave background,” [arXiv:2308.06915 \[astro-ph.CO\]](#).
- [39] Z.-C. Chen, C. Yuan, and Q.-G. Huang, “Pulsar Timing Array Constraints on Primordial Black Holes with NANOGrav 11-Year Dataset,” *Phys. Rev. Lett.* **124** no. 25, (2020) 251101, [arXiv:1910.12239 \[astro-ph.CO\]](#).
- [40] Y. Cai, M. Zhu, and Y.-S. Piao, “Primordial black holes from null energy condition violation during inflation,” [arXiv:2305.10933 \[gr-qc\]](#).
- [41] H.-L. Huang, Y. Cai, J.-Q. Jiang, J. Zhang, and Y.-S. Piao, “Supermassive primordial black holes in multiverse: for

- nano-Hertz gravitational wave and high-redshift JWST galaxies,” [arXiv:2306.17577 \[gr-qc\]](#).
- [42] J. Cang, Y. Gao, Y. Liu, and S. Sun, “High Frequency Gravitational Waves from Pulsar Timing Arrays,” [arXiv:2309.15069 \[astro-ph.CO\]](#).
- [43] G. Domènech, “Scalar Induced Gravitational Waves Review,” *Universe* **7** no. 11, (2021) 398, [arXiv:2109.01398 \[gr-qc\]](#).
- [44] S. Choudhury, K. Dey, and A. Karde, “Untangling PBH overproduction in w -SIGWs generated by Pulsar Timing Arrays for MST-EFT of single field inflation,” [arXiv:2311.15065 \[astro-ph.CO\]](#).
- [45] S. Choudhury, K. Dey, A. Karde, S. Panda, and M. Sami, “Primordial non-Gaussianity as a saviour for PBH overproduction in SIGWs generated by Pulsar Timing Arrays for Galileon inflation,” [arXiv:2310.11034 \[astro-ph.CO\]](#).
- [46] D. Baumann, “Inflation,” in *Theoretical Advanced Study Institute in Elementary Particle Physics: Physics of the Large and the Small*, pp. 523–686. 2011. [arXiv:0907.5424 \[hep-th\]](#).
- [47] D. Baumann, *Cosmology*. Cambridge University Press, 7, 2022.
- [48] D. Baumann, “Primordial Cosmology,” *PoS TASI2017* (2018) 009, [arXiv:1807.03098 \[hep-th\]](#).
- [49] L. Senatore, “Lectures on Inflation,” in *Theoretical Advanced Study Institute in Elementary Particle Physics: New Frontiers in Fields and Strings*, pp. 447–543. 2017. [arXiv:1609.00716 \[hep-th\]](#).
- [50] J. Martin, C. Ringeval, and V. Vennin, “Encyclopædia Inflationaris,” *Phys. Dark Univ.* **5-6** (2014) 75–235, [arXiv:1303.3787 \[astro-ph.CO\]](#).
- [51] J. Martin, C. Ringeval, R. Trotta, and V. Vennin, “The Best Inflationary Models After Planck,” *JCAP* **03** (2014) 039, [arXiv:1312.3529 \[astro-ph.CO\]](#).
- [52] A. Mazumdar and J. Rocher, “Particle physics models of inflation and curvaton scenarios,” *Phys. Rept.* **497** (2011) 85–215, [arXiv:1001.0993 \[hep-ph\]](#).
- [53] D. H. Lyth and A. Riotto, “Particle physics models of inflation and the cosmological density perturbation,” *Phys. Rept.* **314** (1999) 1–146, [arXiv:hep-ph/9807278](#).
- [54] Planck Collaboration, Y. Akrami *et al.*, “Planck 2018 results. X. Constraints on inflation,” *Astron. Astrophys.* **641** (2020) A10, [arXiv:1807.06211 \[astro-ph.CO\]](#).
- [55] Planck Collaboration, N. Aghanim *et al.*, “Planck 2018 results. VI. Cosmological parameters,” *Astron. Astrophys.* **641** (2020) A6, [arXiv:1807.06209 \[astro-ph.CO\]](#). [Erratum: *Astron. Astrophys.* 652, C4 (2021)].
- [56] CMB-S4 Collaboration, K. N. Abazajian *et al.*, “CMB-S4 Science Book, First Edition,” [arXiv:1610.02743 \[astro-ph.CO\]](#).
- [57] NANOGrav Collaboration, G. Agazie *et al.*, “The NANOGrav 15 yr Data Set: Evidence for a Gravitational-wave Background,” *Astrophys. J. Lett.* **951** no. 1, (2023) L8, [arXiv:2306.16213 \[astro-ph.HE\]](#).
- [58] NANOGrav Collaboration, G. Agazie *et al.*, “The NANOGrav 15 yr Data Set: Observations and Timing of 68 Millisecond Pulsars,” *Astrophys. J. Lett.* **951** no. 1, (2023) L9, [arXiv:2306.16217 \[astro-ph.HE\]](#).
- [59] NANOGrav Collaboration, G. Agazie *et al.*, “The NANOGrav 15 yr Data Set: Detector Characterization and Noise Budget,” *Astrophys. J. Lett.* **951** no. 1, (2023) L10, [arXiv:2306.16218 \[astro-ph.HE\]](#).
- [60] NANOGrav Collaboration, A. Afzal *et al.*, “The NANOGrav 15 yr Data Set: Search for Signals from New Physics,” *Astrophys. J. Lett.* **951** no. 1, (2023) L11, [arXiv:2306.16219 \[astro-ph.HE\]](#).
- [61] NANOGrav Collaboration, G. Agazie *et al.*, “The NANOGrav 15 yr Data Set: Constraints on Supermassive Black Hole Binaries from the Gravitational-wave Background,” *Astrophys. J. Lett.* **952** no. 2, (2023) L37, [arXiv:2306.16220 \[astro-ph.HE\]](#).
- [62] NANOGrav Collaboration, G. Agazie *et al.*, “The NANOGrav 15-year Data Set: Search for Anisotropy in the Gravitational-Wave Background,” [arXiv:2306.16221 \[astro-ph.HE\]](#).
- [63] NANOGrav Collaboration, G. Agazie *et al.*, “The NANOGrav 15 yr Data Set: Bayesian Limits on Gravitational Waves from Individual Supermassive Black Hole Binaries,” *Astrophys. J. Lett.* **951** no. 2, (2023) L50, [arXiv:2306.16222 \[astro-ph.HE\]](#).
- [64] NANOGrav Collaboration, A. D. Johnson *et al.*, “The NANOGrav 15-year Gravitational-Wave Background Analysis Pipeline,” [arXiv:2306.16223 \[astro-ph.HE\]](#).
- [65] EPTA Collaboration, J. Antoniadis *et al.*, “The second data release from the European Pulsar Timing Array III. Search for gravitational wave signals,” [arXiv:2306.16214 \[astro-ph.HE\]](#).
- [66] EPTA Collaboration, J. Antoniadis *et al.*, “The second data release from the European Pulsar Timing Array I. The dataset and timing analysis,” [arXiv:2306.16224 \[astro-ph.HE\]](#).
- [67] EPTA Collaboration, J. Antoniadis *et al.*, “The second data release from the European Pulsar Timing Array II. Customised pulsar noise models for spatially correlated gravitational waves,” [arXiv:2306.16225 \[astro-ph.HE\]](#).
- [68] EPTA Collaboration, J. Antoniadis *et al.*, “The second data release from the European Pulsar Timing Array IV. Search for continuous gravitational wave signals,” [arXiv:2306.16226 \[astro-ph.HE\]](#).
- [69] EPTA Collaboration, J. Antoniadis *et al.*, “The second data release from the European Pulsar Timing Array: V. Implications for massive black holes, dark matter and the early Universe,” [arXiv:2306.16227 \[astro-ph.CO\]](#).
- [70] EPTA Collaboration, C. Smarra *et al.*, “The second data release from the European Pulsar Timing Array: VI. Challenging the ultralight dark matter paradigm,” [arXiv:2306.16228 \[astro-ph.HE\]](#).
- [71] D. J. Reardon *et al.*, “Search for an Isotropic Gravitational-wave Background with the Parkes Pulsar Timing Array,” *Astrophys. J. Lett.* **951** no. 1, (2023) L6, [arXiv:2306.16215 \[astro-ph.HE\]](#).
- [72] D. J. Reardon *et al.*, “The Gravitational-wave Background Null Hypothesis: Characterizing Noise in Millisecond Pulsar Arrival Times with the Parkes Pulsar Timing Array,” *Astrophys. J. Lett.* **951** no. 1, (2023) L7, [arXiv:2306.16229 \[astro-ph.HE\]](#).

- [73] A. Zic *et al.*, “The Parkes Pulsar Timing Array Third Data Release,” [arXiv:2306.16230 \[astro-ph.HE\]](#).
- [74] H. Xu *et al.*, “Searching for the Nano-Hertz Stochastic Gravitational Wave Background with the Chinese Pulsar Timing Array Data Release I,” *Res. Astron. Astrophys.* **23** no. 7, (2023) 075024, [arXiv:2306.16216 \[astro-ph.HE\]](#).
- [75] S. Matarrese, O. Pantano, and D. Saez, “A General relativistic approach to the nonlinear evolution of collisionless matter,” *Phys. Rev. D* **47** (1993) 1311–1323.
- [76] S. Matarrese, O. Pantano, and D. Saez, “General relativistic dynamics of irrotational dust: Cosmological implications,” *Phys. Rev. Lett.* **72** (1994) 320–323, [arXiv:astro-ph/9310036](#).
- [77] S. Matarrese, S. Mollerach, and M. Bruni, “Second order perturbations of the Einstein-de Sitter universe,” *Phys. Rev. D* **58** (1998) 043504, [arXiv:astro-ph/9707278](#).
- [78] K. N. Ananda, C. Clarkson, and D. Wands, “The Cosmological gravitational wave background from primordial density perturbations,” *Phys. Rev. D* **75** (2007) 123518, [arXiv:gr-qc/0612013](#).
- [79] D. Baumann, P. J. Steinhardt, K. Takahashi, and K. Ichiki, “Gravitational Wave Spectrum Induced by Primordial Scalar Perturbations,” *Phys. Rev. D* **76** (2007) 084019, [arXiv:hep-th/0703290](#).
- [80] R. Saito and J. Yokoyama, “Gravitational wave background as a probe of the primordial black hole abundance,” *Phys. Rev. Lett.* **102** (2009) 161101, [arXiv:0812.4339 \[astro-ph\]](#). [Erratum: *Phys. Rev. Lett.* 107, 069901 (2011)].
- [81] R. Saito and J. Yokoyama, “Gravitational-wave constraints on the abundance of primordial black holes,” *Progress of theoretical physics* **123** no. 5, (2010) 867–886.
- [82] S. W. Hawking, “Black hole explosions,” *Nature* **248** (1974) 30–31.
- [83] B. J. Carr and S. W. Hawking, “Black holes in the early Universe,” *Mon. Not. Roy. Astron. Soc.* **168** (1974) 399–415.
- [84] B. J. Carr, “The Primordial black hole mass spectrum,” *Astrophys. J.* **201** (1975) 1–19.
- [85] G. F. Chapline, “Cosmological effects of primordial black holes,” *Nature* **253** no. 5489, (1975) 251–252.
- [86] B. J. Carr and J. E. Lidsey, “Primordial black holes and generalized constraints on chaotic inflation,” *Phys. Rev. D* **48** (1993) 543–553.
- [87] J. Yokoyama, “Chaotic new inflation and formation of primordial black holes,” *Phys. Rev. D* **58** (1998) 083510, [arXiv:astro-ph/9802357](#).
- [88] S. G. Rubin, A. S. Sakharov, and M. Y. Khlopov, “The Formation of primary galactic nuclei during phase transitions in the early universe,” *J. Exp. Theor. Phys.* **91** (2001) 921–929, [arXiv:hep-ph/0106187](#).
- [89] M. Y. Khlopov, S. G. Rubin, and A. S. Sakharov, “Strong primordial inhomogeneities and galaxy formation,” [arXiv:astro-ph/0202505](#).
- [90] M. Y. Khlopov, S. G. Rubin, and A. S. Sakharov, “Primordial structure of massive black hole clusters,” *Astropart. Phys.* **23** (2005) 265, [arXiv:astro-ph/0401532](#).
- [91] R. Saito, J. Yokoyama, and R. Nagata, “Single-field inflation, anomalous enhancement of superhorizon fluctuations, and non-Gaussianity in primordial black hole formation,” *JCAP* **06** (2008) 024, [arXiv:0804.3470 \[astro-ph\]](#).
- [92] M. Y. Khlopov, “Primordial Black Holes,” *Res. Astron. Astrophys.* **10** (2010) 495–528, [arXiv:0801.0116 \[astro-ph\]](#).
- [93] B. J. Carr, K. Kohri, Y. Sendouda, and J. Yokoyama, “New cosmological constraints on primordial black holes,” *Phys. Rev. D* **81** (2010) 104019, [arXiv:0912.5297 \[astro-ph.CO\]](#).
- [94] S. Choudhury and S. Pal, “Fourth level MSSM inflation from new flat directions,” *JCAP* **04** (2012) 018, [arXiv:1111.3441 \[hep-ph\]](#).
- [95] D. H. Lyth, “Primordial black hole formation and hybrid inflation,” [arXiv:1107.1681 \[astro-ph.CO\]](#).
- [96] M. Drees and E. Erfani, “Running Spectral Index and Formation of Primordial Black Hole in Single Field Inflation Models,” *JCAP* **01** (2012) 035, [arXiv:1110.6052 \[astro-ph.CO\]](#).
- [97] M. Drees and E. Erfani, “Running-Mass Inflation Model and Primordial Black Holes,” *JCAP* **04** (2011) 005, [arXiv:1102.2340 \[hep-ph\]](#).
- [98] M. P. Hertzberg and M. Yamada, “Primordial Black Holes from Polynomial Potentials in Single Field Inflation,” *Phys. Rev. D* **97** no. 8, (2018) 083509, [arXiv:1712.09750 \[astro-ph.CO\]](#).
- [99] M. Cicoli, V. A. Diaz, and F. G. Pedro, “Primordial Black Holes from String Inflation,” *JCAP* **06** (2018) 034, [arXiv:1803.02837 \[hep-th\]](#).
- [100] O. Özsoy, S. Parameswaran, G. Tasinato, and I. Zavala, “Mechanisms for Primordial Black Hole Production in String Theory,” *JCAP* **07** (2018) 005, [arXiv:1803.07626 \[hep-th\]](#).
- [101] C. T. Byrnes, P. S. Cole, and S. P. Patil, “Steepest growth of the power spectrum and primordial black holes,” *JCAP* **06** (2019) 028, [arXiv:1811.11158 \[astro-ph.CO\]](#).
- [102] J. Martin, T. Papanikolaou, and V. Vennin, “Primordial black holes from the preheating instability in single-field inflation,” *JCAP* **01** (2020) 024, [arXiv:1907.04236 \[astro-ph.CO\]](#).
- [103] J. M. Ezquiaga, J. García-Bellido, and V. Vennin, “The exponential tail of inflationary fluctuations: consequences for primordial black holes,” *JCAP* **03** (2020) 029, [arXiv:1912.05399 \[astro-ph.CO\]](#).
- [104] H. Motohashi, S. Mukohyama, and M. Oliosi, “Constant Roll and Primordial Black Holes,” *JCAP* **03** (2020) 002, [arXiv:1910.13235 \[gr-qc\]](#).
- [105] A. Ashoorioon, A. Rostami, and J. T. Firouzjaee, “EFT compatible PBHs: effective spawning of the seeds for primordial black holes during inflation,” *JHEP* **07** (2021) 087, [arXiv:1912.13326 \[astro-ph.CO\]](#).
- [106] P. Auclair and V. Vennin, “Primordial black holes from metric preheating: mass fraction in the excursion-set approach,” *JCAP* **02** (2021) 038, [arXiv:2011.05633 \[astro-ph.CO\]](#).
- [107] V. Vennin, *Stochastic inflation and primordial black holes*. PhD thesis, U. Paris-Saclay, 6, 2020. [arXiv:2009.08715 \[astro-ph.CO\]](#).
- [108] K. Inomata, E. McDonough, and W. Hu, “Primordial black holes arise when the inflaton falls,” *Phys. Rev. D* **104**

- no. 12, (2021) 123553, [arXiv:2104.03972 \[astro-ph.CO\]](#).
- [109] K.-W. Ng and Y.-P. Wu, “Constant-rate inflation: primordial black holes from conformal weight transitions,” *JHEP* **11** (2021) 076, [arXiv:2102.05620 \[astro-ph.CO\]](#).
 - [110] Q. Wang, Y.-C. Liu, B.-Y. Su, and N. Li, “Primordial black holes from the perturbations in the inflaton potential in peak theory,” *Phys. Rev. D* **104** no. 8, (2021) 083546, [arXiv:2111.10028 \[astro-ph.CO\]](#).
 - [111] S. Kawai and J. Kim, “Primordial black holes from Gauss-Bonnet-corrected single field inflation,” *Phys. Rev. D* **104** no. 8, (2021) 083545, [arXiv:2108.01340 \[astro-ph.CO\]](#).
 - [112] M. Solbi and K. Karami, “Primordial black holes formation in the inflationary model with field-dependent kinetic term for quartic and natural potentials,” *Eur. Phys. J. C* **81** no. 10, (2021) 884, [arXiv:2106.02863 \[astro-ph.CO\]](#).
 - [113] G. Ballesteros, S. Céspedes, and L. Santoni, “Large power spectrum and primordial black holes in the effective theory of inflation,” *JHEP* **01** (2022) 074, [arXiv:2109.00567 \[hep-th\]](#).
 - [114] G. Rigopoulos and A. Wilkins, “Inflation is always semi-classical: diffusion domination overproduces Primordial Black Holes,” *JCAP* **12** no. 12, (2021) 027, [arXiv:2107.05317 \[astro-ph.CO\]](#).
 - [115] C. Animali and V. Vennin, “Primordial black holes from stochastic tunnelling,” [arXiv:2210.03812 \[astro-ph.CO\]](#).
 - [116] D. Frolovsky, S. V. Ketov, and S. Saburov, “Formation of primordial black holes after Starobinsky inflation,” *Mod. Phys. Lett. A* **37** no. 21, (2022) 2250135, [arXiv:2205.00603 \[astro-ph.CO\]](#).
 - [117] A. Escrivà, F. Kuhnel, and Y. Tada, “Primordial Black Holes,” [arXiv:2211.05767 \[astro-ph.CO\]](#).
 - [118] J. Kristiano and J. Yokoyama, “Ruling Out Primordial Black Hole Formation From Single-Field Inflation,” [arXiv:2211.03395 \[hep-th\]](#).
 - [119] J. Kristiano and J. Yokoyama, “Response to criticism on ”Ruling Out Primordial Black Hole Formation From Single-Field Inflation”: A note on bispectrum and one-loop correction in single-field inflation with primordial black hole formation,” [arXiv:2303.00341 \[hep-th\]](#).
 - [120] A. Karam, N. Koivunen, E. Tomberg, V. Vaskonen, and H. Veermäe, “Anatomy of single-field inflationary models for primordial black holes,” [arXiv:2205.13540 \[astro-ph.CO\]](#).
 - [121] A. Riotto, “The Primordial Black Hole Formation from Single-Field Inflation is Not Ruled Out,” [arXiv:2301.00599 \[astro-ph.CO\]](#).
 - [122] A. Riotto, “The Primordial Black Hole Formation from Single-Field Inflation is Still Not Ruled Out,” [arXiv:2303.01727 \[astro-ph.CO\]](#).
 - [123] O. Özsoy and G. Tasinato, “Inflation and Primordial Black Holes,” [arXiv:2301.03600 \[astro-ph.CO\]](#).
 - [124] S. Choudhury, M. R. Gangopadhyay, and M. Sami, “No-go for the formation of heavy mass Primordial Black Holes in Single Field Inflation,” [arXiv:2301.10000 \[astro-ph.CO\]](#).
 - [125] S. Choudhury, S. Panda, and M. Sami, “PBH formation in EFT of single field inflation with sharp transition,” *Phys. Lett. B* **845** (2023) 138123, [arXiv:2302.05655 \[astro-ph.CO\]](#).
 - [126] S. Choudhury, S. Panda, and M. Sami, “Quantum loop effects on the power spectrum and constraints on primordial black holes,” *JCAP* **11** (2023) 066, [arXiv:2303.06066 \[astro-ph.CO\]](#).
 - [127] S. Choudhury, S. Panda, and M. Sami, “Galileon inflation evades the no-go for PBH formation in the single-field framework,” *JCAP* **08** (2023) 078, [arXiv:2304.04065 \[astro-ph.CO\]](#).
 - [128] S. Choudhury, A. Karde, S. Panda, and M. Sami, “Primordial non-Gaussianity from ultra slow-roll Galileon inflation,” *JCAP* **01** (2024) 012, [arXiv:2306.12334 \[astro-ph.CO\]](#).
 - [129] S. Banerjee, S. Choudhury, S. Chowdhury, J. Knaute, S. Panda, and K. Shirish, “Thermalization in quenched open quantum cosmology,” *Nucl. Phys. B* **996** (2023) 116368, [arXiv:2104.10692 \[hep-th\]](#).
 - [130] H. Firouzjahi and A. Riotto, “Primordial Black Holes and Loops in Single-Field Inflation,” [arXiv:2304.07801 \[astro-ph.CO\]](#).
 - [131] H. Firouzjahi, “One-loop Corrections in Power Spectrum in Single Field Inflation,” [arXiv:2303.12025 \[astro-ph.CO\]](#).
 - [132] G. Franciolini, A. Iovino, Junior., M. Taoso, and A. Urbano, “One loop to rule them all: Perturbativity in the presence of ultra slow-roll dynamics,” [arXiv:2305.03491 \[astro-ph.CO\]](#).
 - [133] G. Tasinato, “A large $|\eta|$ approach to single field inflation,” [arXiv:2305.11568 \[hep-th\]](#).
 - [134] H. Motohashi and Y. Tada, “Squeezed bispectrum and one-loop corrections in transient constant-roll inflation,” [arXiv:2303.16035 \[astro-ph.CO\]](#).
 - [135] N. Afshordi, P. McDonald, and D. N. Spergel, “Primordial black holes as dark matter: The Power spectrum and evaporation of early structures,” *Astrophys. J. Lett.* **594** (2003) L71–L74, [arXiv:astro-ph/0302035](#).
 - [136] P. H. Frampton, M. Kawasaki, F. Takahashi, and T. T. Yanagida, “Primordial Black Holes as All Dark Matter,” *JCAP* **04** (2010) 023, [arXiv:1001.2308 \[hep-ph\]](#).
 - [137] B. Carr, F. Kuhnel, and M. Sandstad, “Primordial Black Holes as Dark Matter,” *Phys. Rev. D* **94** no. 8, (2016) 083504, [arXiv:1607.06077 \[astro-ph.CO\]](#).
 - [138] M. Kawasaki, A. Kusenko, Y. Tada, and T. T. Yanagida, “Primordial black holes as dark matter in supergravity inflation models,” *Phys. Rev. D* **94** no. 8, (2016) 083523, [arXiv:1606.07631 \[astro-ph.CO\]](#).
 - [139] K. Inomata, M. Kawasaki, K. Mukaida, Y. Tada, and T. T. Yanagida, “Inflationary Primordial Black Holes as All Dark Matter,” *Phys. Rev. D* **96** no. 4, (2017) 043504, [arXiv:1701.02544 \[astro-ph.CO\]](#).
 - [140] J. R. Espinosa, D. Racco, and A. Riotto, “Cosmological Signature of the Standard Model Higgs Vacuum Instability: Primordial Black Holes as Dark Matter,” *Phys. Rev. Lett.* **120** no. 12, (2018) 121301, [arXiv:1710.11196 \[hep-ph\]](#).
 - [141] G. Ballesteros and M. Taoso, “Primordial black hole dark matter from single field inflation,” *Phys. Rev. D* **97** no. 2, (2018) 023501, [arXiv:1709.05565 \[hep-ph\]](#).
 - [142] M. Sasaki, T. Suyama, T. Tanaka, and S. Yokoyama, “Primordial black holes—perspectives in gravitational wave

- astronomy,” *Class. Quant. Grav.* **35** no. 6, (2018) 063001, [arXiv:1801.05235 \[astro-ph.CO\]](#).
- [143] G. Ballesteros, J. Rey, and F. Rompineve, “Detuning primordial black hole dark matter with early matter domination and axion monodromy,” *JCAP* **06** (2020) 014, [arXiv:1912.01638 \[astro-ph.CO\]](#).
 - [144] I. Dalianis and G. Tringas, “Primordial black hole remnants as dark matter produced in thermal, matter, and runaway-quintessence postinflationary scenarios,” *Phys. Rev. D* **100** no. 8, (2019) 083512, [arXiv:1905.01741 \[astro-ph.CO\]](#).
 - [145] D. Y. Cheong, S. M. Lee, and S. C. Park, “Primordial black holes in Higgs- R^2 inflation as the whole of dark matter,” *JCAP* **01** (2021) 032, [arXiv:1912.12032 \[hep-ph\]](#).
 - [146] A. M. Green and B. J. Kavanagh, “Primordial Black Holes as a dark matter candidate,” *J. Phys. G* **48** no. 4, (2021) 043001, [arXiv:2007.10722 \[astro-ph.CO\]](#).
 - [147] B. Carr and F. Kuhnel, “Primordial Black Holes as Dark Matter: Recent Developments,” *Ann. Rev. Nucl. Part. Sci.* **70** (2020) 355–394, [arXiv:2006.02838 \[astro-ph.CO\]](#).
 - [148] G. Ballesteros, J. Rey, M. Taoso, and A. Urbano, “Primordial black holes as dark matter and gravitational waves from single-field polynomial inflation,” *JCAP* **07** (2020) 025, [arXiv:2001.08220 \[astro-ph.CO\]](#).
 - [149] B. Carr, K. Kohri, Y. Sendouda, and J. Yokoyama, “Constraints on primordial black holes,” *Rept. Prog. Phys.* **84** no. 11, (2021) 116902, [arXiv:2002.12778 \[astro-ph.CO\]](#).
 - [150] O. Özsoy and Z. Lalak, “Primordial black holes as dark matter and gravitational waves from bumpy axion inflation,” *JCAP* **01** (2021) 040, [arXiv:2008.07549 \[astro-ph.CO\]](#).
 - [151] R. Saito and J. Yokoyama, “Gravitational-Wave Constraints on the Abundance of Primordial Black Holes,” *Prog. Theor. Phys.* **123** (2010) 867–886, [arXiv:0912.5317 \[astro-ph.CO\]](#). [Erratum: *Prog.Theor.Phys.* 126, 351–352 (2011)].
 - [152] M. Sasaki, T. Suyama, T. Tanaka, and S. Yokoyama, “Primordial Black Hole Scenario for the Gravitational-Wave Event GW150914,” *Phys. Rev. Lett.* **117** no. 6, (2016) 061101, [arXiv:1603.08338 \[astro-ph.CO\]](#). [Erratum: *Phys.Rev.Lett.* 121, 059901 (2018)].
 - [153] M. Raidal, V. Vaskonen, and H. Veermäe, “Gravitational Waves from Primordial Black Hole Mergers,” *JCAP* **09** (2017) 037, [arXiv:1707.01480 \[astro-ph.CO\]](#).
 - [154] Y. Ali-Haïmoud, E. D. Kovetz, and M. Kamionkowski, “Merger rate of primordial black-hole binaries,” *Phys. Rev. D* **96** no. 12, (2017) 123523, [arXiv:1709.06576 \[astro-ph.CO\]](#).
 - [155] H. Di and Y. Gong, “Primordial black holes and second order gravitational waves from ultra-slow-roll inflation,” *JCAP* **07** (2018) 007, [arXiv:1707.09578 \[astro-ph.CO\]](#).
 - [156] S.-L. Cheng, W. Lee, and K.-W. Ng, “Primordial black holes and associated gravitational waves in axion monodromy inflation,” *JCAP* **07** (2018) 001, [arXiv:1801.09050 \[astro-ph.CO\]](#).
 - [157] V. Vaskonen and H. Veermäe, “Lower bound on the primordial black hole merger rate,” *Phys. Rev. D* **101** no. 4, (2020) 043015, [arXiv:1908.09752 \[astro-ph.CO\]](#).
 - [158] M. Drees and Y. Xu, “Overshooting, Critical Higgs Inflation and Second Order Gravitational Wave Signatures,” *Eur. Phys. J. C* **81** no. 2, (2021) 182, [arXiv:1905.13581 \[hep-ph\]](#).
 - [159] A. Hall, A. D. Gow, and C. T. Byrnes, “Bayesian analysis of LIGO-Virgo mergers: Primordial vs. astrophysical black hole populations,” *Phys. Rev. D* **102** (2020) 123524, [arXiv:2008.13704 \[astro-ph.CO\]](#).
 - [160] H. V. Ragavendra, P. Saha, L. Sriramkumar, and J. Silk, “Primordial black holes and secondary gravitational waves from ultraslow roll and punctuated inflation,” *Phys. Rev. D* **103** no. 8, (2021) 083510, [arXiv:2008.12202 \[astro-ph.CO\]](#).
 - [161] A. Ashoorioon, A. Rostami, and J. T. Firouzjaee, “Examining the end of inflation with primordial black holes mass distribution and gravitational waves,” *Phys. Rev. D* **103** (2021) 123512, [arXiv:2012.02817 \[astro-ph.CO\]](#).
 - [162] H. V. Ragavendra, L. Sriramkumar, and J. Silk, “Could PBHs and secondary GWs have originated from squeezed initial states?,” *JCAP* **05** (2021) 010, [arXiv:2011.09938 \[astro-ph.CO\]](#).
 - [163] T. Papanikolaou, V. Vennin, and D. Langlois, “Gravitational waves from a universe filled with primordial black holes,” *JCAP* **03** (2021) 053, [arXiv:2010.11573 \[astro-ph.CO\]](#).
 - [164] Z. Teimoori, K. Rezazadeh, M. A. Rasheed, and K. Karami, “Mechanism of primordial black holes production and secondary gravitational waves in α -attractor Galileon inflationary scenario,” [arXiv:2107.07620 \[astro-ph.CO\]](#).
 - [165] M. Cicoli, F. G. Pedro, and N. Pedron, “Secondary GWs and PBHs in string inflation: formation and detectability,” *JCAP* **08** no. 08, (2022) 030, [arXiv:2203.00021 \[hep-th\]](#).
 - [166] A. Ashoorioon, K. Rezazadeh, and A. Rostami, “NANOGrav signal from the end of inflation and the LIGO mass and heavier primordial black holes,” *Phys. Lett. B* **835** (2022) 137542, [arXiv:2202.01131 \[astro-ph.CO\]](#).
 - [167] T. Papanikolaou, “Gravitational waves induced from primordial black hole fluctuations: the effect of an extended mass function,” *JCAP* **10** (2022) 089, [arXiv:2207.11041 \[astro-ph.CO\]](#).
 - [168] T. Papanikolaou, “Primordial black holes in loop quantum cosmology: the effect on the threshold,” *Class. Quant. Grav.* **40** no. 13, (2023) 134001, [arXiv:2301.11439 \[gr-qc\]](#).
 - [169] T. Papanikolaou, A. Lymperis, S. Lola, and E. N. Saridakis, “Primordial black holes and gravitational waves from non-canonical inflation,” *JCAP* **03** (2023) 003, [arXiv:2211.14900 \[astro-ph.CO\]](#).
 - [170] X. Wang, Y.-I. Zhang, R. Kimura, and M. Yamaguchi, “Reconstruction of Power Spectrum of Primordial Curvature Perturbations on small scales from Primordial Black Hole Binaries scenario of LIGO/VIRGO detection,” [arXiv:2209.12911 \[astro-ph.CO\]](#).
 - [171] W. Ahmed, M. Junaid, and U. Zubair, “Primordial black holes and gravitational waves in hybrid inflation with chaotic potentials,” *Nucl. Phys. B* **984** (2022) 115968, [arXiv:2109.14838 \[astro-ph.CO\]](#).
 - [172] Z. Yi, Z.-Q. You, Y. Wu, Z.-C. Chen, and L. Liu, “Exploring the NANOGrav Signal and Planet-mass Primordial Black

- Holes through Higgs Inflation,” [arXiv:2308.14688 \[astro-ph.CO\]](#).
- [173] C. Yuan and Q.-G. Huang, “A topic review on probing primordial black hole dark matter with scalar induced gravitational waves,” [arXiv:2103.04739 \[astro-ph.GA\]](#).
 - [174] M. Aghaie, G. Armando, A. Dondarini, and P. Panci, “Bounds on Ultralight Dark Matter from NANOGrav,” [arXiv:2308.04590 \[astro-ph.CO\]](#).
 - [175] C. Burrage, C. de Rham, D. Seery, and A. J. Tolley, “Galileon inflation,” *JCAP* **01** (2011) 014, [arXiv:1009.2497 \[hep-th\]](#).
 - [176] S. Choudhury, “Large fluctuations in the Sky,” [arXiv:2403.07343 \[astro-ph.CO\]](#).
 - [177] S. Choudhury, A. Karde, P. Padiyar, and M. Sami, “Primordial Black Holes from Effective Field Theory of Stochastic Single Field Inflation at NNNLO,” [arXiv:2403.13484 \[astro-ph.CO\]](#).
 - [178] B. Jain and J. Khoury, “Cosmological Tests of Gravity,” *Annals Phys.* **325** (2010) 1479–1516, [arXiv:1004.3294 \[astro-ph.CO\]](#).
 - [179] R. Gannouji and M. Sami, “Galileon gravity and its relevance to late time cosmic acceleration,” *Phys. Rev. D* **82** (2010) 024011, [arXiv:1004.2808 \[gr-qc\]](#).
 - [180] A. Ali, R. Gannouji, and M. Sami, “Modified gravity a la Galileon: Late time cosmic acceleration and observational constraints,” *Phys. Rev. D* **82** (2010) 103015, [arXiv:1008.1588 \[astro-ph.CO\]](#).
 - [181] C. de Rham and L. Heisenberg, “Cosmology of the Galileon from Massive Gravity,” *Phys. Rev. D* **84** (2011) 043503, [arXiv:1106.3312 \[hep-th\]](#).
 - [182] C. Burrage and D. Seery, “Revisiting fifth forces in the Galileon model,” *JCAP* **08** (2010) 011, [arXiv:1005.1927 \[astro-ph.CO\]](#).
 - [183] A. De Felice and S. Tsujikawa, “Generalized Brans-Dicke theories,” *JCAP* **07** (2010) 024, [arXiv:1005.0868 \[astro-ph.CO\]](#).
 - [184] A. De Felice, S. Mukohyama, and S. Tsujikawa, “Density perturbations in general modified gravitational theories,” *Phys. Rev. D* **82** (2010) 023524, [arXiv:1006.0281 \[astro-ph.CO\]](#).
 - [185] E. Babichev, C. Deffayet, and R. Ziour, “The Recovery of General Relativity in massive gravity via the Vainshtein mechanism,” *Phys. Rev. D* **82** (2010) 104008, [arXiv:1007.4506 \[gr-qc\]](#).
 - [186] A. De Felice and S. Tsujikawa, “Cosmology of a covariant Galileon field,” *Phys. Rev. Lett.* **105** (2010) 111301, [arXiv:1007.2700 \[astro-ph.CO\]](#).
 - [187] A. De Felice and S. Tsujikawa, “Generalized Galileon cosmology,” *Phys. Rev. D* **84** (2011) 124029, [arXiv:1008.4236 \[hep-th\]](#).
 - [188] K. Hinterbichler, M. Trodden, and D. Wesley, “Multi-field galileons and higher co-dimension branes,” *Phys. Rev. D* **82** (2010) 124018, [arXiv:1008.1305 \[hep-th\]](#).
 - [189] T. Kobayashi, M. Yamaguchi, and J. Yokoyama, “G-inflation: Inflation driven by the Galileon field,” *Phys. Rev. Lett.* **105** (2010) 231302, [arXiv:1008.0603 \[hep-th\]](#).
 - [190] C. Deffayet, O. Pujolas, I. Sawicki, and A. Vikman, “Imperfect Dark Energy from Kinetic Gravity Braiding,” *JCAP* **10** (2010) 026, [arXiv:1008.0048 \[hep-th\]](#).
 - [191] S. Mizuno and K. Koyama, “Primordial non-Gaussianity from the DBI Galileons,” *Phys. Rev. D* **82** (2010) 103518, [arXiv:1009.0677 \[hep-th\]](#).
 - [192] J. Khoury, “Theories of Dark Energy with Screening Mechanisms,” [arXiv:1011.5909 \[astro-ph.CO\]](#).
 - [193] A. De Felice, R. Kase, and S. Tsujikawa, “Matter perturbations in Galileon cosmology,” *Phys. Rev. D* **83** (2011) 043515, [arXiv:1011.6132 \[astro-ph.CO\]](#).
 - [194] K. Kamada, T. Kobayashi, M. Yamaguchi, and J. Yokoyama, “Higgs G-inflation,” *Phys. Rev. D* **83** (2011) 083515, [arXiv:1012.4238 \[astro-ph.CO\]](#).
 - [195] T. Kobayashi, M. Yamaguchi, and J. Yokoyama, “Primordial non-Gaussianity from G-inflation,” *Phys. Rev. D* **83** (2011) 103524, [arXiv:1103.1740 \[hep-th\]](#).
 - [196] A. De Felice and S. Tsujikawa, “Primordial non-Gaussianities in general modified gravitational models of inflation,” *JCAP* **04** (2011) 029, [arXiv:1103.1172 \[astro-ph.CO\]](#).
 - [197] J. Khoury, J.-L. Lehnert, and B. A. Ovrut, “Supersymmetric Galileons,” *Phys. Rev. D* **84** (2011) 043521, [arXiv:1103.0003 \[hep-th\]](#).
 - [198] M. Trodden and K. Hinterbichler, “Generalizing Galileons,” *Class. Quant. Grav.* **28** (2011) 204003, [arXiv:1104.2088 \[hep-th\]](#).
 - [199] C. Burrage, C. de Rham, and L. Heisenberg, “de Sitter Galileon,” *JCAP* **05** (2011) 025, [arXiv:1104.0155 \[hep-th\]](#).
 - [200] T. Kobayashi, M. Yamaguchi, and J. Yokoyama, “Generalized G-inflation: Inflation with the most general second-order field equations,” *Prog. Theor. Phys.* **126** (2011) 511–529, [arXiv:1105.5723 \[hep-th\]](#).
 - [201] L. Perreault Levasseur, R. Brandenberger, and A.-C. Davis, “Defrosting in an Emergent Galileon Cosmology,” *Phys. Rev. D* **84** (2011) 103512, [arXiv:1105.5649 \[astro-ph.CO\]](#).
 - [202] P. Brax, C. Burrage, and A.-C. Davis, “Laboratory Tests of the Galileon,” *JCAP* **09** (2011) 020, [arXiv:1106.1573 \[hep-ph\]](#).
 - [203] A. De Felice and S. Tsujikawa, “Inflationary non-Gaussianities in the most general second-order scalar-tensor theories,” *Phys. Rev. D* **84** (2011) 083504, [arXiv:1107.3917 \[gr-qc\]](#).
 - [204] X. Gao and D. A. Steer, “Inflation and primordial non-Gaussianities of ‘generalized Galileons’,” *JCAP* **12** (2011) 019, [arXiv:1107.2642 \[astro-ph.CO\]](#).
 - [205] E. Babichev, C. Deffayet, and G. Esposito-Farese, “Constraints on Shift-Symmetric Scalar-Tensor Theories with a Vainshtein Mechanism from Bounds on the Time Variation of G ,” *Phys. Rev. Lett.* **107** (2011) 251102,

- arXiv:1107.1569 [gr-qc].
- [206] A. De Felice, T. Kobayashi, and S. Tsujikawa, “Effective gravitational couplings for cosmological perturbations in the most general scalar-tensor theories with second-order field equations,” *Phys. Lett. B* **706** (2011) 123–133, arXiv:1108.4242 [gr-qc].
 - [207] J. Khoury, G. E. J. Miller, and A. J. Tolley, “Spatially Covariant Theories of a Transverse, Traceless Graviton, Part I: Formalism,” *Phys. Rev. D* **85** (2012) 084002, arXiv:1108.1397 [hep-th].
 - [208] T. Qiu, J. Evslin, Y.-F. Cai, M. Li, and X. Zhang, “Bouncing Galileon Cosmologies,” *JCAP* **10** (2011) 036, arXiv:1108.0593 [hep-th].
 - [209] S. Renaux-Petel, S. Mizuno, and K. Koyama, “Primordial fluctuations and non-Gaussianities from multifield DBI Galileon inflation,” *JCAP* **11** (2011) 042, arXiv:1108.0305 [astro-ph.CO].
 - [210] A. De Felice and S. Tsujikawa, “Conditions for the cosmological viability of the most general scalar-tensor theories and their applications to extended Galileon dark energy models,” *JCAP* **02** (2012) 007, arXiv:1110.3878 [gr-qc].
 - [211] A. De Felice, R. Kase, and S. Tsujikawa, “Vainshtein mechanism in second-order scalar-tensor theories,” *Phys. Rev. D* **85** (2012) 044059, arXiv:1111.5090 [gr-qc].
 - [212] A. De Felice and S. Tsujikawa, “Cosmological constraints on extended Galileon models,” *JCAP* **03** (2012) 025, arXiv:1112.1774 [astro-ph.CO].
 - [213] S.-Y. Zhou and E. J. Copeland, “Galileons with Gauge Symmetries,” *Phys. Rev. D* **85** (2012) 065002, arXiv:1112.0968 [hep-th].
 - [214] G. Goon, K. Hinterbichler, A. Joyce, and M. Trodden, “Gauged Galileons From Branes,” *Phys. Lett. B* **714** (2012) 115–119, arXiv:1201.0015 [hep-th].
 - [215] N. Shirai, K. Bamba, S. Kumekawa, J. Matsumoto, and S. Nojiri, “Generalized Galileon Model: Cosmological reconstruction and the Vainshtein mechanism,” *Phys. Rev. D* **86** (2012) 043006, arXiv:1203.4962 [hep-th].
 - [216] G. Goon, K. Hinterbichler, A. Joyce, and M. Trodden, “Galileons as Wess-Zumino Terms,” *JHEP* **06** (2012) 004, arXiv:1203.3191 [hep-th].
 - [217] C. de Rham, “Galileons in the Sky,” *Comptes Rendus Physique* **13** (2012) 666–681, arXiv:1204.5492 [astro-ph.CO].
 - [218] A. Ali, R. Gannouji, M. W. Hossain, and M. Sami, “Light mass galileons: Cosmological dynamics, mass screening and observational constraints,” *Phys. Lett. B* **718** (2012) 5–14, arXiv:1207.3959 [gr-qc].
 - [219] Z.-G. Liu and Y.-S. Piao, “A Galileon Design of Slow Expansion: Emergent universe,” *Phys. Lett. B* **718** (2013) 734–739, arXiv:1207.2568 [gr-qc].
 - [220] S. Choudhury and S. Pal, “DBI Galileon inflation in background SUGRA,” *Nucl. Phys. B* **874** (2013) 85–114, arXiv:1208.4433 [hep-th].
 - [221] S. Choudhury and S. Pal, “Primordial non-Gaussian features from DBI Galileon inflation,” *Eur. Phys. J. C* **75** no. 6, (2015) 241, arXiv:1210.4478 [hep-th].
 - [222] A. Barreira, B. Li, C. M. Baugh, and S. Pascoli, “Linear perturbations in Galileon gravity models,” *Phys. Rev. D* **86** (2012) 124016, arXiv:1208.0600 [astro-ph.CO].
 - [223] P. de Fromont, C. de Rham, L. Heisenberg, and A. Matas, “Superluminality in the Bi- and Multi- Galileon,” *JHEP* **07** (2013) 067, arXiv:1303.0274 [hep-th].
 - [224] F. Arroja, N. Bartolo, E. Dimastrogiovanni, and M. Fasiello, “On the Trispectrum of Galileon Inflation,” *JCAP* **11** (2013) 005, arXiv:1307.5371 [astro-ph.CO].
 - [225] M. Sami and R. Myrzakulov, “Late time cosmic acceleration: ABCD of dark energy and modified theories of gravity,” *Int. J. Mod. Phys. D* **25** no. 12, (2016) 1630031, arXiv:1309.4188 [hep-th].
 - [226] J. Khoury, “Les Houches Lectures on Physics Beyond the Standard Model of Cosmology,” arXiv:1312.2006 [astro-ph.CO].
 - [227] C. Burrage, D. Parkinson, and D. Seery, “Beyond the growth rate of cosmic structure: Testing modified gravity models with an extra degree of freedom,” *Phys. Rev. D* **96** no. 4, (2017) 043509, arXiv:1502.03710 [astro-ph.CO].
 - [228] K. Koyama, “Cosmological Tests of Modified Gravity,” *Rept. Prog. Phys.* **79** no. 4, (2016) 046902, arXiv:1504.04623 [astro-ph.CO].
 - [229] P. Brax, C. Burrage, and A.-C. Davis, “The Speed of Galileon Gravity,” *JCAP* **03** (2016) 004, arXiv:1510.03701 [gr-qc].
 - [230] I. D. Saltas and V. Vitagliano, “Covariantly Quantum Galileon,” *Phys. Rev. D* **95** no. 10, (2017) 105002, arXiv:1611.07984 [hep-th].
 - [231] LISA Collaboration, P. Amaro-Seoane *et al.*, “Laser Interferometer Space Antenna,” arXiv:1702.00786 [astro-ph.IM].
 - [232] J. Crowder and N. J. Cornish, “Beyond LISA: Exploring future gravitational wave missions,” *Phys. Rev. D* **72** (2005) 083005, arXiv:gr-qc/0506015.
 - [233] S. Kawamura *et al.*, “The Japanese space gravitational wave antenna: DECIGO,” *Class. Quant. Grav.* **28** (2011) 094011.
 - [234] D. Reitze *et al.*, “Cosmic Explorer: The U.S. Contribution to Gravitational-Wave Astronomy beyond LIGO,” *Bull. Am. Astron. Soc.* **51** no. 7, (2019) 035, arXiv:1907.04833 [astro-ph.IM].
 - [235] M. Punturo *et al.*, “The Einstein Telescope: A third-generation gravitational wave observatory,” *Class. Quant. Grav.* **27** (2010) 194002.
 - [236] LIGO Scientific Collaboration, J. Aasi *et al.*, “Advanced LIGO,” *Class. Quant. Grav.* **32** (2015) 074001, arXiv:1411.4547 [gr-qc].
 - [237] VIRGO Collaboration, F. Acernese *et al.*, “Advanced Virgo: a second-generation interferometric gravitational wave detector,” *Class. Quant. Grav.* **32** no. 2, (2015) 024001, arXiv:1408.3978 [gr-qc].

- [238] **KAGRA** Collaboration, T. Akutsu *et al.*, “KAGRA: 2.5 Generation Interferometric Gravitational Wave Detector,” *Nature Astron.* **3** no. 1, (2019) 35–40, [arXiv:1811.08079 \[gr-qc\]](#).
- [239] A. Nicolis, R. Rattazzi, and E. Trincherini, “The Galileon as a local modification of gravity,” *Phys. Rev. D* **79** (2009) 064036, [arXiv:0811.2197 \[hep-th\]](#).
- [240] C. Deffayet, G. Esposito-Farese, and A. Vikman, “Covariant Galileon,” *Phys. Rev. D* **79** (2009) 084003, [arXiv:0901.1314 \[hep-th\]](#).
- [241] S. Choudhury, A. Karde, S. Panda, and M. Sami, “Realisation of the ultra-slow roll phase in Galileon inflation and PBH overproduction,” [arXiv:2401.10925 \[astro-ph.CO\]](#).
- [242] K. Inomata, M. Kawasaki, K. Mukaida, Y. Tada, and T. T. Yanagida, “Inflationary primordial black holes for the LIGO gravitational wave events and pulsar timing array experiments,” *Phys. Rev. D* **95** no. 12, (2017) 123510, [arXiv:1611.06130 \[astro-ph.CO\]](#).
- [243] K. Kohri and T. Terada, “Semianalytic calculation of gravitational wave spectrum nonlinearly induced from primordial curvature perturbations,” *Phys. Rev. D* **97** no. 12, (2018) 123532, [arXiv:1804.08577 \[gr-qc\]](#).